Investigating Non-Image Forming Photoreception in a Mouse Model of Autosomal Dominant Optic Atrophy

Georgia Perganta MD

Green Templeton College

Trinity Term 2011

Master of Science by Research (Nuffield Laboratory of Ophthalmology -University of Oxford)

SUPERVISOR: Prof Robert E MacLaren

CO-SUPERVISOR: Dr Sumathi Sekaran

Abstract

Autosomal Dominant Optic Atrophy (ADOA) is a progressive optic neuropathy affecting mainly the retinal ganglion cells (RGCs). It is associated with mutations in the *Opa1* gene and is phenotypically characterized by decreased visual acuity, central field deficits and colour vision defects. Experimental work on *Opa1* mutant mice (B6; C3-*Opa1*$^{+/Q285STOP}$) has permitted further characterisation of the pathophysiology of the disease. A specific functional visual deficit in the photopic negative response of the electroretinogram has been described in these mice, possibly due to altered dendritic pruning of RGCs. However, non-image-forming (NIF) visual function, which is regulated by a subset of RGCs that express the photopigment melanopsin, has not yet been extensively investigated in *Opa1* mutant mice. We were interested in whether RGC dysfunction in *Opa1* mutants affects NIF behaviours. We evaluated circadian behaviour, sleep behaviour and melanopsin expression in *Opa1* mutant mice (*Opa1*$^{+/Q285STOP}$) and littermate controls (*Opa1*$^{+/+}$). *Opa1* mutant mice were able to entrain their behaviour rhythm to a normal 12:12 hr light/dark cycle, confining their activity to the dark phase. The suppression of activity by acute light exposure at night (negative masking) was equivalent between genotypes. Circadian phase shift responses to 480 nm or 520 nm light pulses during the subjective night were preserved in *Opa1*$^{+/Q285STOP}$ mice relative to wildtype controls. The acute induction of sleep by light exposure at night was also present in *Opa1*$^{+/Q285STOP}$ mice and not significantly different to *Opa1*$^{+/+}$ animals. Immunohistochemical characterisation of melanopsin cells in flatmount retinae revealed no significant differences in cell numbers betweeen genotypes. Melanopsin (*Opn4*) transcript levels were also equivalent between *Opa1* wildtype and mutant mice. There was also no obvious difference in melanopsin cell stratification patterns. The data overwhelmingly support

the preservation of the NIF visual system in *Opa1* mutant mice. The findings are consistent with patient studies suggesting increased resistance of melanopsin-expressing RGCs in conditions of mitochondrial optic atrophy. Further work is needed to extend our understanding of the possible neuroprotective mechanism involved which could lead to exciting therapeutic strategies.

Acknowledgements

It is a pleasure for me to thank all people who contributed in some way to this thesis.

First and foremost I want to express my gratitude to my principal supervisor Prof Robert E MacLaren for his support, advice and inspiration. Thanks for believing in me and giving me the opportunity to be part of his successful research group. It has been an honor to work with him.

I would like also to thank my second supervisor Dr Sumathi Sekaran for helping me set up the experiments. Her guidance and assistance was priceless. I appreciate all her contributions of time and ideas to make my MSc experience productive.

My special thanks also go to Dr Alun Barnard and Dr Christiana Katti for their great help and directions when I run my experiments.

Thanks to Dr Stuart Peirson, Dr Sofia Godinho, Dr Simon Fisher and everyone at the Nuffield Laboratory of Ophthalmology for their valuable support.

I also wish to acknowledge the advice and suggestions of Dr Kingsley Micklem from the Nuffield Department of Clinical Laboratory Sciences.

I also appreciate all my colleagues in the team of Robert MacLaren to make my experience at the Nuffield Laboratory of Ophthalmology and Oxford a very pleasant memory.

Lastly, I would like to thank my parents and my sister for all their love and encouragement. They raised me with a love of science and supported me in all my pursuits. And most of all, my loving, encouraging and patient husband Thano whose faithful support during all stages of this thesis is so appreciated.

List of Figures

Tables

Glossary of Acronyms

AC-Amacrine cell

ADOA -Autosomal Dominant Optic Atrophy

BC-Bipolar cell

BME- β-mercaptoethanol

B2m- β2 microglobulin

ChAT- Choline Acetyltransferase

CT- Circadian Time

DD- Constant Darkness

DNA- Deoxyribonucleic Acid

ERG- Electroretinogram

Gapdh- (Glyceraldehyde-3-phosphate dehydrogenase)

GCL- Ganglion cell layer

h-Hour

HC- Horizontal cell

ICC- Immunocytochemistry

IGL- Intergeniculate leaflet

INL- Inner nuclear layer

IPL- Inner plexiform layer

LD- (Light-Dark cycle)

LEDs- (Light -emitting diodes)

LGd- Dorsal lateral geniculate nucleus

LHb- Lateral habenula

LHON- Leber's hereditary optic neuropathy

LL- Constant Light

min- Minute

NAT- (N-acetyltransferase)

NIF- Non-image forming

ONL- Outer nuclear layer

OPA1- Optic atrophy gene 1

OPL- Outer plexiform layer

OPN- Olivery Pretectal Nucleus

Opn4- Melanopsin

Opn4L- Melanopsin Long

Opn4S- Melanopsin Short

PACAP- (Pituitary adenylate cyclase –activating polypeptide)

PBS- Phosphate buffered saline

PCR- Polymerase chain reaction

PFA- Paraformaldeyde

PhNR- Photopic Negative Response

PLR- Pupillary light reflex

PRGCs-Photosensitive Retinal Ganglion Cells

Psmb2- Proteasome subunit beta type-2

rd/rd cl- rodless/coneless

RGCs- Retinal Ganglion Cells

RHT- Retinohypothalamic tract

RNA- Ribonucleic Acid

Rpm - Revolutions per minute

RT PCR- Reverse Transcription PCR

SAD- Seasonal Affective Disorder

SC- Superior colliculus

SCN- Suprachiasmatic nucleus

SZP- Ventral subparaventicular zone

VEP- Visual evoked potential

VLPO- Ventrolateral preoptic nucleus

ZT- Zeitgeber Time

Contents

Chapter 1

Introduction

1.1 Melanopsin and Non-Image Forming Photoreception

1.1.1 Discovery of melanopsin

The retina is a stratified tissue which has two functions: the generation of a visual image of the surroundings (image forming photoreception which is dependent on fine resolution contrast detection) and also the perception of ambient lighting levels to entrain our internal circadian oscillator to the external light cycle (non-image-forming vision which requires longer term measurements of the overall quantity of environmental light i.e. irradiance detection). The retina has been the subject of research study for many years and until recently it was assumed that in mammals only two classes of photoreceptors existed, the rods and cones in the outer retina. The generation of a mouse model that contained no rods or cones, (rodless/coneless or *rd/rd cl*) revealed that the eye contained a third photoreceptor class. Despite the loss of the entire outer retina, *rd/rd cl* mice retained non visual photic tasks such as circadian photoentrainment (Freedman et al., 1999), melatonin suppression (Lucas et al., 1999), the suppressing influence of bright light on the activity of nocturnal rodents (negative masking, (Mrosovsky et al., 2001) and the pupillary light reflex (Lucas et al., 2001). It was subsequently determined that retinal ganglion cells (RGCs) innervating the suprachiasmatic nucleus (SCN), the site of the central circadian pacemaker, were intrinsically photosensitive (Berson et al., 2002, Sekaran et al., 2003). This subset of the RGCs depolarized in response to

light even when all synaptic input from rods and cones were blocked. Other studies revealed the involvement of an opsin/vitamin A based photopigment with a peak spectral sensitivity of approximately 480nm, which lies in the blue/cyan range of the visible light spectrum (Lucas et al., 2001, Hattar et al., 2002). It is now known that this third photoreceptive system is localized to intrinsically photosensitive retinal ganglion cells (pRGCs) expressing the photopigment melanopsin (Berson et al., 2002, Hattar et al., 2002, Provencio et al., 2000).

Melanopsin was initially isolated from the brain, eye and dermal melanophores of *Xenopus* (Provencio et al., 1998). These areas are directly photosensitive in amphibians. In dermal melanophores of frogs, melanopsin was found to be responsible for redistribution of the skin pigment in direct response to light (Provencio et al., 1998). An orthologue of this opsin, was also found to be exclusively expressed in a small subset of ganglion cells in the mouse retina and further work demonstrated that these cells send their axons to the SCN (Gooley et al., 2001, Hattar et al., 2002, Provencio et al., 2002). Electrophysiological recordings from melanopsin expressing ganglion cells revealed an intrinsic light-evoked response (Hattar et al., 2002, Sekaran et al., 2003). The melanopsin cells co-express the neurotransmitter, pituitary adenylate cyclase-activating polypeptide (PACAP) (Hannibal et al., 2002). Related sequences of melanopsin have also been identified in humans (Provencio et al., 2000), fish (Bellingham et al., 2002, Drivenes et al., 2003), birds (Chaurasia et al., 2005) and other species.

1.1.2 Morphological and physiological properties of melanopsin expressing RGCs

Hydrophobicity analysis of the melanospin amino-acid sequence predicted a 7-transmembrane structure, common to all G-protein coupled receptors (Provencio et al., 1998). Interestingly,

melanopsin shares more homology with invertebrate rhabdomeric opsins (r-opsins) than with ciliary opsins of vertebrate species (c-opsins) in primary structure and in the ability to use light both, to initiate the signaling cascade and to reisomerize the retinal chromophore (Provencio et al., 2000, Koyanagi et al., 2005, Melyan et al., 2005, Mure et al., 2007, Panda et al., 2005, Walker et al., 2008). This and the fact that pRGCs depolarise in response to light (Berson et al., 2002), suggested that melanopsin may signal light through a different mechanism to that used in vertebrate rods and cones.

Melanopsin-expressing RGCs represent a small subset (1% - 3%) of the RGC population (Hattar et al., 2002, Hattar et al., 2006). Their dendritic profiles are large, spanning roughly 500 μm, and form an extensive overlapping plexus within the retinal inner plexiform layer (IPL) (Figure 1.1) (Hattar et al., 2002, Provencio et al., 2002). The dendrites of melanopsin expressing RGCs terminate mainly in the outer-most sublayer of the IPL (sublamina a) (Viney et al., 2007, Hattar et al., 2006, Schmidt and Kofuji., 2009, Berson et al., 2010, Hattar et al., 2002). These cells have been classified as M1 cells (Hattar et al., 2006). A second plexus of melanopsin-positive dendrites is also present in the inner IPL (sublamina b) corresponding to a second population of melanopsin-expressing cells - M2 cells (Hattar et al., 2006). M1 cells have higher melanopsin immunoreactivity (Viney et al., 2007, Hattar et al., 2006, Schmidt and Kofuji., 2009, Berson et al., 2010, Hattar et al., 2002) and their somata have diameters of ~15 μm. Although the M1 cells constitute just 1% (~700–900 overall) of the total mouse RGC population, their ~300μm diameter dendritic fields overlap to cover the entire retina (Berson et al.,2010, Hattar et al., 2002, Provencio et al., 2002). M2 cells have larger (~20 μm) somata and more regular branching dendrites covering a larger area (~400 μm) compared to M1 cells (Berson et al., 2010, Hattar et al., 2006, Viney et al., 2007).

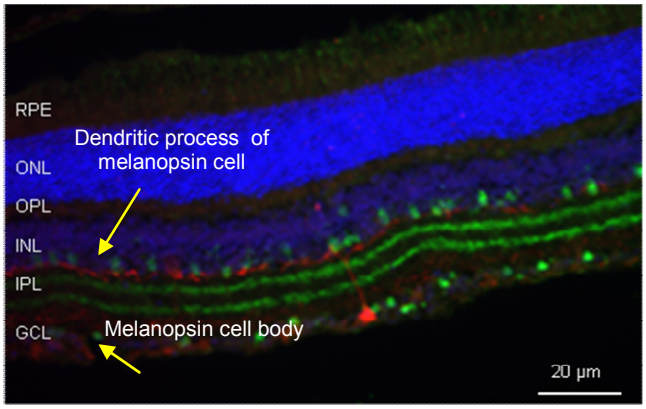

Figure 1.1: Immunostaining of mouse retinal sections with antibodies against melanopsin (red) and choline acetyl- transferase (*ChAT*) (green). The dendrites of this melanopsin cell terminate in outer layer of the IPL. The characteristic synaptic banding pattern of the IPL is visualised by ChAT staining which also labels amacrine cell bodies. Nuclei are stained blue with DAPI. Figure is the result of work done by author. N –terminal rabbit anti-melanopsin antibody (UF006) and polyclonal rabbit anti-chAT (ab68779) antibody were used.

In addition to the M1 and M2 subtypes, several other subtypes have been described. M3 cells stratify in both sublaminae of the IPL (Berson et al., 2010, Schmidt et al., 2008, Viney et al., 2007, Hattar et al., 2006). M3 cells comprise ~20% of the pRGC population (Schmidt and Kofuji, 2011) and their dendritic spread does not cover the entire retina. M3 cells have intrinsic membrane properties that are similar to M2 cells (Schmidt and Kofuji, 2011, Schmidt et al., 2008, Viney et al., 2007) M4 cells have also been described which are characterized by a large soma size and dendritic field and the rare M5 classification has small, bushy dendritic arbors (Berson et al., 2010, Ecker et al., 2010). Recent studies have revealed that different sub-types of melanopsin-expressing RGCs project to different retino-recipient brain areas and therefore may drive different functional outputs (Baver et al., 2008, Chen et al., 2011). Two distinct isoforms of mouse melanopsin, *Opn4L* (Long) and *Opn4S* (Short), have also been identified which are generated by alternate splicing of the *Opn4* locus. These isoforms are differentially expressed in ipRGC subtypes of the adult mouse retina, with both *Opn4*L and *Opn4*S detected in M1 type ipRGCs, and only *Opn4*L detected in M2 type pRGCs. Quantitative PCR showed also that *Opn4S* is expressed at levels 40 greater than *Opn4L* (Pires et al., 2009).

The critical role of melanopsin in the transduction of light information in pRGCs was determined from gene replacement/ablation studies. Three such models have been generated. Panda et al., (2002) developed melanopsin null mice (*Opn4*$^{-/-}$) by replacing exon 1 of the melanopsin gene with a neomycin-resistance gene by homologous recombination in embryonic stem cells. Hattar et al., (2002) targeted a *tau-lacZ* cassette into the melanopsin gene locus to enable identification of the cells and there axonal projections by β-galactosidase expression. Ruby et al., (2002) generated knockout mice with a targeted disruption of the melanopsin gene. Mice in which the melanopsin gene was absent (*Opn4*$^{-/-}$) exhibited attenuated phase-shifting and pupillary responses to light as well as reduced period

lengthening in constant light (LL) (Panda et al., 2002, Ruby et al., 2002, Lucas et al., 2003). Further description of circadian clock outputs are described in section 1.2. Moreover in mice lacking the *Opn*^{4} gene, light–mediated sleep induction was found to be markedly reduced even at very bright irradiances (Lupi et al., 2008; Altimus et al., 2008). Masking behaviour was also attenuated in *Opn4*$^{-/-}$ mice (Mrosovsky and Hattar, 2003).

Mice in which the melanopsin cells are completely destroyed have shown: i) attenuated entrainment to normal LD cycles (Guler et al., 2008, Hatori et al., 2008, Goz et al., 2008), ii) absence of entrainment to brief light pulses (Guler et al., 2008), iii) absence of the suppression of locomotor activity to light exposure at night "negative masking" (Hatori et al., 2008, Goz et al., 2008), iv) loss of the acute induction of sleep to brief light pulses (Lupi et al., 2008, Altimus et al., 2008) and v) reduction of the pupil light reflex (Guler et al., 2008, Hatori et al., 2008). This more severe phenotype demonstrates the importance of the melanopsin cells in relaying rod and cone information to non-image-forming functions via dendritic inputs (see section 1.1.3). All previous experiments were done on mouse models in which melanopsin cells were ablated rather than just the melanopsin gene. Goz et al., (2008) developed a saporin-based immunotoxin (UF008/SAP) that specifically ablates pRGCs in the fully-differentiated adult retina. Guler et al., (2008) introduced an attenuated diphtheria toxin A subunit (*aDTA*) 20 into the mouse melanopsin gene locus to eliminate pRGCs. Hatori et al., (2008) used a Cre- inducible diphtheria toxin receptor (iDTR) expression approach to ablate melanopsin cells.

1.1.3 Intraretinal connectivity

Although melanopsin expressing RGCs can function as photoreceptors, they also receive intraretinal synaptic input from rods and cones. The dendrites of the melanopsin cells stratify in the IPL, the layer of synaptic contact for amacrine and bipolar cells to convey rod and cone signals to ganglion cells (Berson, 2003). Using electron microscopy, Belenky et al. identified synaptic contacts between amacrine cells and presumed ON-bipolar cells with melanopsin-immunopositive processes in the inner IPL (Belenky et al., 2003). Additionally it has been suggested that there are some ON cone bipolar cells which make ectopic synapses in the outer IPL (OFF sublamina) where they costratify with and contact the dendrites of M1 and dopaminergic amacrine cells (Dumitrescu et al., 2009, Hoshi et al., 2009). Also, as demonstrated in both rats and primates, in addition to their intrinsic melanopsin-based light response, pRGCs respond to light through synaptically mediated input from rods and cones (Berson et al., 2002, Dacey et al., 2005, Perez-Leon et al., 2006, Wong et al., 2007).

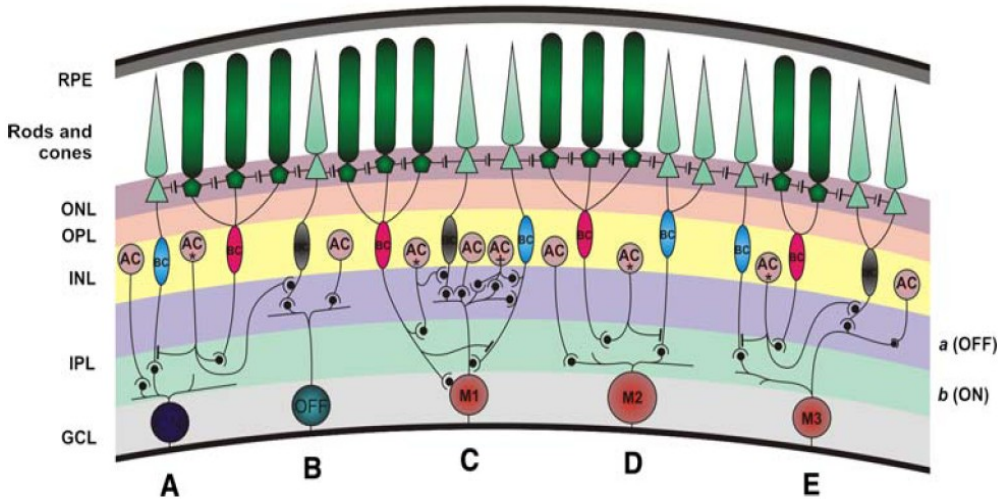

Figure 1.2: A schematic diagram of retinal connections relevant to pRGCs in the rodent retina. (Reproduced from Bailes and Lucas, 2010). Dendrites of M1 pRGCs stratify at the outer border of the IPL (OFF; sublamina a), M2 cells stratify in the inner sublamina of the IPL (ON; sublamina b) and M3 cells are bistratified with dendrites in both OFF and ON sublamina. ON bipolar cells have unusual ectopic contacts with the M1 cell type in the OFF sublamina. *ONL:* outer nuclear layer; *OPL:* outer plexiform layer; *INL:* inner nuclear layer; *IPL:* inner plexiform layer; *GCL:* ganglion cell layer; *HC:* horizontal cell; *AC:* amacrine cell;,*BC:* bipolar cell. *Blue* body = *cone* ON BC; *red* BC body = *rod* BC (ON); *grey* BC body = *cone* OFF BC.

1.1.4 Projections of melanopsin expressing RGCs

One of the differences of melanopsin expressing RGCs relative to the classical rod and cone photoreceptors is that they project directly to the brain (Figure 1.3). They transmit light information directly to the SCN, through a monosynaptic pathway called the retinohypothalamic tract (RHT), allowing photoentainment to the external light-dark cycle (Gooley et al., 2001, Berson et al., 2002, Hannibal et al., 2002, Hattar et al., 2002). Other major projections of melanopsin expressing RGCs include the intergeniculate leaflet (IGL) which also participates in circadian photoentrainment and the olivery pretectal nucleus(OPN) which controls pupil constriction (Hattar et al., 2002). The melanopsin cells also project to brain centres involved in the promotion of sleep (the ventrolateral preoptic nucleus-VLPO), gaze control (superior colliculus) and image-forming vision (dorsal lateral geniculate nucleus) (Hattar et al., 2006).

The melanopsin cell sub-classes differentially project to retinorecipient targets. M1 cells form the primary projection to the SCN (80% M1/20% M2), while M1 and M2 cells project to the OPN in approximately equivalent proportions (45% M1/55% M2) (Baver et al., 2008). Ecker et al., showed that M2-M4 cells send processes to diverse brain regions, including areas involved in visual processing such as the dorsal and ventral subregions of the lateral geniculate nucleus and the superior colliculus (Ecker et al., 2010). According to Chen et al., M1 pRGCs are composed of at least two different subtypes which have distinct brain targets and are involved in different non-image forming visual functions (Chen et al., 2011). Brn3b-positive M2 pRGCs make up the majority of projections to the OPN, whereas Brn3b-negative M1 cells project mainly to the SCN.

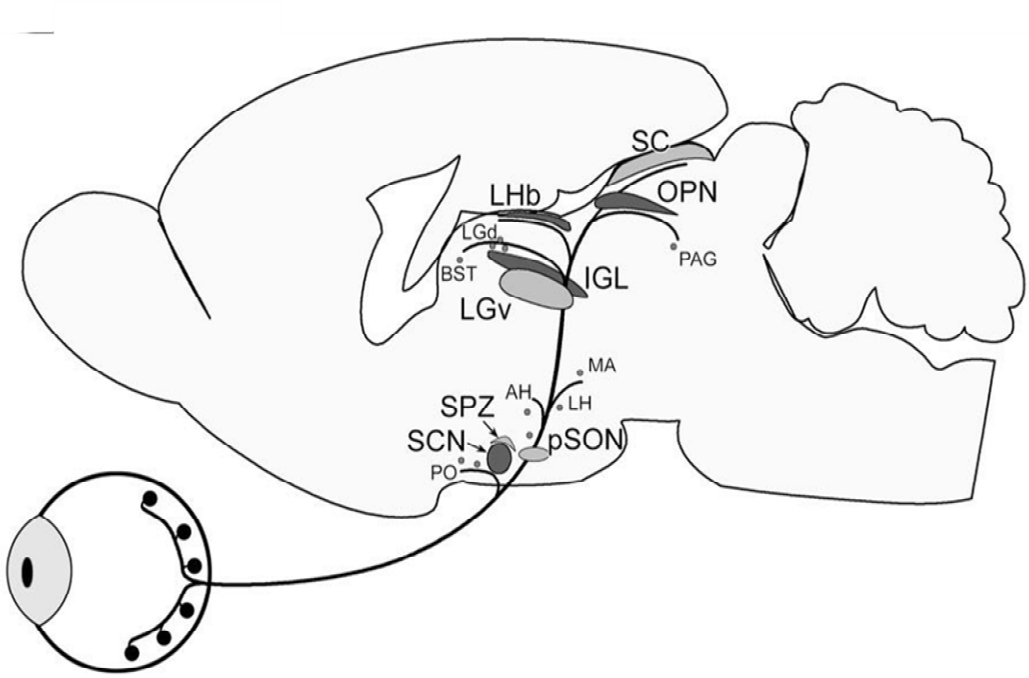

Figure 1.3: Schematic representation of brain targets of melanopsin expressing RGCs.

From Hattar et al., (2006) (Central projections of melanopsin-expressing retinal ganglion cells in the mouse. J Comp Neurol 497:326–349). Targets of melanopsin retinal ganglion cell axons include the suprachiasmatic nucleus (SCN), the intergeniculate leaflet (IGL), the lateral geniculate nucleus (LGv), the olivary pretectal nucleus (OPN), the ventral subparaventricular zone (SZP), the ventrolateral preoptic nucleus (VLPO- not shown here), the dorsal lateral geniculate nucleus (LGd), the superior colliculus (SC), the lateral habenula (LHb) and the amygdale. Principles targets are shown in dark grey and secondary targets in light grey.

1.2 Outputs of the Circadian Clock

1.2.1 General Features of a circadian system

The term *circadian* comes from the Latin circa , meaning "around", and *diem* or *dies*, meaning "day". Although circadian rhythms are endogenous ("built-in", self-sustained), they are adjusted (entrained) to the environment by external cues called zeitgebers. The primary zeitgeber is daylight and, in this case, the synchronisation with the environment is referred to as photoentrainment *(*review: Jud et al., 2005). Other zeitgebers include temperature, humidity, and food availability. Circadian rhythms have been widely observed in plants, animals, fungi and cyanobacteria. Examples of circadian rhythms in humans include the sleep-wake cycle, the core body temperature cycle and the cycles in which a number of hormones are secreted such as melatonin and cortisol. All circadian systems are composed of 3 components: an input (the entrainment pathway), an oscillator (the endogenous clock) and output pathways driving physiological functions. In mammals, light is received by pRGCs in the eye and this information is transmitted via the RHT (input) to the SCN (oscillator) which, in turns, acts to control the output of the system. The circadian oscillator is composed of conserved transcriptional–translational feedback loops which drive molecular oscillations of clock-controlled genes (for reviews see Dunlap, 1999, Shearman et al., 2000, King and Takahashi, 2000). The following sections describe functional outputs of the non image forming system.

1.2.2 Locomotor activity rhythm and phase shift behaviour.

One of the most prevalent outputs of the circadian system in mammals is the locomotor activity rhythm. In rodents, this can be monitored by placing animals in a cage with a running

wheel. By plotting wheel running activity counts against time, locomotor activity rhythms can be represented as a graph called an *actogram*. In a lighting schedule of 12 hours of light and 12 hours of darkness (LD 12:12), diurnal mammals confine their activity to the light phase and nocturnal animals to the dark phase. In this 24 hour rhythm, light is the zeitgeber (ZT). ZT0 is defined as "lights on" (the beginning of the light phase) and ZT12 corresponds to "lights off" (the end of the light phase; Fig 1.4A). The dark period of the LD cycle is also called *scotophase* and the light period called *photophase*.

The endogenous period length of the internal clock is often slightly shorter or longer than 24 hours and differs from species to species. This is revealed in the absence of external cues in conditions of constant darkness (DD) where organisms display a free-running rhythm. In DD conditions, time is expressed in circadian time (CT) units. One circadian cycle is divided into 24 equally sized circadian units (or *circadian hours*) with one unit being defined as the division of the internal period length by 24 hours. In nocturnal organisms, one circadian unit is usually less than 1 hour because the internal rhythm of these animals is typically shorter than 24 hours. CT0 designates the beginning of the subjective day (the rest phase in nocturnal rodents) and CT12 that of the subjective night (their activity phase). (Fig 1.4 B)

An entraining stimulus such as light pulse applied to an animal in constant darkness will shift the onset of the activity rhythm ("phase shift") (Pittendrigh, 1976). However, the amplitude of the shift produced depends on both the signal strength and the circadian time at which it is applied. Light administered early in the subjective night causes a phase delay, and light administered late in the night causes a phase advance, whereas light administered during the subjective day has little effect, producing a "dead zone" of response (Fig 1.5). A phase response curve represents the amplitude of the phase shift response plotted against the time

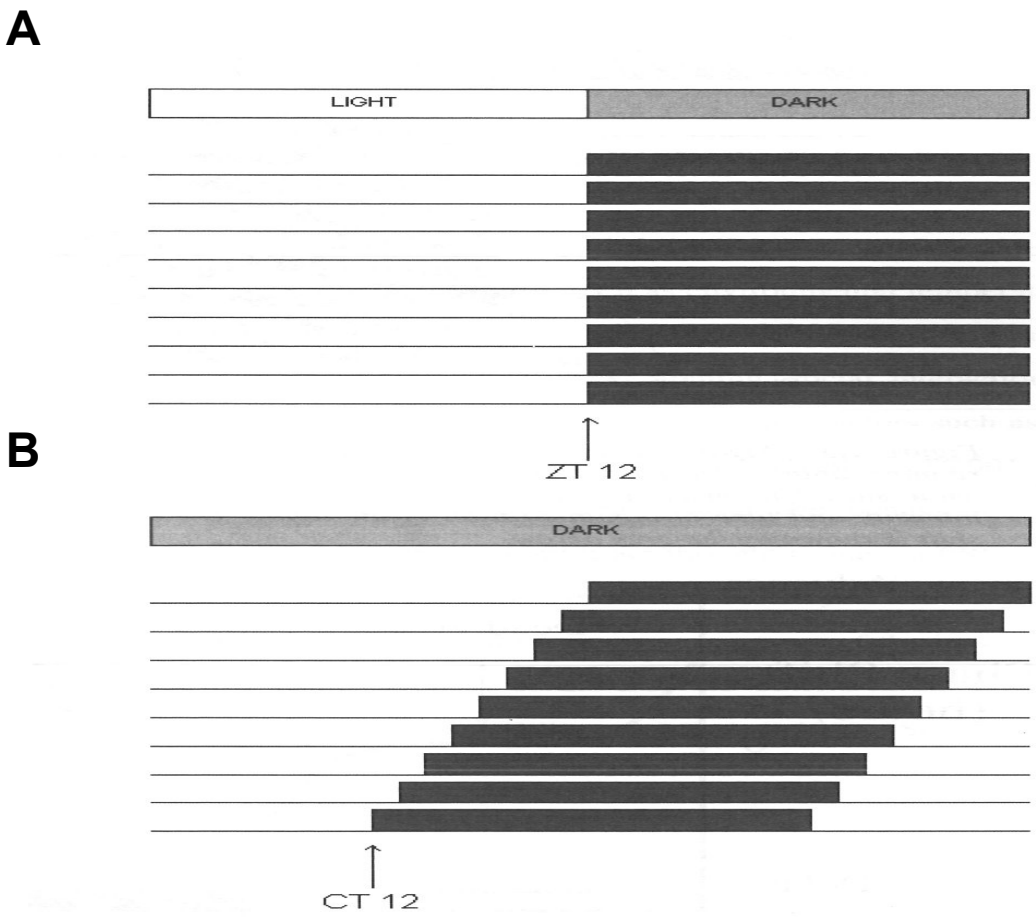

Figure 1.4: Actograms demonstrating wheel running activity profiles.

Bar at top indicates light conditions. Each horizontal line represents a 24 hour period. Solid blocks indicate wheel running activity A: Schematic example of an actogram in a 12:12 hr light-dark cycle. The period of the activity rhythm is 24 hr (ZT 12 = start of dark phase and activity onset) B: Schematic example of an actogram in conditions of constant darkness. In this case, a free running rhythm with a period of < 24 hr is observed (CT 12 = activity onset).

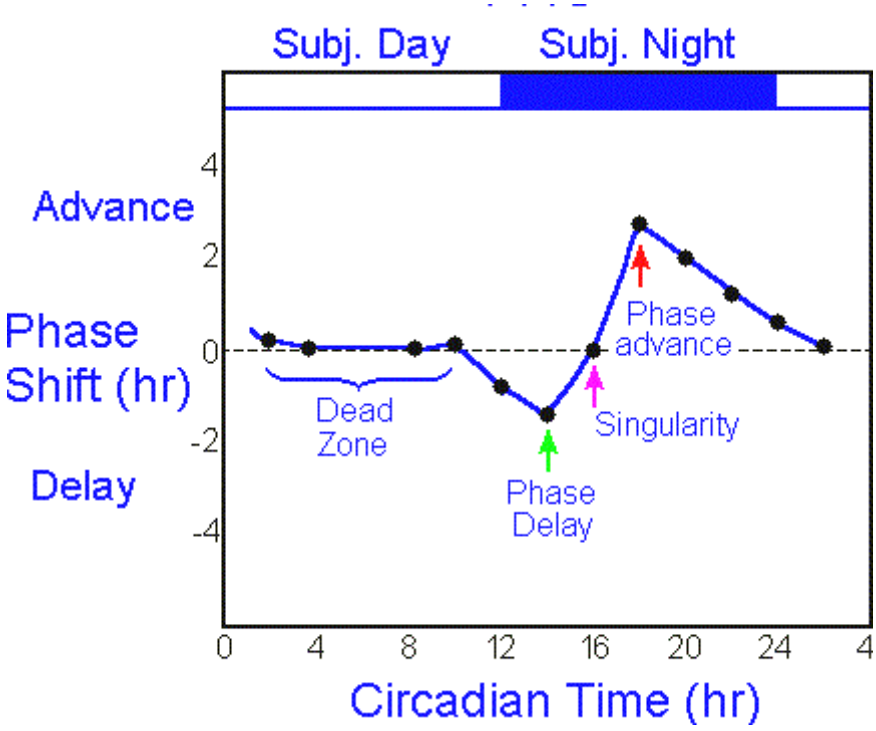

Figure 1.5: Phase response curve demonstrating the effects of light on the circadian clock. (http://scienceblogs.com/clock/2009/07/clock_tutorial_13_using_the_ph_3.php) Circadian time (CT) is shown along the horizontal axis and the phase shift in response to a brief light pulse is plotted on the vertical axis. Light given early in the subjective night causes a phase delay in the onset of activity and light late in the subjective night causes a phase advance. The dead zone, where light has no effect, is indicated.

the light pulse was administered across the circadian cycle. Phase shift behavior can be used as a tool to probe circadian function.

Although light is the most powerful zeitgeber, a variety of stimuli can be used to phase shift in its absence or to modify its effects. For example environmental temperature variation in heterothermic species (reviewed by Rensing and Ruoff, 2002) and various non-photic signals including behavioural arousal, induced wheel running, social interaction, running wheel size (Deboer and Tobler, 2000) and cage familiarity (Galani et al., 2001) can phase shift the clock.

1.2.3 Negative Masking

Acute light stimuli directly modulate activity by a mechanism independent of the pacemaker. It has two forms: a suppression of activity usually caused by a bright light in the dark period (negative masking) and an enhancement of activity caused by either a dark pulse in the light period or dim light during the dark period (positive masking) (Mrosovsky, 1999). Positive masking is completely lost in retinally degenerative mice (Mrosovsky, 1999) and thus is mediated by the classical photoreceptor system and does not rely on pRGC function.

Mice lacking rods and cones retain negative masking (Mrosovsky et al., 2001). Mice lacking the melanopsin gene display normal negative masking to dim light pulses but demonstrate impaired suppression of activity to bright light pulses (Mrosovsky and Hattar, 2003). This would suggest that rods, cones and pRGCs all contribute to the negative masking response. Indeed, mice lacking all three photoreceptors do not display negative masking (Hattar et al., 2003). Interestingly, mice in which the melanopsin cells are ablated demonstrate a complete absence of negative masking (Hatori et al., 2008, Goz et al., 2008). This would imply that rod and cone contributions to negative masking are relayed via the melanopsin expressing RGCs.

1.2.4 Sleep induction by acute light at night

In addition to the ability of acute light exposure to suppress activity levels, it can also induce sleep in nocturnal animals. The acute induction of sleep by light uses a different central pathway to circadian behaviours. A direct projection from the photosensitive RGCs to sleep/wake regulatory brain centres (including the ventrolateral preoptic nucleus and superior colliculus) have been implicated (Lupi et al., 2008). The influence of light on sleep requires both rod-cone and melanopsin signalling through pRGCs and is independent of image formation (Altimus et al., 2008).

The critical role for both the rod-cone and melanopsin systems in mediating the effects of light on sleep imply that humans with deficits in either retinal pathway could be vulnerable to acute effects of light on sleep. It has been argued that the threshold for inducing sleep by light is higher than the threshold for inhibiting wheel-running activity, possibly because light has to overcome both circadian and homeostatic mechanisms (Altimus et al., 2008).

1.2.5 Pupil light reflex

Melanopsin retinal ganglion cells provide a major contribution to the afferent limb of the pupillary light reflex (PLR). These neurons send a direct projection to the olivary pretectal nucleus (OPN) of the midbrain. Neurons of the OPN project to the Edinger-Westphal nucleus, which sends efferents to the ciliary ganglion. The axons of these ganglia innervate the sphincter pupillae muscle which induces pupil constriction. The pupillary reflex is retained in mice lacking rods and cones but with a reduced sensitivity, identifying a crucial input from the rods and cones to the PLR (Lucas et al., 2001). Mice in which the melanopsin gene is

ablated showed a pupillary light reflex indistinguishable from that of the wild types at low irradiances, but at high irradiances the reflex was incomplete suggesting that the melanopsin-associated system and the classical rod/cone system are complementary in function (Lucas et al., 2003).

1.2.6 Melatonin rhythm

Melatonin is a hormone normally secreted from the pineal gland with peak levels seen at night (Lewy, 1980). It serves as the signal of "darkness" in the organism, and as such plays an important role in the physiological regulation of circadian rhythms. The generation of melatonin rhythms can be largely attributed to N-acetyltransferase (NAT), the rate limiting enzyme in the melatonin biosynthetic pathway. Melanospin expressing retinal ganglion cells project to the SCN which sends inhibitory projections to the paraventricular nucleus controlling melatonin secretion via the sympathetic system. Acute light exposure at night suppresses melatonin release (Moore, 1996, Malpaux et al., 2001).

1.3 Melanopsin and applications in health and disease

It is becoming increasingly apparent that dysfunction of the melanopsin RGC system can have direct implications in human health and disease. For example, a mutation in the melanopsin gene may be associated with seasonal affective disorder (SAD) (Roecklein et al., 2009), an effective treatment of which is to deliver intense light to the eyes, particularly light enriched in blue (Terman and Terman, 2005). It has also been found that pRGCs mediate the light-induced exacerbation of migraine pain and therefore blocking the melanopsin expressing RGC signalling pathway may offer a new therapy for pain management (Noseda et al., 2010). Disruption of the circadian system has also been found in diabetes, cardiovascular disease, obesity, and even cancer (Green et al., 2008, Laposky et al., 2008, Reid and Zee, 2009, Takahashi et al., 2008, Sahar and Sassone-Corsi, 2009).

It would be predicted that in ocular disorders that affect the retinal ganglion cells, non image forming visual outputs should be disrupted. It has been found that the melanopsin–expressing RGCs and circadian behaviour were compromised in rat glaucoma models (Wang et al., 2008, de Zavalia et al., 2011, Drouyer et al., 2008) but see (Li et al., 2006). Glaucoma patient studies have suggested abnormal circadian rhythms of melatonin secretion and of light–induced melatonin secretion (Jean-Louis et al., 2008, Perez-Rico et al., 2010). This would confirm that in some conditions of optic neuropathy, melanopsin RGC function is compromised.

However, in certain conditions of optic neuropathy/damage preservation of the melanopsin expressing RGCs has been observed. Preservation of melanopsin expressing pRGCs has been observed in a model of axotomy (Robinson and Madison, 2004). Furthermore, preservation of pupil light responses has been found in patients with Leber's hereditary optic neuropathy

(LHON) and autosomal dominant optic neuropathy (ADOA) (Wakakura and Yokoe, 1995, Bremner et al., 1999, Chambille and Serviere, 1993, Kawasaki et al., 2010, La Morgia et al., 2010). Preservation of acute light induced melatonin suppression was also observed in these patient groups (La Morgia et al., 2010). La Morgia et al., also found a relative sparing of the melanopsin expressing RGCs relative to the rest of the RGC population. Both ADOA and LHON affect mitochondrial function in RGCs. The evidence would suggest that melanopsin RGCs are resistant to degeneration in mitochondrial optic neuropathies. However, full characterisation of circadian behaviour in conditions of mitochondrial optic neuropathy has not yet been investigated.

1.4 Autosomal Dominant Optic Atrophy

Autosomal dominant optic atrophy (ADOA) is the most common form of inherited optic neuropathy in humans with a disease prevalence ranging between 1 to 10,000 and 1 to 50,000 in different populations (Kjer, 1959, Delettre et al., 2002). It is clinically characterized by a moderate to severe decrease in visual acuity, central visual field defects, colour vision defects (mainly tritanopia) and temporal or diffuse optic nerve pallor (Johnston et al., 1979, Votruba et al., 1998) (Figure 1.6). Disease onset is mainly in childhood with a progressive visual loss (Jaeger, 1974, Lorenz, 1994). However the progression and severity of visual deficits show variability between affected families and there is range from asymptomatic carriers to legally blind patients (Caldwell et al., 1971, Kline and Glaser, 1979, Roggeveen et al., 1985). The fundamental pathology of the disease is RGC degeneration (affecting mainly those of the papillomacular bundle) associated with loss of optic nerve myelin. Postmortem studies of two patients with ADOA identified diffuse atrophy of the RGC layer, loss of myelin and fibrillary gliosis along the anterior visual pathways extending to the lateral geniculate body (Johnston et al., 1979, Kjer et al., 1983). Visual loss was moderate to severe, 6/12 (20/40) to 3/60 (10/200).

A major gene locus for ADOA was found on chromosome region 3q28-q29 (Eiberg et al., 1994) and mutations in the optic atrophy gene 1 (*OPA1*) are implicated in most of patients with ADOA (Alexander et al., 2000, Delettre et al., 2000). To date 62 OPA1 mutations have been identified (Figure 1.7) in 201 patients with ADOA (Alexander et al., 2000, Delettre et al., 2000). Most mutations are predicted to result in truncated *OPA1* polypeptides either by nonsense mutations, small deletions and/or insertions and splicing mutations. Delettre et al., (2001) screened 19 unrelated patients and found 17 mutations. Of these, 15 were different (Table 1), of which 8 were novel and 7 had been previously described (Alexander et al. 2000; Delettre et al. 2000; Pesch et al. 2001; Toomes et al. 2001). Recently, Hudson et al., (2008)

described a novel heterozygous mis-sense mutation in OPA1 leading to multiple mtDNA deletions in skeletal muscle and a mosaic defect of cytochrome c oxidase. The disorder presented with visual failure and optic atrophy in childhood, followed by progressive external ophthalmoplegia, ataxia, deafness and a sensory-motor neuropathy in adult life. Morever isolated mutations in the OPA1 gene have also been shown to cause a 'DOA plus syndrome', in which optic atrophy is accompanied by sensorineural deafness, ataxia, axonal sensory-motor polyneuropathy, chronic progressive external ophthalmoplegia and mitochondrial myopathy with cytochrome c oxidase negative and Ragged Red Fibres (Amati-Bonneau et al., 2009, Huang et al., 2009, Milone et al., 2009 and Yu-Wai-Man et al., 2010). Remarkably, it has recently shown that, in rare cases, OPA1 mutations can be associated with hearing loss, ptosis and oculomotor deficits in the absence of any detectable optic atrophy (Milone et al., 2009).

Haploinsufficiency is believed to be the major disease mechanism in *OPA1*-linked ADOA (Marchbank et al., 2002). The *OPA1* gene consists of 30 coding exons spanning 70 to 90 kb of genomic DNA. Alternative splicing of exons 4,4b and 5b leads to eight transcript isoforms with open reading frames for polypeptides of 960-1015 amino acids (Figure 1.8). In mice, although the structure is similar to humans, exon 4 is present in *Opa1* mRNA. As in human OPA1, mouse Opa1 contains a putative mitochondrial targeting signal, GTPase and dynamin central region domains and two predicted coiled-coil structures (upstream the GTPase domain and in the C-terminal domain) with 97 % overall identity with the human sequence.

Figure 1.6: Color fundus photograph from a patient with dominant optic atrophy.

The fundus photograph shows almost diffuse pallor of the left optic disk of a patient with dominant optic atrophy. The best-corrected visual acuity of the patient was 20/120 (6/36 m). (Picture courtesy of Prof Robert MacLaren)

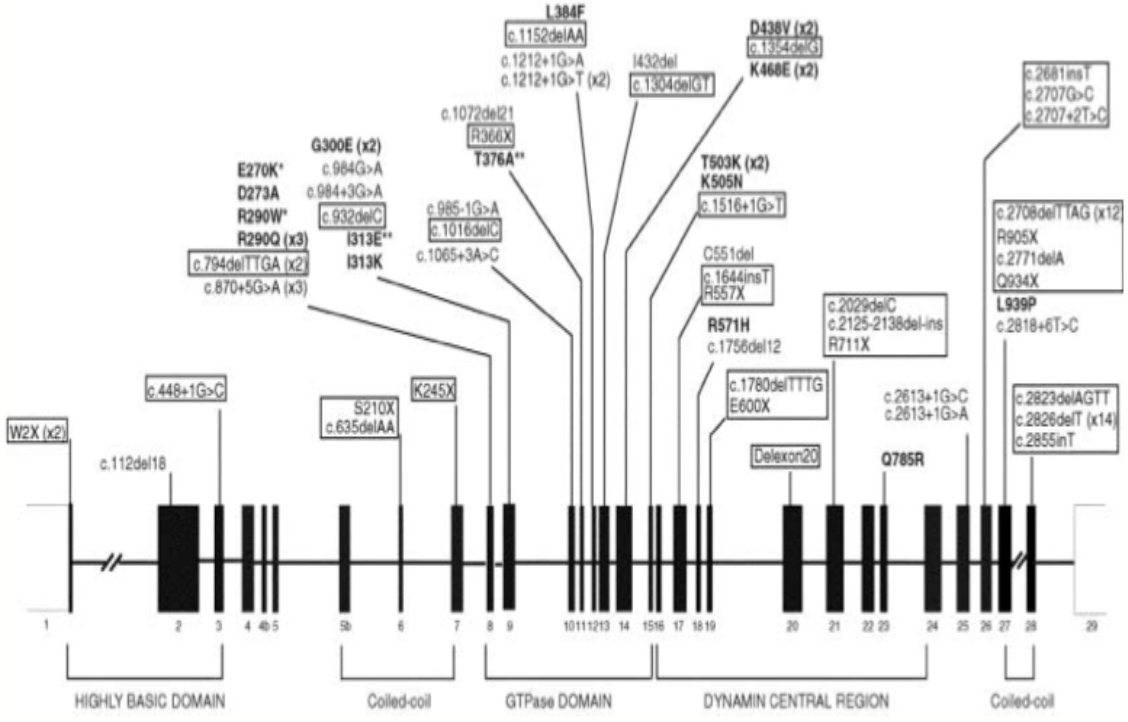

Figure 1.7: *OPA1* mutations. Adapted from Delettre et al., (2001) (Mutation spectrum and splicing variants in the OPA1 gene. Hum Genet, 109**,** 584-91). Structure of human *OPA1* (black boxes and numbers depicting exons) and positions of mutations identified in ADOA patients. Missense mutations are in bold, and trunca-tive mutations that cause loss of a C-terminal part of the protein are boxed. In-frame deletions either by deletion of nucleotides or by exon skipping resulting from splicing mutations are in plain text. The numbers in parentheses indicate the frequency. Exons en- coding the different domains of the protein are bracketed.

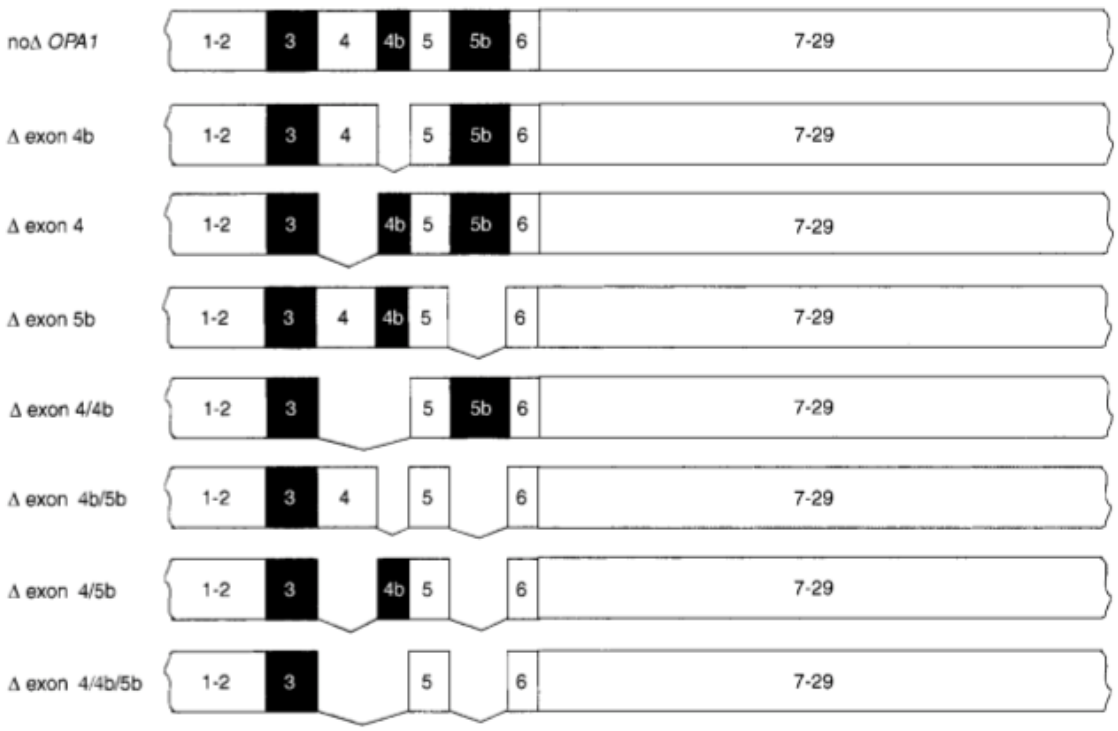

Figure 1.8: Alternative splicing patterns in human *OPA1.* From Delettre et al., (2002) (OPA1 (Kjer type) dominant optic atrophy: a novel mitochondrial disease. Mol Genet Metab, 75**,** 97-107). Schematic representation of the 8 alternative transcripts of human *OPA1* found by RT-PCR. Numbers indicate exons.

Nucleotide change	Amino acid change/effect on mRNA	Location	Protein domain	No. of families	Reference
c.794delTTGA	Frameshift Ile265	Exon 8	GTPase domain	1	Toomes et al. (2001)
c.869G>A	Arg290Gln	Exon 8	GTPase domain	1	Alexander et al. (2000); Toomes et al. (2001)
c.870+5G>A	Splice defect with skipping of exon 8	Intron 8	GTPase domain	1	Toomes et al. (2001)
c.984G>A	Splice defect with skipping of exon 9	Exon 9	GTPase domain	1	Novel
c.985–1G>A	Splice defect with skipping of exon 10	Intron 9	GTPase domain	1	Delettre et al. (2000)
c.1096C>T	Arg366STOP	Exon 11	GTPase domain	1	Alexander et al. (2000)
c.1212+1G>T	Splice defect with putative frameshift	Intron 12	GTPase domain	2	Novel
c.2029delC	Frameshift Leu677	Exon 21	Dynamin central region	1	Novel
c.2131C>T	Arg711STOP	Exon 21	Dynamin central region	1	Novel
c.2354A>G	Gln785Arg	Exon 23	Dynamin central region	1	Pesch et al. (2001)
c.2681insT	Frameshift Leu894	Exon 26	–	1	Novel
c.2707G>C	Splice defect with skipping of exon 26	Exon 26	–	1	Novel
c.2708delTTAG	Frameshift Val903	Exon 27	Coiled-coil region	2	Delettre et al. (2000); Pesch et al. (2001); Toomes et al. (2001)
c.2816T>C	Leu939Pro	Exon 27	Coiled-coil region	1	Novel
c.2855insT	Frameshift Phe952	Exon 28	Coiled-coil region	1	Novel

Table 1.1: Mutations detected in human *OPA1*. From Delettre et al. (2001) (Mutation spectrum and splicing variants in the OPA1 gene. Hum Genet 109: 584–591). 19 unrelated patients were screened and 17 mutations were found. Of these, 15 were different, of which 8 were novel and 7 had been previously described (Alexander et al. 2000; Delettre et al. 2000; Pesch et al. 2001; Toomes et al. 2001). They were distributed in the GTPase domain, the dynamin central region and the coiled-coil C-terminal domain.

OPA1 gene encodes the OPA1 protein, a dynamin –related GTPase which is located mainly to the inner membrane of mitochondria facing the intermembrane space (Delettre et al., 2000, Olichon et al., 2002, Satoh et al., 2003). OPA1 protein regulates mitochondrial fusion and thus its role in the maintenance of the mitochondrial network and morphology is critical (Cipolat et al., 2004, Cipolat et al., 2006). According to Cipolat et al., (2004) OPA1 induces mitochondrial tubulation and levels of OPA1 determine the shape of mitochondrial reticulum. OPA1 shares significant homology with Mgm1 from *S.cerevisiae* and Msp1 from *S.pombe,* genes known to be important for mitochondrial inheritance and maintenance (Pelloquin et al., 1999). The *Mgm1* gene is located on the right arm of chromosome XV between STE4 and PTP2. Sequence analysis revealed a single open reading frame of 902 residues capable of encoding a protein with an approximate molecular mass of 101 kDa. Loss of *Mgm1* resulted in slow growth on rich medium, failure to grow on non-fermentable carbon sources, and loss of mitochondrial DNA (Farh et al., 1993). The *Msp1* gene is a novel family of putative ATPase whose overexpression causes mislocalization of the 61mC1 fusion protein to the inner membrane of mitochondria, probably via the inter-membrane space, and thereby allows the host cells to grow on glycerol (Nakai et al., 1993). The predicted Msp1 protein (Msp1) is a hydrophilic 40-kDa polypeptide containing a putative membrane-spanning domain near the amino terminus (Nakai et al., 1993). When Opa1 expression was down-regulated by RNA interference in HeLa cells, the result was fragmentation of the mitochondrial network, loss of the mitochondrial membrane potential and a disorganization of the cristae. Moreover, release of cytochrome c from mitochondria and caspase-dependent activation of the apoptotic cascade was detected (Olichon et al., 2003, Lee et al., 2004).

The molecular mechanism and pathophysiology of ADOA has not been completely determined. An important question that remains unresolved is why the phenotype in most

cases is restricted to visual deficits despite broad expression of the *OPA1* gene throughout the body (Alexander et al., 2000, Bette et al., 2005). The use of mouse models which combine the clinical and genetic traits of ADOA has contributed to the better understanding of the ADOA phenotype.

1.5 Mouse Models of Autosomal Dominant Optic Atrophy

Two mouse models of *Opa1* ADOA have been published so far. These are the B6; C3-*Opa1*$^{329\text{-}355del}$ *Opa1* mutant mouse (Alavi et al., 2007) and the B6; C3-*Opa1* $^{+Q285STOP}$ *Opa1* mutant mouse (Davies et al., 2007). Both mutations result in 50% reduction in protein levels suggesting that similar to ADOA in patients, haploinsufficiency plays a critical role in the pathophysiology of disease in these mouse models.

1.5.1 B6; C3-Opa1$^{329\text{-}355del}$ Opa1 mouse model

The B6; C3-*Opa1*$^{329\text{-}355del}$ *Opa1* mouse is an ENU mutant which has a splice site mutation in *Opa1* intron 10 (c.1065+5G→A) (Alavi et al., 2007). These mice showed a normal electroretinogram (ERG) even in late ages (Heiduschka et al., 2010). However, a reduction in the amplitude of photopic visual evoked potentials (VEPs) recorded from the striate cortex was detected suggesting dysfunction in the transmission of light information from the eye to the brain. In terms of optic nerve pathology, this mouse model displayed a complete loss of large axons and a significant loss of small axons by 8 months of age indicative of RGC degeneration (Alavi et al., 2007).

1.5.2 B6; C3-Opa1 ^{Q285STOP} Opa1 mouse model

The B6;C3-*Opa1*$^{+/Q285STOP}$ *Opa1* mutant mouse was generated by screening an ENU-mutagenized DNA archive for point mutations in *Opa1* exons. An *Opa1* mutant carrying a nonsense mutation in exon 8 (coding for a C-T transition at 1051 bp (Q285STOP)) was selected (Davies et al., 2007). Homozygous progeny were not viable. Heterozygous mice displayed late onset and slow progression of morphological and functional visual outcomes. Significant abnormalities in the optic nerve were observed in *Opa1*$^{+/Q285STOP}$ mice from 9 months to 18 months of age (Davies et al., 2007, White et al., 2009). Large abnormal whirls

of myelin associated with intra-axonal changes were detected. No significant cell loss in the retinal ganglion cell layer across all age groups was observed using Haematoxylin and Eosin, Hoechst 33258 and TUNEL staining (Davies et al., 2007, Williams et al., 2010). Gross retinal morphology was also normal in *Opa1*$^{+/Q285STOP}$ mice. However, specific changes in RGC dendritic morphology were noted using diolistic labelling of the retinal ganglion cell layer at 10 months of age (Williams et al., 2010). Dendritic pruning of RGCs in *Opa1* mutant mice was localized exclusively to sublamina b (ON-centre layer) of the inner plexiform layer. RGC dendrites stratifying in the outer OFF layer of the IPL were unaffected. It was suggested that this differential effect may be due to different energy and neurotransmitter requirements of ON- and OFF- centre RGCs (Marc et al., 2008, Xu and Tian, 2007). Dendritic changes in the RGC population preceded visual dysfunction and optic nerve defects.

Visual acuity in *Opa1* mutant mice has been assessed by the optokinetic response test (Davies et al., 2007). *Opa1*$^{+/Q285STOP}$ mice at 12 months of age demonstrated a reduction in acuity relative to age matched wildtype controls. Non-image forming responses to light have not been examined in any detail in this mouse model. Davies et al., did note a difference in negative masking in *Opa1* mutant mice relative to wildtype controls (but see section 3.2 of results) (Davies et al., 2007).

On concluding, the two murine models are a useful resource for the study of DOA disease mechanisms since they display a broad correlation with the human ADOA phenotype. The B6; C3-Opa1$^{329\text{-}355del}$ mouse develop visual dysfunction as a result of RGC loss and an ascending optic neuropathy, whilst the earliest changes detected in the B6; C3-Opa1^{Q285STOP} mouse are RGC dendritic changes leading to dysfunctional RGCs. Ocular and CNS tissue from patients with ADOA is scarce and the published histology of ADOA has come from a

very small number of elderly patients with severe disease (Johnston et al., 1979, Kjer et al., 1983). This limitation has created the need for an animal model of ADOA. However, it should be recognised that although these mutant animals are a good model for ADOA disease, they are not perfect. The two mouse models have been generated by mutations in the GTPase domain and cannot replicate the functional effect of a mutation in a different gene domain or even a mutation within the same domain but in a different region. As we have already described there are many human Opa1 mutations in different domains of the gene.

1.6 Aim of thesis

Although considerable research has been devoted to assessing visual deficits in murine models of ADOA, non image forming responses to light have not been characterised in any detail. Due to the RGC pathology in *Opa1* mutant mice, dysfunction of non-image forming responses to light might be predicted. Here, in this study, we aimed to assess the non image forming visual system in 11-13 month old heterozygous B6; C3-*Opa1*$^{+/Q285STOP}$ mice and age/sex matched wildtype littermate controls. Main objectives included:

1) To investigate the photic regulation of circadian and sleep behaviour in *Opa1* mutant and wildtype mice including assessment of entrainment to a light/dark cycle, phase shift responses to brief light pulses of two different wavelengths, acute light-induced sleep and masking responses.

2) To detect any differences in melanopsin expression between *Opa1* mutant and wildtype mice at the protein level by immunohistochemistry in retinal flatmounts and at the transcript level by real-time quantitative PCR.

Chapter 2

Materials and Methods

2.1 Animal Methodology

11-13 month old *Opa1* mutant (B6; C3-*Opa1*$^{+/Q285STOP}$; Davies et al., 2007) male heterozygous mice (n=7) and an equal number of age/sex matched wildtype littermate controls (*Opa1*$^{+/+}$; n=7) were singly housed in animal care facilities under a 12-h light/12-h dark cycle (lights on at 7.00am and off at 7.00pm) at 19-23°C and 45-55% humidity with food and water provided *ad libitum*. All animal care and experimental procedures were performed with the approval of the Oxford University Institutional Animal Care and Use Committee and in accordance with the UK/British Home Office Animals (Scientific Research) Act, 1986.

2.2 Wheel running-activity monitoring

2.2.1 Animals and Housing

Seven 11-13 month old *Opa1*$^{+/Q285STOP}$ male mice (n=7) and age/sex matched *Opa1*$^{+/+}$ littermate controls (n=6) were transferred from the colony room and housed individually in standard plastic laboratory cages (45 cm ×28 cm ×13 cm, made by North Kent Plastics, UK) equipped with a steel running wheel (17.5 cm in diameter). The cages contained sawdust bedding and one nestlet (5×5 cm). Mice had access to food and water ad libitum. They were checked daily for any problems (lack of food or water, leaky water bottles, dysfunctional switches, inactivity or high activity). The water bottle was changed normally once per week while waste tray was changed once every fifteen days. Animal care procedures were

performed without light exposure using an infrared viewer when the animals were kept in DD or during the dark portion of the LD cycle.

The cages were placed inside a custom made light-tight box which offered space for 6 wheel running cages (Figure 2.1). These isolation cabinets were ventilated and contained two fluorescent light bulbs mounted on the ceiling of the cabinet. A light intensity of 200 lux, measured with a luxmeter (Macam Photometrics, UK) at the bottom of cage, was used for all behavioural assays unless otherwise stated. The provision of this white artificial light source was controlled by a timer without opening the box. This timer regulated daily light exposure by turning lights either "on" or "off ". Circadian rhythms can be influenced by several environmental cues such as light, noise, humidity, temperature or vibration (Albrecht and Foster, 2002). Therefore the room in which the wheel running experiments were performed was isolated and air-conditioned. Additionally the box doors had 2-3 heavy brass latches which were locked at all times to secure the doors closed. In order to minimize reflection of light, the interior of the isolation box or chamber was black and non-reflective.

Each cage was connected via a magnetic switch to a computer which collected the wheel activity data in 10-min bins using Clocklab circadian collection and analysis software (Actimetrics Software, IL, USA) from the MatLab Software package (The Mathwork, MA, USA). On each rotation of the running wheel, the magnetic switch was once opened and closed and signals were registered on the computer. A unique file specific for each animal was created for data acquisition. The computer also controlled whether the lights were "on" or "off " within the cabinet. Data files were copied at the end of each part of the experiment for analysis.

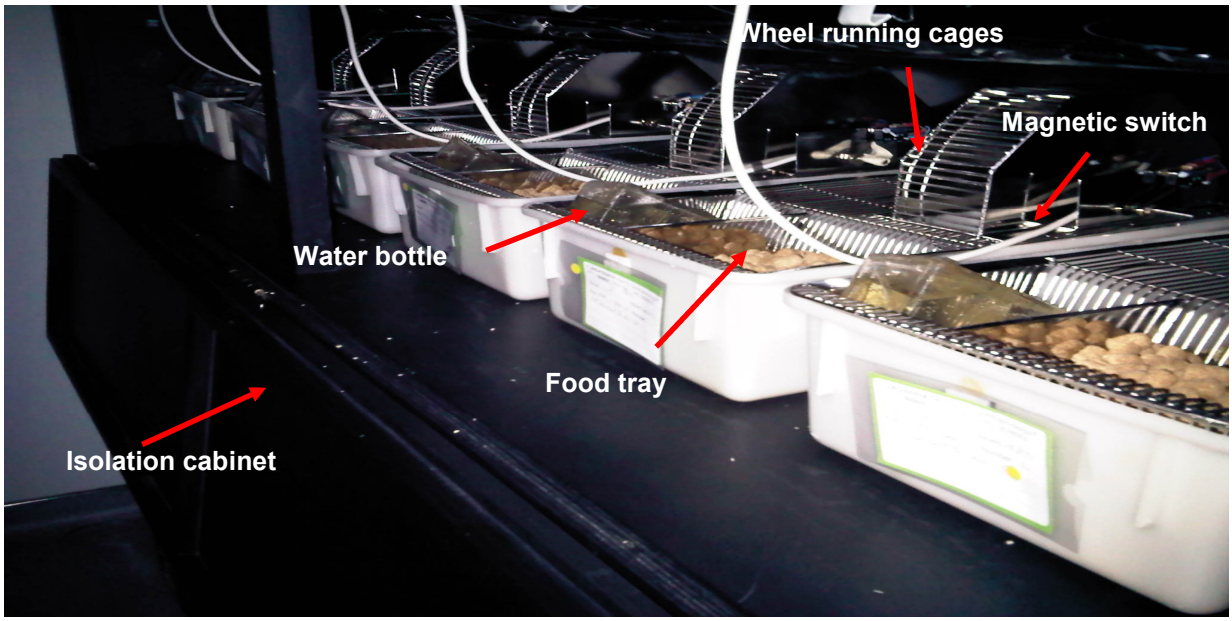

Figure 2.1: Representative image from the light-tight isolation chambers. Wheel running activity in the cages is monitored by a magnetic switch which is activated upon each wheel revolution. This information from each cage is relayed to a computer. The water bottles and food tray are also shown.

Before placing *Opa1* mice in cages, each wheel was lubricated with silicon spray and spun for detection of any bent wheels. The cages were placed in position in the light-tight box and connected to the appropriate microswitch. The wheels were spun again to ensure that each wheel revolution activated the microswitch. Once the mice were placed in the wheel cages, water bottles and food were added and the data collection on the computer was activated (Figure 2.1).

2.2.2 Entrainment to 12:12 h LD cycle

Before the start of the experiments, it was essential for the mice to be fully adapted to the isolation cabinets, to the cage and wheel. For this the animals were entrained to a standard LD cycle consisting of 12h of light (200 lux) and 12h of darkness. Lights in the isolation cabinet were switched on at 3am and switched off at 3pm on this 12/12 h LD cycle. *Opa1*$^{+/Q285STOP}$ mice and wildtypes were adapted to these conditions for 5 weeks before circadian behaviour testing. Normal entrainment to the 12:12 LD cycle was examined over a period of 7 days. The onset and offset of activity, length of the active phase, total activity levels, activity levels in the light and dark phases and the period length were calculated using Clocklab software (Actimetrics, USA).

2.2.3 Negative masking test

To examine the acute effects of bright light during the night on locomotor activity (negative masking), a 3-h pulse of white fluorescent light was applied to *Opa1*$^{+/+}$ and *Opa1*$^{+/Q285STOP}$ mice starting at zeitgeber time (ZT) 14 (the light pulse started 2h after the lights were switched off (at ZT12)). The “masking” light pulse was at 200 lux using the fluorescent light source in the light tight chambers. Subsequently all animals were re-entrained to the LD 12:12 cycle .The response to light was scored as a percentage of the number of wheel revolutions

made by the same animal during the same hour on the previous night when there was no light (i.e., a baseline day (Mrosovsky, 1999). Total activity during the masking pulse and an hourly breakdown of activity levels were also calculated.

2.2.4 Phase shift assays

After 10 days of stable entrainment*, Opa1* mutant mice and wildtype controls were released into DD for 10 days. In DD, animals began to free run with an internal period of less than 24 hours. On the first 2-3 days animals often display unstable period lengths. These days were excluded from analyses. Phase shifts were studied using a 15-min monochromatic light pulse of equivalent irradiance of 10.397×10^{10} photons/cm^2/s at two different wavelengths (480 nm and 525 nm; half peak bandwidth 10 nm). The light stimulus was applied four circadian hours (CT 16) after the onset of daily activity, at the time when light produces the maximal phase shift in most inbred mouse strains (Van Den Pol et al., 1998, Yoshimura et al., 1994). The administration of the light pulse occurred in a light-tight chamber with full internal reflectance (Honig Lichttechnik, Germany) (Figure 2.2). Animals were transferred to the light pulse chamber in their own home cages with no food or water bottles to enable full exposure to the light stimulus. The chamber was coated with reflective neutral white enamel and had a full range of different wavelength light-emitting diodes (LEDs). The intensity of the light pulse at 525 nm and 480 nm was photon matched ($10.397\ 10^{10}$ photons/s/cm^2) The irradiance of the stimulus was measured in microwatts per centimetres squared and converted to photons per centimetres squared per second based on the energy per photon for λ=525nm and λ=480 nm. Onset and duration of the light pulse were controlled with electronic timers.

After the first light pulse of 525 nm at CT16, mice were returned to their isolation cabinets and activity was monitored in DD for an additional 10 days before the next light pulse (at 480 nm). Moreover all *Opa1* mice were given a control dark sham 15-min pulse 10 days after the

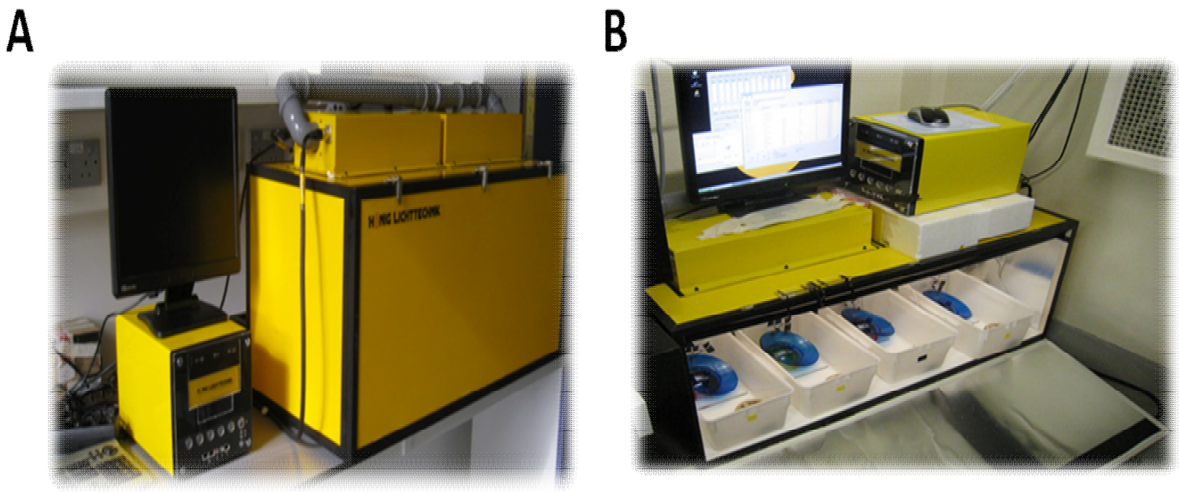

Figure 2.2: Light –tight chamber for the administration of phase shift pulses A. External view: B. From inside. The Honig Lichttechnik (Germany) chamber was used to administer the light pulses. A computer was used for the setting of appropriate irradiance and wavelength of light pulses

last pulse at CT 16. Animals were treated exactly as for the light pulse condition but remained in darkness during the procedure. Mice were allowed to free-run for a further 10 days, and the magnitudes of the phase shifts were calculated with ClockLab software, using the difference between a regression line through steady state activity onsets prior to and after the pulse. (Foster et al., 1991) (Foster et al., 1991) (ignoring the first 3 days after the pulse).

2.3 Sleep screening

Six (n=6) *Opa1*$^{+/Q285STOP}$ male mice and age/sex matched wild type littermate controls (*Opa1*$^{+/+}$ n=5) were housed in individual plastic cages with free access to food and water. Cages were placed in light-tight isolation cabinets equipped with night vision CCTV cameras (Sentient Mini-night vision CCTV camera, Maplin, UK; Figure 2.3A). Cages were ventilated and contained two fluorescent light bulbs mounted on the ceiling of the cabinet which provided a light intensity of 200 lux. A miniature of the camera and HDD security 16-channel digital hard-drive recorder (VXM4B-16, Videcon PLC, UK; 25 frames per second with a resolution of 704 x 576 pixels) used for recording activity is shown in Figure 2.3B.

Before starting the experiments, all cages were positioned under the camera and the area containing each animal was located in the centre of the field of view on the monitor. A large perspex block was placed under the food hopper area to permit full visability of the mouse in the cage. Initial background shots of the empty cage were performed in the light and dark (5 minutes for each) recording the exact time. We placed a very small amount of white bedding in each cage (1/4 square) and put animals into cages without disturbing the position of cage.

A

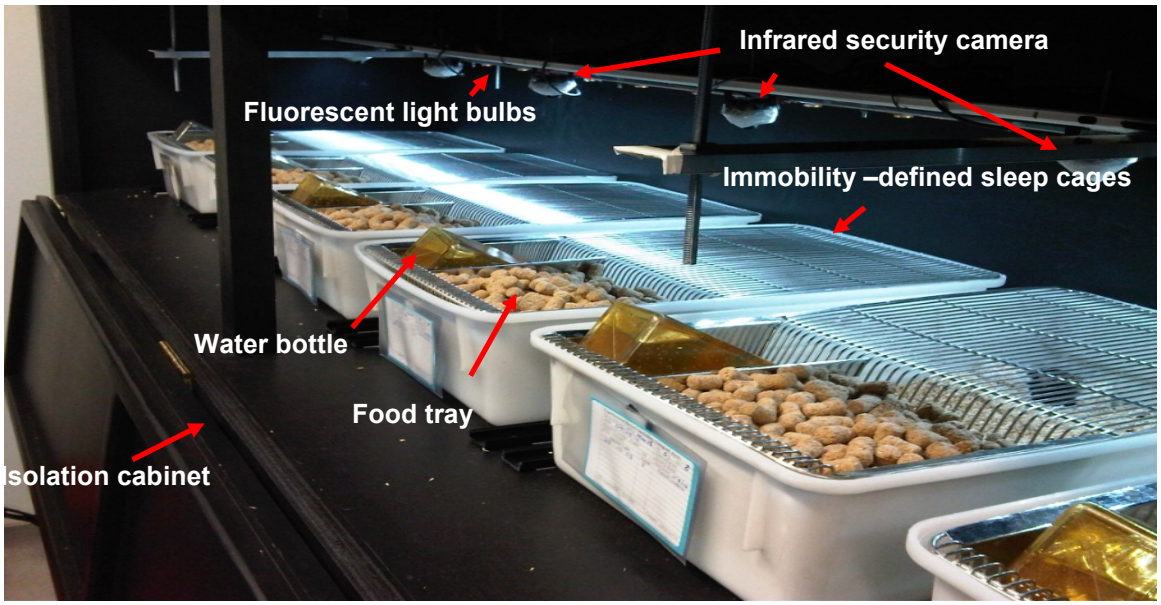

B

Figure 2.3: Equipment used for videotracking experiments. (A) Representative image from the isolation cabinet for videotracking. The water bottles and food tray are shown here as well as the two fluorescent light bulbs mounted on the ceiling of the cabinet. The infrared cameras are mounted above each cage. (B) Representative infrared camera (right) and HDD security recorder (left) used in sleep screening. Right figure is an illustration of the night vision CCTV camera which allowed us to see and capture mouse movement even in total darkness while the left one illustrates the HDD security 16-channel digital hard-drive recorder which recorded the activity of mice during sleep experiments.

Videotracking monitoring of immobility was recorded for each mouse in one full 12:12 hr LD cycle (baseline) (Figure 2.3 A). To determine the modulation of sleep behaviour by light in *Opa1* mutant and control mice, we exposed mice to a 1-h white light pulse (200 lux) during the dark phase of the 12:12 hr LD cycle starting at ZT14. Consistent with previous reports that videotracking monitoring of immobility has extremely high concordance (>95%) with EEG recordings for sleep determination (Fisher et al., 2012), we assessed the immobility-defined sleep period for each mouse using video tracking software (Anymaze Version 4.5, Stoelting, US). Sleep was defined as a period of immobility greater than 40 sec. At the start of the next light phase, mice were released into constant darkness and immobility monitored for 12 hours. Thus, immobility-defined sleep data was collected for the following conditions: i) ZT0 -24 - one baseline 12-h light/12-h dark schedule (1h resolution), ii) ZT 12-18 on the day of light pulse where ZT 14-15 is the time of light pulse administration (10 min resolution) iii) ZT 12-18 on the previous day (baseline) which was used as the control period for the light pulse (10 min resolution), iv) ZT 0-12 in darkness. Sleep latency (defined as the time between the onset of the light exposure and the first 2min of continuous immobility) was determined. The total amount of sleep spent during the light exposure was also calculated.

2.4 Immunocytochemistry (ICC)

2.4.1 Tissue collection and preparation

All animals were maintained in stable 12:12 LD conditions for at least 20 days before sacrifice. Three 11-13 month old *Opa1*$^{+/Q285STOP}$ male mice (n=3) and an equal number of age/sex matched wildtype littermate controls (n=3) were killed at ZT12 by cervical dislocation in accordance with UK Home Office guidelines. Eyes were removed, punctured at the limbus and a slit cut was made in sclera to remove the cornea, lens and vitreous. One eye from each animal

was processed for immunocytochemistry for the visualization of pRGCs in wholemount tissue and the retina from the other eye was dissected and snap frozen on dry ice at -80° C for q PCR.

2.4.2 Immunohistochemistry in flat mounted retinas

Using a Leica dissection microscope, free-floating retinas of three 11-13 month old *Opa1*$^{+/Q285STOP}$ male mice (n=3) and an equal number of age/sex matched wildtype littermate controls (*Opa1*$^{+/+}$) were carefully removed from the eyecups and fixed in freshly prepared 4% paraformaldehyde (PFA)(Thermoscientific, Pierce, Rockford, IL) for 2 h at 4ºC. Following fixation, free-floating retinas were immersed in 30% sucrose at 4ºC overnight. The following day, the samples were washed with PBS (5 min×3) and incubated in 0.4% Triton X-100 in PBS at room temperature for 20 min to enhance permeability. Unspecific binding was blocked with 10 % normal donkey serum, 0.1% Triton X-100 in PBS for one hour at room temperature. After washes with PBS (5 min × 3) retinae were incubated with polyclonal rabbit melanopsin antibody (PAS8331, Pires et al., 2009) 1:500 diluted in 1% Donkey serum, 0.1% Triton X-100 in PBS) for 4 days at 4ºC. Following further washes with 0.01% Tween-20 in PBS, a fluorescently-conjugated secondary antibody (Alexa Fluor 488 donkey anti-rabbit IgG (Invitrogen, UK) 1:400 diluted in 0.1 % Triton X-100 in PBS) was applied for 2h at 4ºC. Retinae were washed and subsequently flat mounted on glass slides with the ganglion cell layer side up. Four slits were made in the retina before being flat-mounted. Slides were cover-slipped and sealed for examination.

A fluorescent microscope (Zeiss Axioskop Germany - camera Hamamatsu Orca Japan) was used to image melanopsin positive cells with a 20x objective. Open Lab software (USA) was used to create a composite image of the entire whole- mount. (48 tiles of 1280x1022pixels at 1.07um/pixel = 1.37x1.09mm. Image total 7.49mm square). The location of melanopsin cell

bodies was mapped using Adobe Photoshop, USA. The total number of melanopsin cells was counted using Adobe Photoshop. To exclude any variations in the distribution of pRGCs, we also counted melanopsin positive cells 2 mm around optic disk which is the area of retina with the highest density of pRGCs at least in primates and humans (Dakey et al., 2005, Jusuf et al., 2007, La Morgia et al., 2010). To examine the morphology and stratification patterns of the melanopsin cells, stacked confocal images were captured using a Laser scanning confocal microscope (Zeiss LSM510, Germany). The following parameters were measured using the image analysis software package Image J（Maryland, USA http://rsb.info.nih.gov/ij/.: i) the diameter of soma: a line was drawn outlining the shape of each soma and the largest was used to calculate the area ii) number of dendrites: number of primary dendrites just emerging from the soma iii) axon diameter: the mean diameter of the axonal process 3 μm from the soma.

2.5 RNA Extraction

2.5.1 RNA preparation

To obtain RNA from frozen retina tissue, the AllPrep RNA/Protein kit from Qiagen (Germany) was used. All centrifugation and mixing steps were performed at room temperature. To ensure an RNase free working environment, all surfaces and instruments were cleaned with RNaseZap (Ambion, USA). Before starting, a volume of buffer RLT (containing guanidine thiocyanate) was mixed with β-mercaptoethanol (BME, Sigma, USA) at a ratio of 10μl BME per 1ml buffer RLT and 4 volumes of ethanol were added to buffer RPE.

Retinas of 11-13 month old *Opa1*$^{+/Q285STOP}$ male mice (n=5) and an equal number of age/sex matched wildtype littermate controls (n=5) were thawed on ice and were homogenised with a pestle. 100 μl of lysis buffer APL was added and the homogenization was continued at room

temperature by pipetting up and down several times followed by incubation for 5 min at room temperature. The RNA and protein in the lysate was then separated using an AllPrep spin column (Qiagen (Germany). The protein was purified and frozen for later use. The RNA bound to the AllPrep column was eluted with 350 µl RLT. Subsequently 1 volume (100 µl) of 70% ethanol was added and mixed well by pipetting. Up to 700µl of sample was then pipetted into an RNeasy spin column (Qiagen (Germany) which was placed within a 2ml collection tube. The samples were centrifuged at 10000 rpm for 1 minute and the flow through discarded. 350µl of wash buffer RW1 (containing ethanol) was added to each sample, centrifuged at 10000 rpm for 15 seconds and the flow through discarded.

To perform DNaseI digestion, 80µl of DNaseI incubation mix (made by adding 10µl of DNaseI stock solution to 70µl of buffer RDD) was added directly to the spin column membrane and incubated at room temperature for 15 minutes. Repeated washes using buffer RW1 and RPE were performed and after the final wash and centrifugation at 10000rpm for 30 seconds the flow through was discarded. To elute the RNA, the spin columns were placed in a sterile, RNase free 1.5ml microcentrifuge tube, 30µl of RNase free water was added and the samples were centrifuged at 10000rpm for 1 minute. The eluted RNA was pipetted back into the spin column and centrifuged at 10000rpm for another 1 minute. The RNA was quantified (section 2.5.2) and sample stored at -70^{O}C.

2.5.2 Quantification of RNA

For each RNA sample obtained, the nucleic acid concentration and $A_{260/280}$ ratio were obtained using a NanoPhotometer (Nanodrop 1000; Thermo Fisher Scientific (MA, USA)). The ratio of the absorbance at 260 and 280nm ($A_{260/280}$) is used to assess the purity of nucleic acids. For pure DNA, $A_{260/280}$ is ~1.8 and for pure RNA $A_{260/280}$ is ~2. . If the ratio is

appreciably lower in either case, it may indicate the presence of protein, phenol or other contaminants that absorb strongly at or near 280 nm. In our case, an A260:280 ratio of 1.8-2.1 was considered acceptable.

2.6 Reverse transcriptase PCR analysis (RT-PCR)

2.6.1 First strand synthesis

Samples of RNA to be tested were thawed on ice. RNA was reverse transcribed into cDNA using the SuperScript®III Reverse-Transcriptase system (Invitrogen, UK). Up to 500 µg total RNA, 5µl random 6-mer/9-mer Primers and RNA-free water to a total volume of 30.5 µl were combined. The mixture was then incubated at 85^{O}C for 15 minutes and placed on ice for 2 minutes. The cDNA synthesis master mix was prepared in a 1.5ml microcentrifuge tube by adding for each sample: 10µl of First strand buffer, 5µl of 0.1M DTT, 2.5µl of d NTP and 1µl of RNaseOUT Inhibitor. 18.5µl of synthesis mix was added to each RNA/primer mix, mixed gently and collected by brief centrifugation. The samples were incubated at RT for 2 minutes. 1µl Superscript III Reverse Transcriptase (Life Technologies) was added to each tube and incubated at 25^{O}C for 5 minutes, then at 50 ^{O}C for 1 hour. cDNA was stored at -20^{O}C. The primers were designed with NCBI Primer-BLAST. Primers were designed to be 18 – 24 nucleotides in length, with a high G + C content of 45 – 55%, to span exon - exon junctions and with an optimum melting temperature of 60^{o}C (NCBI Primer BLAST, Bethesda MD, USA). The primers used are described in table 2.1.

2.6.2 PCR Set Up

Brilliant II Ultra-Fast SYBR® Green QPCR Master Mix (Agilent, NYSE, USA) and the StepOnePlus Real Time PCR System (Applied Biosystems, Foster City, CA, USA) was used for qRT-PCR. The master mix contained *Taq* DNA polymerase, dNTPs, Mg^{2+}, a buffer

specially formulated for fast cycling and the double–stranded DNA-binding dye SYBR Green I. Each reaction (performed in triplicate) contained 10 µl SYBR, 1 µl of forward and reverse primer, 0.3 µl of Reference Dye, 6.7 µl of RNAse free water and 1 µl of template DNA in a total volume of 20 µl. A no template control was run for each gene to confirm the absence of contamination. Real time PCR consisted of 1 cycle of 3 minutes at 95 ^{O}C, 40 cycles of 5 seconds at 95 ^{O}C , 10 seconds at 60 ^{O}C and 15 seconds at the annealing temperature of each gene.

2.6.3 Data analysis

Data were analysed initially using SDS 1.7 (Applied Biosystems) and raw values were exported to Excel (Microsoft) and analysed as efficiency-corrected expression (Peirson et al., 2003). To normalise variations in RT-PCR efficiency and errors in sample quantification (e.g. loading errors), gene expression was normalised to endogenous unrelated reference genes. Previous studies have demonstrated the benefits of using mutliple internal control genes (Vandesomple et al., 2002). Therefore expression of the genes of interest was normalised to the geometric mean of Glyceraldehyde-3-phosphate dehydrogenase (*Gapdh*), Proteasome subunit beta type-2 (*Psmb2*) and β2 microglobulin (*B2m*) expression (see table 2.1) which have been previously used as internal control genes in the retina (Hughes et al., 2012; Peirson et al., 2007). The quantitative PCR results from *Opa1*$^{+/Q285STOP}$ retinae are expressed relative to the wildtype control.

2.7 Statistical analysis

All results are expressed as mean ± SEM. The quantification of wheel running activity (average period (τ), total activity levels, activity levels during light and dark phase, length of active phase and onset and offset of the activity rhythm) was analyzed using unpaired

Student's t test (Excel Statistics 2010). The same test was applied to assess the quantification of sleep latency and total sleep amount between two genotypes and quantification of melanopsin-expressing cell numbers and melanopsin transcript levels. The average wheel running revolutions on the night of the masking light pulse was examined by the one-way analysis-of-variance (ANOVA) whereas the hourly breakdown of the total activity during the masking pulse was analysed by a two -way ANOVA (SPSS Statistics 17.0). The size of the phase shift responses was evaluated by a two-way ANOVA and the period length before and after the phase shift pulses by one-way ANOVA analysis (SPSS Statistics 17.0).

	Primer sequence	Exon position	T (^{O}C)
Rhodopsin	Forward: TGTTCCTGCTCATCGTGCTGG	1	82.5
	Reverse: GGAAGTTGCTCATCGGCTTGC	2	
Thy1	Forward: CTCCCGCGTCACCCTCTCCA	2	80.5
	Reverse: GCAGGCTTATGCCGCCACACT	3	
Brn3b	Forward: GATGCGGAGAGCTTGTCTTC	1	82.5
	Reverse: GATGGTGGTGGTGGCTCTT	2	
Opa1	Forward: TGACAAACTTAAGGAGGCTGTG	22	77.5
	Reverse: CATTGTGCTGAATAACCCTCAA	23	
Opn4	Forward: TCACAGGGATGCTGGGCAATC	2	80.5
	Reverse: TTCTTGTAGAGGCTGCTGGCAAAG	3	
Short Opn4	Forward: GCTACCGCTCTACCCACC	8	83
	Reverse: CTACATCCCGAGATCCAGACT	10	
Long Opn4	Forward: GCTACCGCTCTACCCACC	8	83
	Reverse: CTACAGATGTCTGAGAGTCAC	9b	
GAPDH	Forward: TGCACCACCAACTGCTTAG	4	82.5
	Reverse GATGCAGGGATGATGTTC	5	
PSMB2	Forward: AAATGCGGAATGGATATGAAT	2-3	80.5
	Reverse: GAAGACAGTCAGCCAGGTT	3	
B2M	Forward: GCTATCCAGAAAACCCCTCAA	1-2	80
	Reverse: CATGTCTCGATCCCAGTAGACGG	2-3	

Table 2.1: Primer sequences. Sequence, exon position and optimal amplification temperature of primers used in RT-PCR analysis (all primers obtained from Invitrogen, UK).

Chapter 3

Results

3.1 *Opa1*$^{+/Q285STOP}$ mice exhibit normal entrainment to a 12:12 hour LD cycle

Wheel running activity of *Opa1*$^{+/Q285STOP}$ mice and littermate wildtype controls was continuously monitored during a 12:12 h LD cycle (see section 2.2). Activity levels (black bars) are plotted against time on an actogram with each horizontal line corresponding to one day (Figure 3.1). During exposure to a 12:12 LD cycle *Opa1*$^{+/Q285STOP}$ mice displayed a daily rhythm in behaviour confining their wheel running activity to the dark phase, typical of nocturnal species. The onset and offset of locomotor activity approximately coincided with the onset of night and day respectively. The time of activity onset, the time of activity offset and the length of the active phase were calculated for all mice for 7 consecutive days in LD (Table 1). There were no significant differences between heterozygous mice and wildtype controls for any of the parameters measured.

Wheel running activity counts were also quantified in the normal LD cycle (Table 3.1). Total activity (average number of wheel revolutions per day) was slightly higher in *Opa1*$^{+/Q285STOP}$ animals compared to the wild type controls but this difference was not significant ($p = 0.60$,

unpaired Student's t test). There were also no significant differences between genotypes in the activity levels during the light phase or dark phase of the LD cycle.

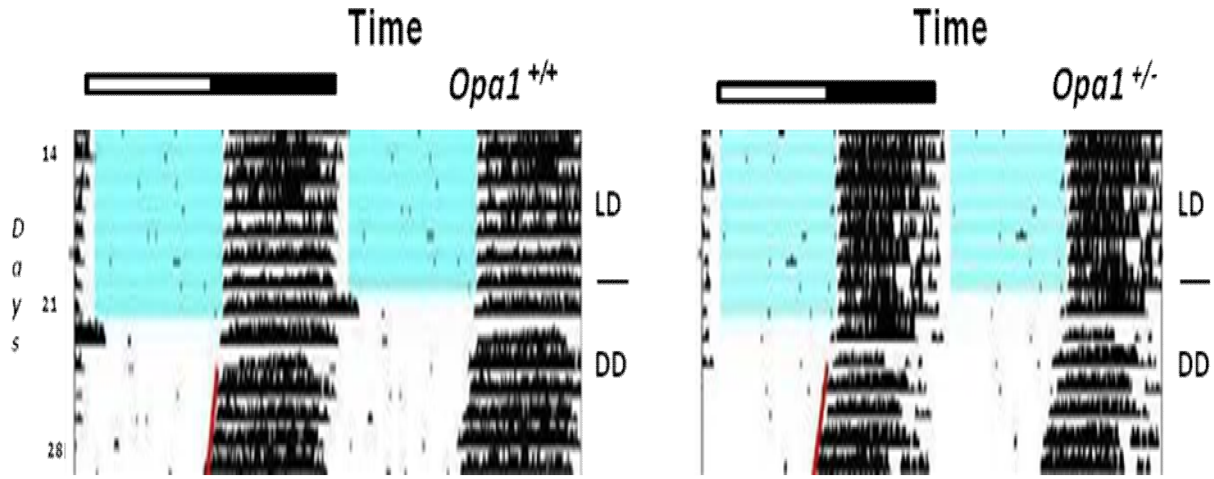

Figure 3.1 Circadian behaviour in *Opa1*$^{+/+}$ and *Opa1*$^{+/Q285STOP}$ mice. Representative double plotted actograms from an *Opa1*$^{+/+}$ (left) and *Opa1*$^{+/Q285STOP}$ (right) mouse. The animals were exposed to 7 days of a normal 12:12 hr LD cycle and then released into constant darkness for 7 days. Each horizontal line corresponds to one day and the black vertical bars represent the number of wheel revolutions. The shaded areas represent light exposure in 12:12 hr LD cycle. The white and black bar at the top refers to rest and activity respectively.

Parameter	Condition	Opa1 $^{+/+}$	Opa1 $^{+/-}$	*p* value
Period (hr)	LD	23.98±0.01	23.99±0.01	0.44
Total activity (wheel rev.)	LD	14549±3982	17244±2717	0.58
Activity during light phase (wheel rev.)	LD	907±280	849±263	0.88
Activity during dark phase (wheel rev.)	LD	13642±3800	16395±2756	0.56
Length of active phase (hr)	LD	10.32±0.44	10.04±0.88	0.80
Average Zeitgeber time of activity onset(hr)	LD	14.36±0.2	13.45±0.86	0.34
Average Zeitgeber time of activity offset(hr)	LD	24.8±0.4	23.3±0.57	0.78

Table 3.1 Quantification of wheel running activity from *Opa1*$^{+/+}$ and *Opa1*$^{+/Q285STOP}$ mice in LD. Table showing average period (τ), total activity levels, activity levels during light and dark phase, length of active phase, and onset and offset of the activity rhythm in LD. There were no significant differences between genotypes (unpaired students t-test; *p* values are shown). All data represent mean ± SEM (n = 6 and 7 for *Opa1*$^{+/+}$ and *Opa1*$^{+/Q285STOP}$ respectively).

The period (τ) of the rhythm in LD was calculated by use of chi^2 periodogram analysis (Clocklab) over 7 consecutive days. An almost identical τ was observed in *Opa1*$^{+/+}$ and *Opa1*$^{+/Q285STOP}$ mice at ~24 hrs (p = 0.44, unpaired Student's t test) (Table 3.1).

When *Opa1* mice were released and kept in constant darkness (DD), they continued to exhibit a rhythmic pattern of activity but with a shorter period (Table 3.2). The period length in DD was almost identical between genotypes at 23.7 hr (p = 0.97). On the first day in DD, the onset of activity was coincident with the previous onset of the dark phase suggesting the animals were entrained to the light cycle (Figure 3.1) rather than a demonstration of masking behaviour.

We calculated the time of the onset and offset of activity, the length of the active phase, total activity levels and activity during the subjective day and subjective night phases for *Opa1*$^{+/+}$ mice and *Opa1*$^{+/Q285STOP}$ mice for 7 consecutive days in DD (ignoring the first 3 days after entering constant dark conditions). We found no significant differences in any of these parameters between genotypes (Table 3.2).

Parameter	Condition	Opa1 $^{+/+}$	Opa1 $^{+/-}$	*p* value
Period (hr)	DD	23.69±0.05	23.68±0.05	0.97
Total activity (wheel rev.)	DD	14727±4120	17323±2304	0.58
Activity during subjective day phase (wheel rev.)	DD	1003±386	962±331	0.94
Activity during subjective night phase (wheel rev.)	DD	13724±3909	16361±2300	0.56
Length of active phase (hr)	DD	9.15±0.65	9.33±0.65	0.85
Average Zeitgeber time of activity onset(hr)	DD	13.87±0.97	13 ±0.42	0.43
Average Zeitgeber time of activity offset(hr)	DD	22.7±0.97	22.3±0.6	0.75

Table 3.2 Quantification of wheel running activity from *Opa1*$^{+/+}$ and *Opa1*$^{+/Q285STOP}$ mice in DD. Table showing average period (τ), total activity levels, activity levels during the subjective day and subjective night phases, length of active phase and onset and offset of the activity rhythm in DD. There were no significant differences between genotypes for each parameter (unpaired students t-test; *p* values are shown). All data represent means ± SEM (n = 6 and 7 for *Opa1*$^{+/+}$ and *Opa1*$^{+/Q285STOP}$ respectively).

3.2 *Opa1*$^{+/Q285STOP}$ mice display a normal negative masking response.

The suppressing influence of bright light at night on the activity of nocturnal rodents is called negative masking (Mrosovsky, 1999). The assessment of this phenomenon in *Opa1*$^{+/Q285STOP}$ and *Opa1*$^{+/+}$ mice was performed by administering a 3 hr 200 lux light pulse two hours after lights off (ZT 14; see section 2.2) (Mrosovsky and Hattar, 2003). The wheel running activity counts (10 minute binned data) on the day of the masking pulse were normalised to baseline data obtained in the same period the previous night (Figure 3.2A). *Opa1*$^{+/Q285STOP}$ and *Opa1*$^{+/+}$ mice stopped running in an acute way for the majority of the first hour of the light pulse. Activity levels gradually increased in the subsequent 2 hours in both genotypes (Mrosovsky and Hattar, 2003). ANOVA analysis found no significant effect of genotype on the baseline corrected wheel running data ($p = 0.468$).

An hourly breakdown of the total activity during the masking pulse is presented in Figure 3.2B. For the first hour of the pulse, the average wheel counts were very low and similar for both genotypes. For the second and third hour of light pulse administration, all mice (*Opa1*$^{+/+}$ and *Opa1*$^{+/Q285STOP)}$ become more active compared to the first hour but still retained low levels of activity. This would suggest the masking response was maintained for the whole period of light exposure. This is consistent to previous findings of Mrosovsky and Hattar, (2003). Two–way ANOVA analysis using activity in each hour of the light pulse and genotype as factors revealed a significant effect of the hour of light pulse ($p < 0.005$) but no significant effect of genotype ($p = 0.143$) on wheel running activity counts during the masking pulse.

Taking all these results together, we conclude that the negative masking response is present for both heterozygote mutants and wildtype controls at the illumination level of 200 lux.

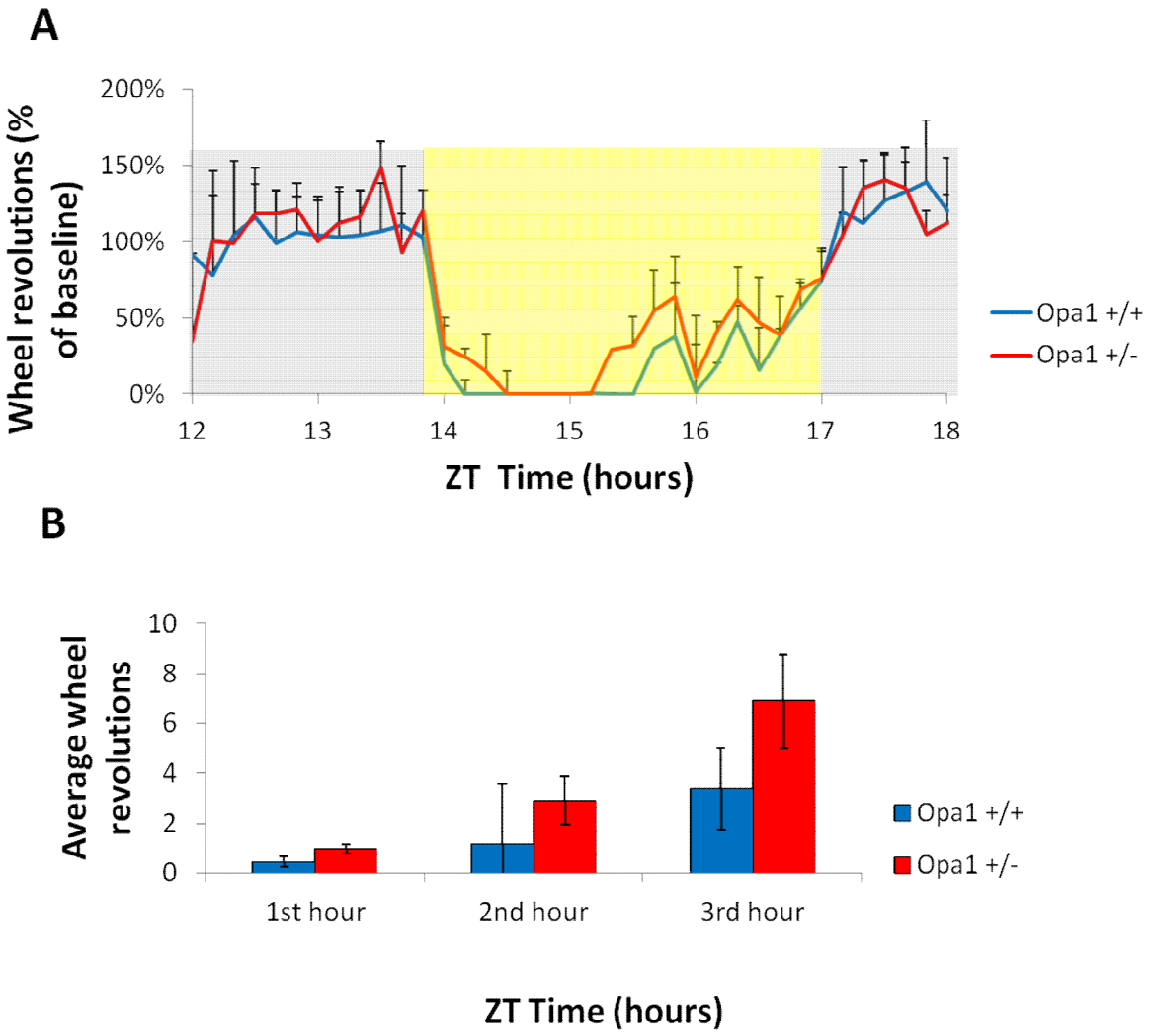

Figure 3.2: Masking response in *Opa1*$^{+/+}$ and *Opa1*$^{+/Q285STOP}$ mice. A. Average wheel running revolutions on the night of the light pulse are plotted relative to the baseline levels (the night before the pulse). 0% indicates complete suppression and 100% no change compared to baseline activity. A 200 lux white light pulse (yellow background) was applied for 3 hours (ZT 14-17) during the dark phase of the LD cycle (gray background). The masking pulse completely suppressed activity in both genotypes immediately after lights ON. ANOVA analysis found no significant effect of genotype on the baseline corrected activity levels ($p = 0.468$) **B**. Bar graph showing hourly breakdown of activity during masking pulse. A 2-way ANOVA using activity in each hour of light pulse and genotype as factors found a significant effect of hour of light pulse ($p < 0.005$) but no significant effect of genotype

(p = 0.143) and no interaction between genotype and light pulse hour (p = 0.359). All data represent means ± SEM, (n = 6 and 7 for *Opa1*$^{+/+}$ and *Opa1*$^{+/Q285STOP}$ respectively).

3.3 Phase shift responses are normal in *Opa1*$^{+/Q285STOP}$ mice

We tested whether there were differences in the phase-shifting response of the free-running clock to brief light pulses of different wavelengths between *Opa1*$^{+/+}$ and *Opa1*$^{+/Q285STOP}$ mice (see section 2.2). A 15 minute 525 nm light pulse was presented at CT16 to animals maintained in constant darkness (Fig 3.3 A, white arrowhead). The light pulse provoked a phase delay in the onset of activity in both wildtype and heterozygous mice of ~ 40 and 26 min respectively (i.e. negative values). Although the phase-shift magnitude was lower in *Opa1*$^{+/Q285STOP}$ mice than in wildtype controls, this difference was not statistically significant (two-way ANOVA; Fig 3.3B). A 15 minute 480 nm light pulse at CT16 (Fig 3.9A, black arrow) also induced a delay in the onset of activity of approximately 35 min for *Opa1*$^{+/+}$ mice and 20 min for *Opa1*$^{+/Q285STOP}$ mice. This difference again was not statistically significant (two-way ANOVA; Fig 3.3B). Mice in a sham control condition, which didn't received a light pulse but were handled in the same way (Fig 3.3A, white arrow), showed no significant phase shift with no significant differences between genotypes (two-way ANOVA; Fig 3.3B).

Further statistical analysis was performed by way of a two-way ANOVA with genotype and wavelength as factors. There was no significant effect of wavelength ($F(1, 22) = 0.203$, $p = 0.657$) or genotype ($F(1, 22) = 1.998$, $p = 0.171$) on the phase shift response. The interaction of genotype and wavelength was also not significant ($F(1, 22) = 0.013$, $p = 0.909$).

To determine if the phase shift pulses had an effect on the period length, the average τ was calculated (for 7 consecutive days) in DD, following the administration of the 525 nm light pulse, after the 480 nm light pulse, and after the dark sham pulse control (Table 3.3). In all cases there were no significant differences in the endogenous period lengths between genotypes (p values and statistical analysis in table; one-way ANOVA).

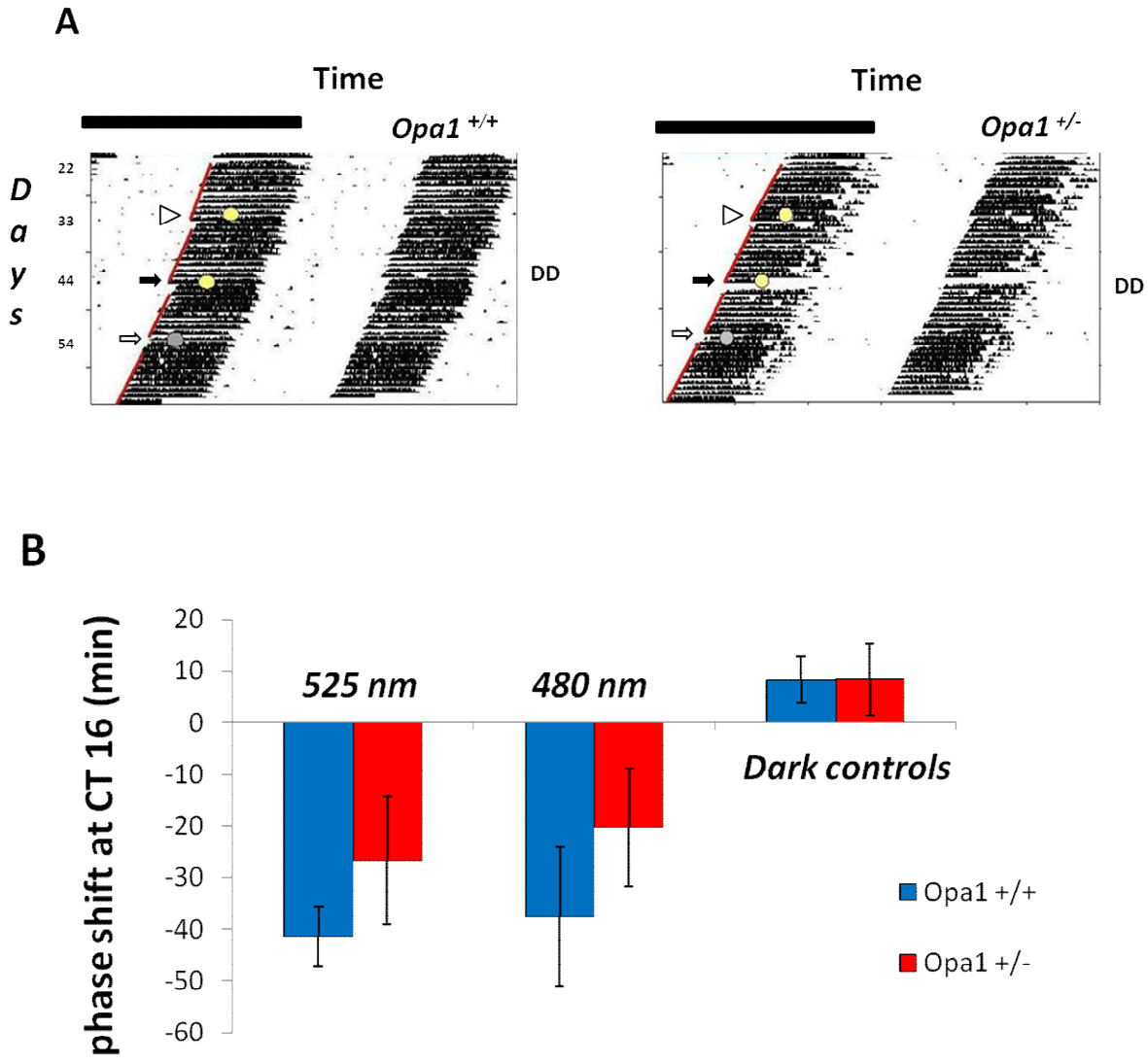

Figure 3.3: Phase shift behaviour in *Opa1*$^{+/+}$ and *Opa1*$^{+/Q285STOP}$ mice. A. Representative double plotted actograms from *Opa1*$^{+/+}$ (right) and *Opa1*$^{+/Q285STOP}$ (left) mice in DD conditions. Animals were exposed to light pulses every ~15 days. Photon matched light pulses at 525 nm (white arrowhead) or 480 nm (black arrow; 10.397 $\times 10^{10}$ photons/cm^2/s) were applied at CT16. Animals were also exposed to a dark sham condition (white arrow). **B.** The size of the phase shift responses were quantified and are plotted for the 525 nm, 480 nm and sham conditions (n = 6 and 7 for *Opa1*$^{+/+}$ and *Opa1*$^{+/Q285STOP}$ respectively). A two-way ANOVA with genotype and wavelength as factors was performed. There was no significant effect of wavelength ($F(1, 22) = 0.203$, $p = 0.657$) or genotype ($F(1, 22) = 1.998$, $p = 0.171$) and the interaction of genotype and wavelength was not significant ($F(1, 22) = 0.013$, $p = 0.909$).

Parameter	Condition	Opa1 $^{+/+}$	Opa1 $^{+/-}$	*p* value
Period (hr)	Before light pulse (525 nm)	23.686±0.05	23.685±0.05	0.30
	Before light pulse (480 nm)	23.64±0.08	23.63±0.08	0.77
	Before sham pulse	23.6±0.095	23.63±0.06	0.86
	After sham pulse	23.53±0.098	23.54±0.091	0.4

Table 3.3 Period length of *Opa1*$^{+/Q285STOP}$ and *Opa1*$^{+/+}$ mice kept in constant darkness before application of phase shift pulses. Average period lengths are shown over a period of 7 consecutive days before the light pulse at 525 nm, before the light pulse at 480 nm, before the sham pulse and after the sham pulse. All data represent mean ± SEM (n = 6 and 7 for *Opa1*$^{+/+}$ and *Opa1*$^{+/Q285STOP}$ respectively). There were no significant differences between genotypes. (One-way ANOVA, *p* values are shown).

3.4 The induction of sleep by acute light is preserved in *Opa1*$^{+/Q285STOP}$ mice

Acute light exposure at night promotes sleep in nocturnal animals. This direct photic regulation of sleep in mice is mainly dependent on the melanopsin-based pRGC system (Altimus et al., 2008, Lupi et al., 2008). To assess the effects of acute light on sleep we used videotracking to assess immobility-defined sleep (Fisher et al., 2012). Sleep was defined as a period of immobility greater than 40 sec (see section 2.3).

Baseline readings were determined by measuring the immobility-defined sleep parameter in a normal 12:12 hr LD cycle (i.e. ZT0 to ZT24; data binned into 1 hour blocks; Figure 3.4A*)* *Opa1*$^{+/Q285STOP}$ mice similar to their littermate wild-type controls, confined their sleep to the light portion of the day whereas they were less immobile during the dark period of the LD 12:12 cycle, as expected. To confirm the involvement of the circadian oscillator in the day/night sleep pattern we assessed immobility in conditions of constant darkness (Figure 3.4 B). The immobility defined sleep parameter was quantified in one 24 hr period of constant darkness (i.e. lights remained OFF from the end of the previous night phase). Regardless of the continuous dark exposure *Opa1*$^{+/Q285STOP}$ mice similar to their littermate wild-type controls were largely immobile during the first 12 hour period, whereas they were less immobile during the second 12 hour period.

To determine the modulation of sleep behaviour by acute light exposure in *Opa1* mutant and control mice, we exposed them to a 1-h white light pulse (200 lux) during the dark phase of the 24-h LD cycle starting 2h after “lights OFF” (Zeitgeber time (ZT) 14) when the homeostatic drive for sleep is low. After light administration both genotypes became more immobile for the time of the exposure (Figure 3.4 D, ZT14-15 white

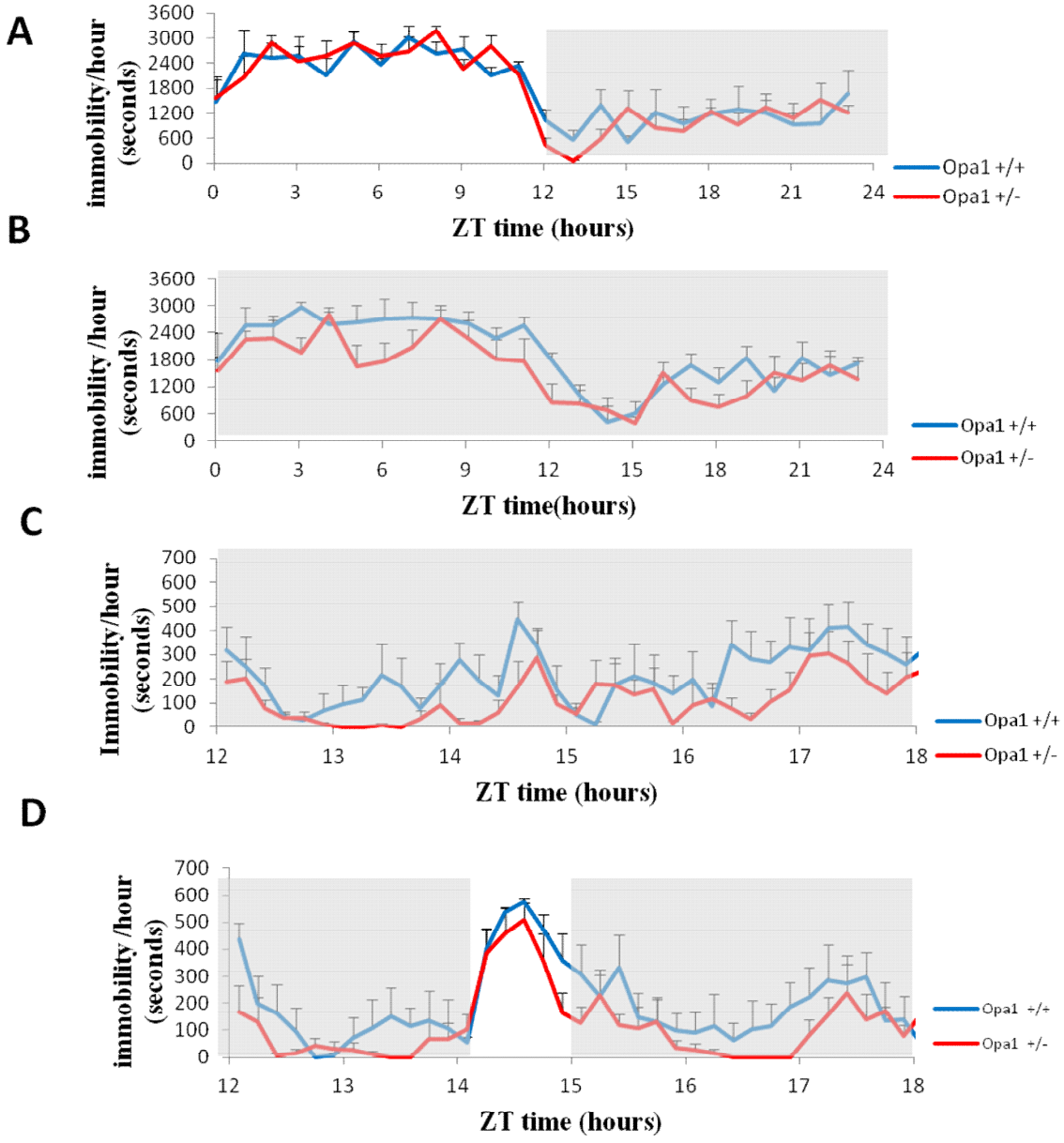

Figure 3.4:Immobility-defined sleep recordings. ***A****:* The time mice spent immobile (in seconds) is plotted against the daily time (zeitgeber time (ZT); 1 hour resolution). White background indicates the light portion and the gray background the dark portion of the 24-hr LD cycle. ***B***: Immobility –defined sleep recordings during one 24 hour cycle of complete darkness (1 hour resolution). ***C****:* Immobility – defined sleep recordings the previous night of the day of light pulse (baseline) where mice were in darkness (gray background, ZT 12-18; 10 min resolution) ***D*****:** The administration of the 1-h light pulse (white background) at ZT 14 during the dark phase (gray background) induced an increase in immobility in both genotypes (10 min resolution). Two-way ANOVA with genotype and time as factors was performed. There was significant effect of genotype ($F(1, 9) = 6.115$, $p = 0.015$) and time

(F (1, 9) = 2.51, p = 0.007) on immobility. The interaction of genotype and time was not significant (F (1, 9) = 1.172, p = 0.315).

background) compared to the previous night where the mice were kept in darkness. (Figure 3.4 C, ZT 14-15 gray background). Statistical analysis was performed by way of a two-way ANOVA with genotype and time as factors. There was significant effect of genotype ($F(1, 9) = 6.115$, $p = 0.015$) and time ($F(1, 9) = 2.51$, $p = 0.007$) on immobility. The interaction of genotype and time was not significant ($F(1, 9) = 1.172$, $p = 0.315$).

Therefore acute light exposure induced sleep in both wildtype and *Opa1* mutant mice as measured by an increase in immobility.

We quantified the amount of time it takes to fall asleep after the lights have been turned off, particularly the time to the first 2 minutes of continuous immobility ("sleep latency"). There was no significant difference in the sleep latency between genotypes ($p = 0.8$ unpaired Student's t-test) (Figure 3.5 A). In *Opa1* mutant mice, white light induced sleep within 15 min and for wildtype controls animals sleep induction was observed within 16 min. To determine whether $Opa1^{+/Q285STOP}$ mice sustained the inhibitory response to light exposure we calculated the total sleep during the light pulse for both genotypes. We found that the total time spent asleep was not significantly different between wild type and mutant mice ($p = 0.24$**,** unpaired Student's t-test) (Figure 3.5 B).

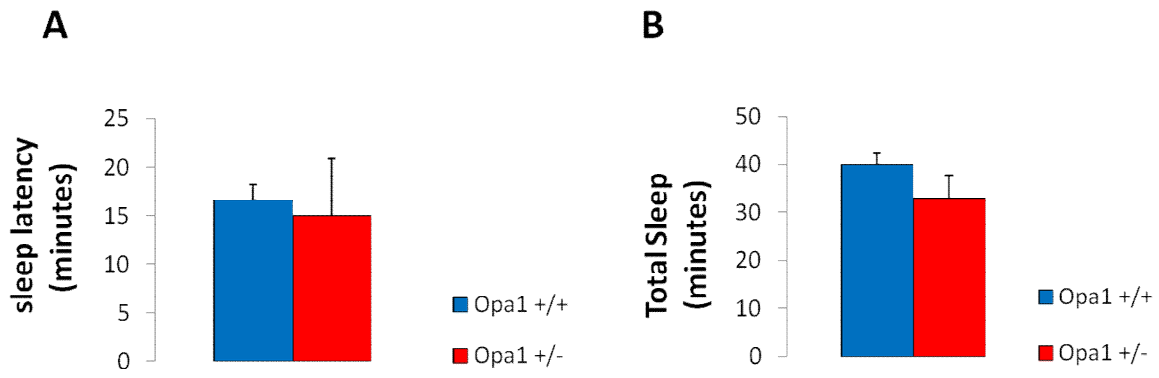

Figure 3.5: Sleep latency and total sleep during acute light exposure at night.

A. Quantification of sleep latency for *Opa1*$^{+/Q285STOP}$ and *Opa1*$^{+/+}$ mice (defined as the time between the beginning of the light exposure and the first 2 min of continuous immobility *(p* = 0.8, unpaired Student's t-test). **B**. Quantification of total sleep amount during light exposure (ZT14-15) in the two genotypes *(p* = 0. 24, unpaired Student's t-test). All data represent means ± SEM (n = 5 and 6 for *Opa1*$^{+/+}$ and *Opa1*$^{+/Q285STOP}$ mice respectively).

3.5 Melanopsin expression in *Opa1*$^{+/+}$ and *Opa1*$^{+/Q285STOP}$ mice

3.5.1 *Opa1* defect has no effect on number of melanopsin-expressing RGCs.

We used immunohistochemistry to visualize the cell bodies and processes of melanopsin – positive RGCs with an antibody against melanopsin (see section 2.4). Images of melanopsin expressing RGCs in sections of flatmounted retinas were captured with a fluorescent microscope. A composite image of the retinae was generated with Open Lab software (Figure 3.6). Melanopsin –expressing cells were observed throughout the retina from *Opa1*$^{+/+}$ and *Opa1*$^{+/Q285STOP}$ mice, in both peripheral and central regions. The number of melanopsin cells was counted using Adobe Photoshop software (Figure 3.7).

Our results revealed that *Opa1*$^{+/Q285STOP}$ mice displayed a slight reduction in the total number of pRGCs relative to wildtype controls but this decrease was not statistically significant (n = 3; $p < 0.05$, unpaired students t-test ; Figure 3.8A). Comparison of cell counts from the central retina also revealed no difference in the number of pRGCs in heterozygous and wildtype retinas (Figure 3.8B). Additionally in the periphery of the retina the number of pRGCs was identical in both genotypes (Figure 3.8C). The results suggest there was no significant degeneration in melanopsin positive cells in *Opa1* mutant mice despite the *Opa1* defect.

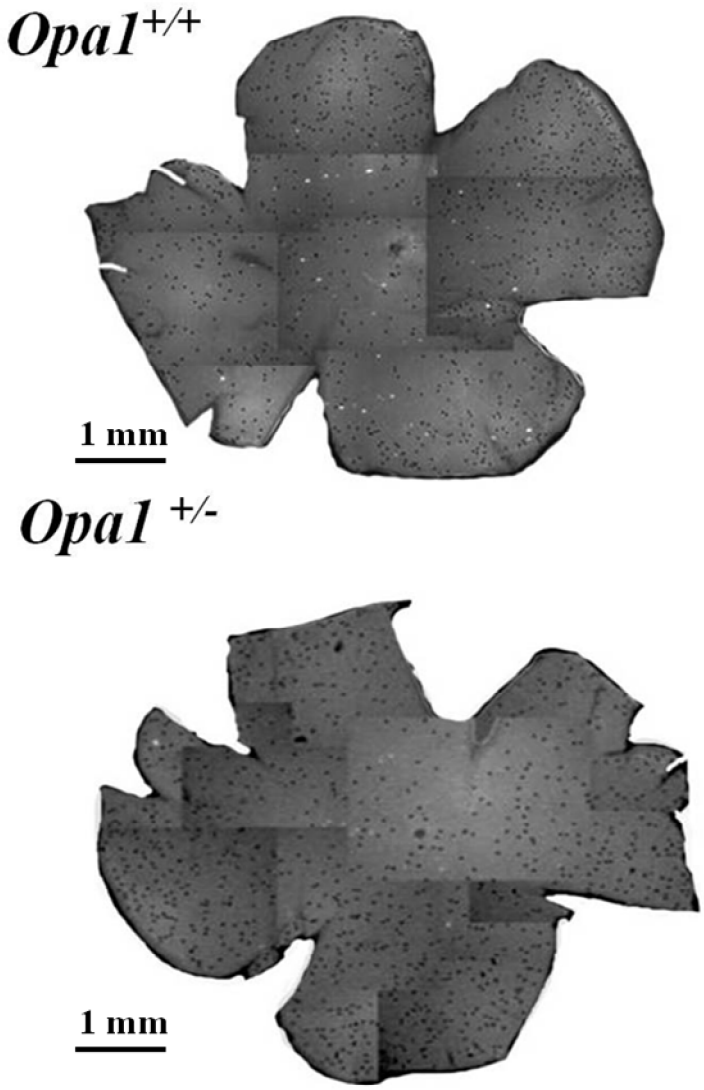

Figure 3.6: Melanopsin expression in the retina.

Composite images showing a typical flat-mounted retina from an *Opa1*$^{+/+}$ and *Opa1*$^{+/Q285STOP}$ mouse immunostained for melanopsin. Polyclonal rabbit melanopsin antibody (PAS8331) (Pires et al., 2009) was used. Images from each quadrant of the retina were taken with a fluorescent microscope and a composite image of the whole retina was produced with OpenLab software. Scale bar 1 mm.

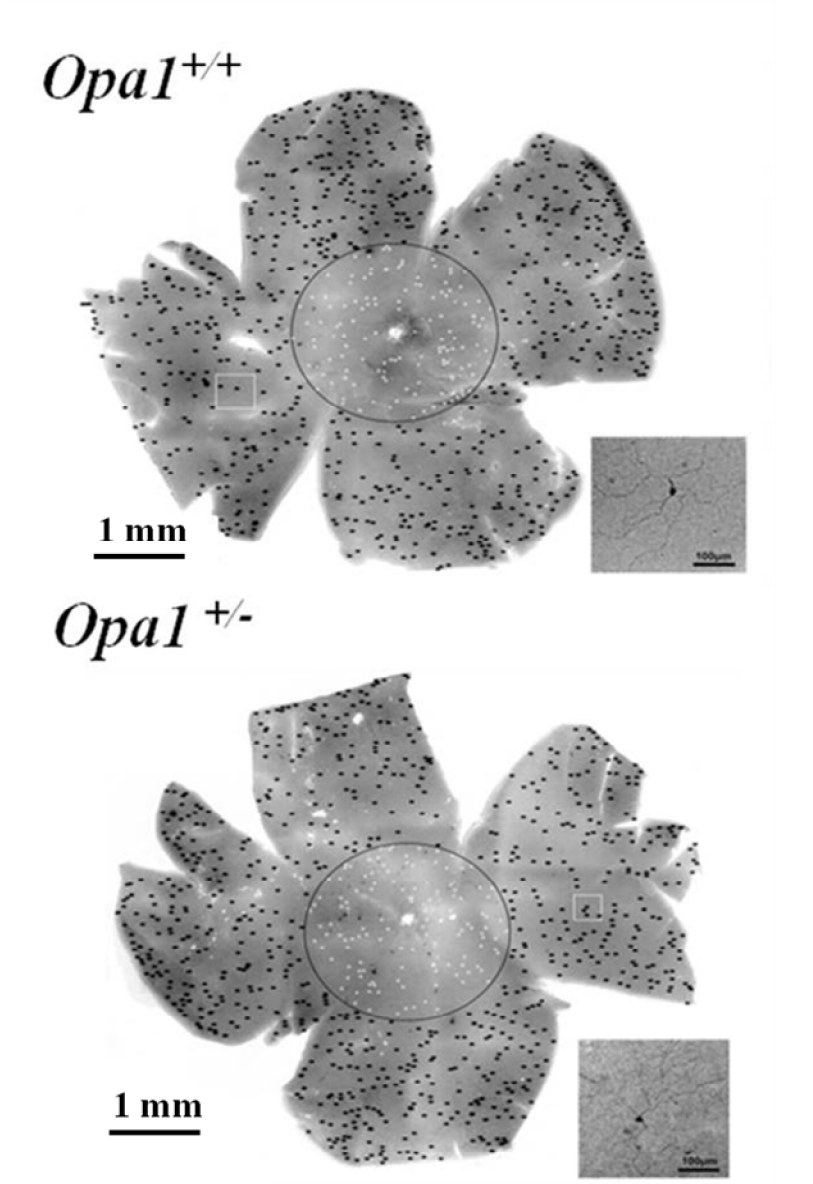

Figure 3.7: Quantificantion of melanopsin cell numbers. Overall distribution of melanopsin-positive RGCs in a typical flatmounted retina from an *Opa1*$^{+/+}$ and an *Opa1*$^{+/Q285STOP}$ mouse. Polyclonal rabbit melanopsin antibody (PAS8331) (Pires et al., 2009) was used. Each cell body is represented by a black (in periphery) and white (in the centre) dot. Insert represents a high power magnification of a single cell in the flatmount. Scale bar of the inset image 100 μm and of flatmount image 1mm.

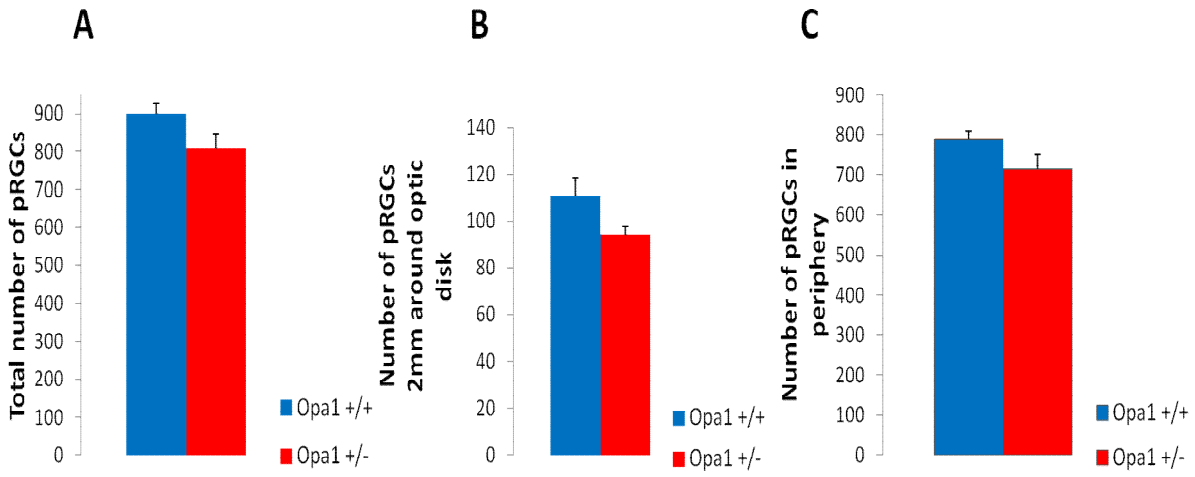

Figure 3.8. Quantification of melanopsin-expressing cell numbers in *Opa1*$^{+/+}$ and *Opa1*$^{+/Q285STOP}$ retina.

A. Total number of melanopsin expressing cells in the retina. **B**. Number of melanopsin expressing cells within 2mm of the optic disc. **C**. Number of melanopsin expressing cells in the peripheral retina. No significant differences were observed between genotypes (Total: p = 0.13; Central: p = 0.14; Peripheral: p = 0.16; unpaired student's t-test). All data represent mean ± SEM.

3.5.2 *Opa1* defect has no effect on melanopsin-expressing RGC morphology

To assess melanopsin cell morphology, stacked confocal images (from the inner plexiform layer to ganglion cell layer) were taken in central (2mm from optic disc; Figure 3.9) and peripheral (Figure 3.10) regions. In the examples shown, each confocal stack covered a retinal area of 325.75μm x 325.75μm. The depth of confocal stack in central and peripheral regions was 7.07 μm and 11.31 μm respectively. In both the central and peripheral retina, we observed melanopsin cells stratifying in the OFF and ON sublaminas of the IPL in wildtype and mutant mice. No obvious differences in stratification patterns were observed between genotypes.

Quantification of the mean soma diameter of pRGCs revealed similar cell sizes in *Opa1*$^{+/+}$ and *Opa1*$^{+/Q285STOP}$ mice of approximately 14 μm (Figure 3.12) .We also quantified the number of primary dendrites just emerging from the cell body and the mean axon diameter (at 3μm from the cell body). These parameters were almost identical between genotypes (Fig 3.11 and 3.12).

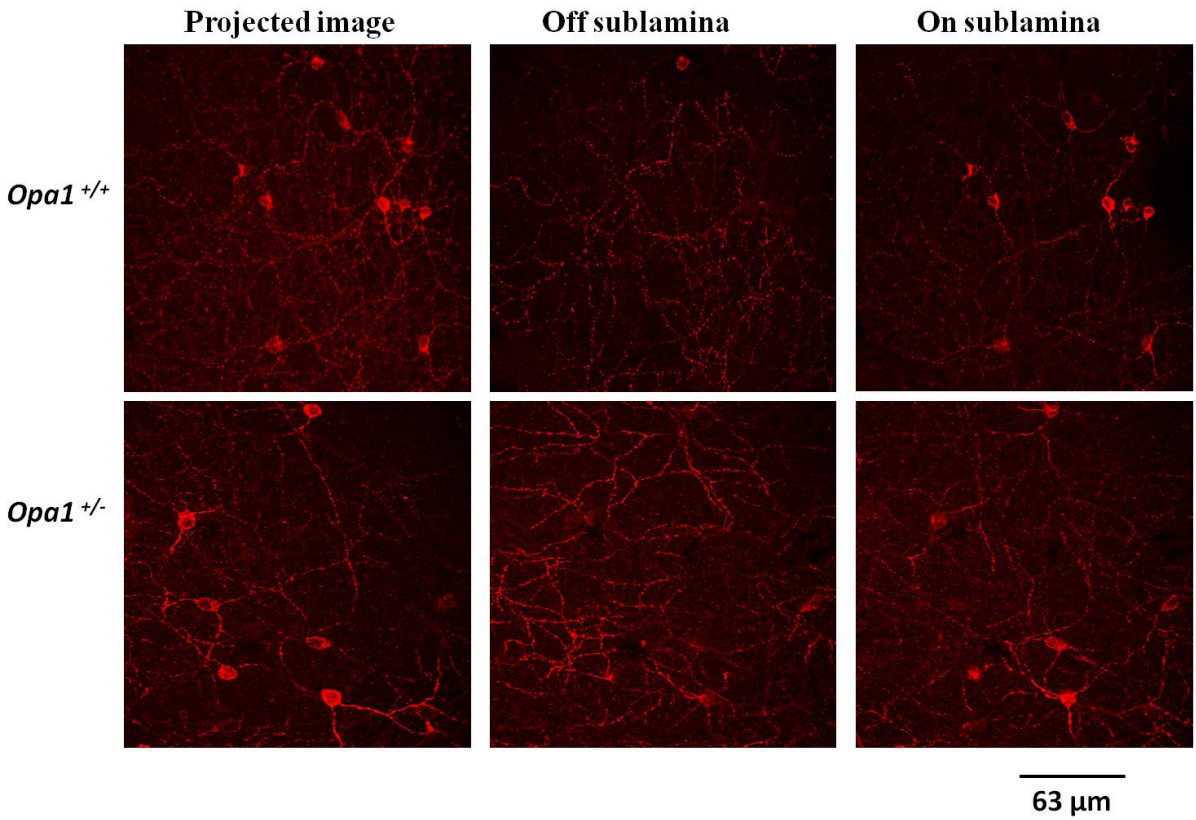

Figure 3.9: Confocal images of melanopsin expressing RGCs within 2 mm of the optic disc. Representative confocal images of melanopsin-immunostained cells from *Opa1*$^{+/+}$ and *Opa1*$^{+/Q285STOP}$ retinae. Polyclonal rabbit melanopsin antibody (PAS8331) (Pires et al., 2009) was used for immunostaining. A projected image of a confocal stack (from the inner plexiform layer to the ganglion cell layer) is shown for each genotype. An image at the level of sublamina a (Off sublamina) and an image at the level of sublamina b (On sublamina) from the same image stacks is also shown. Each confocal stack covered a retinal area of 325.75µm x 325.75µm and the depth was 7.07 µm.

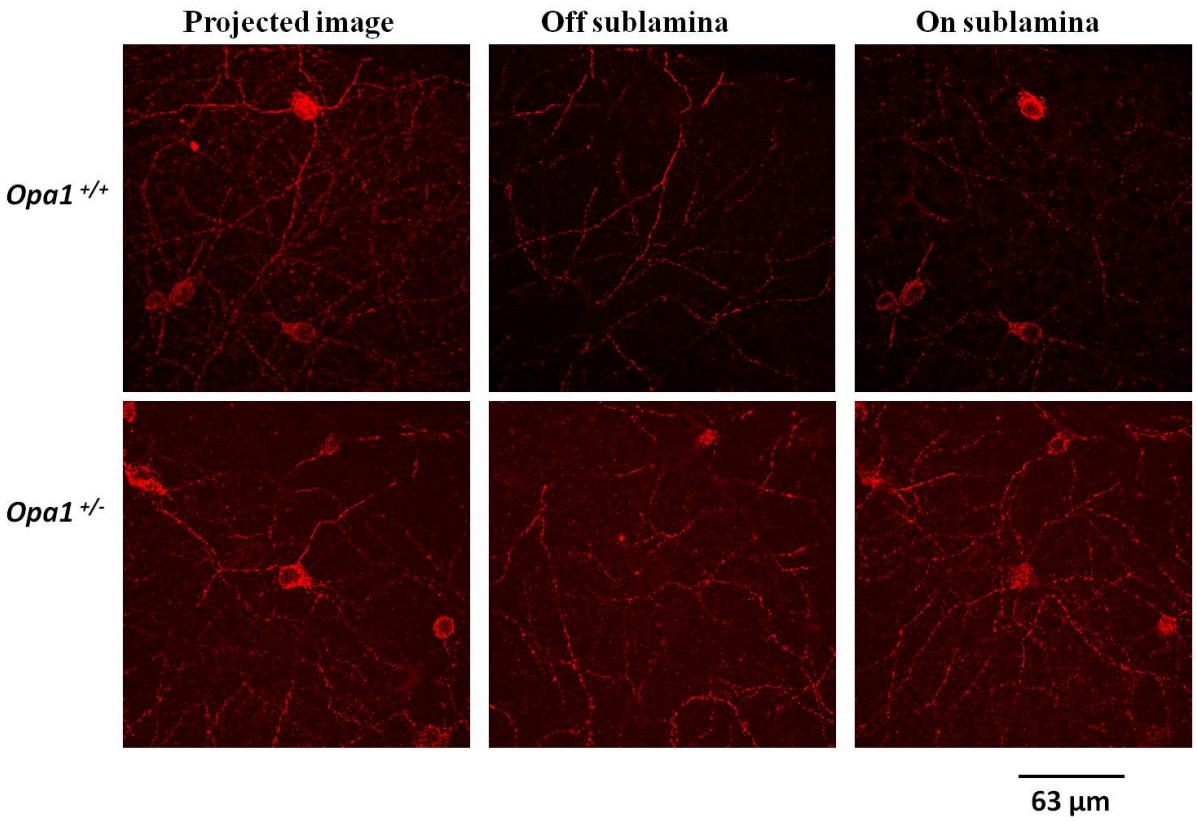

Figure 3.10: Confocal images of melanopsin expressing RGCs in the peripheral retina. Representative confocal images of melanopsin-immunostained cells from *Opa1*$^{+/+}$ and *Opa1*$^{+/Q285STOP}$ retinae. Polyclonal rabbit melanopsin antibody (PAS8331) (Pires et al., 2009) was used for immunostaining. A projected image of a confocal stack (from the inner plexiform layer to the ganglion cell layer) is shown for each genotype. An image at the level of sublamina a (Off sublamina) and an image at the level of sublamina b (On sublamina) from the same image stacks is also shown. Each confocal stack covered a retinal area of 325.75µm x 325.75µm and the depth was 11.31 µm.

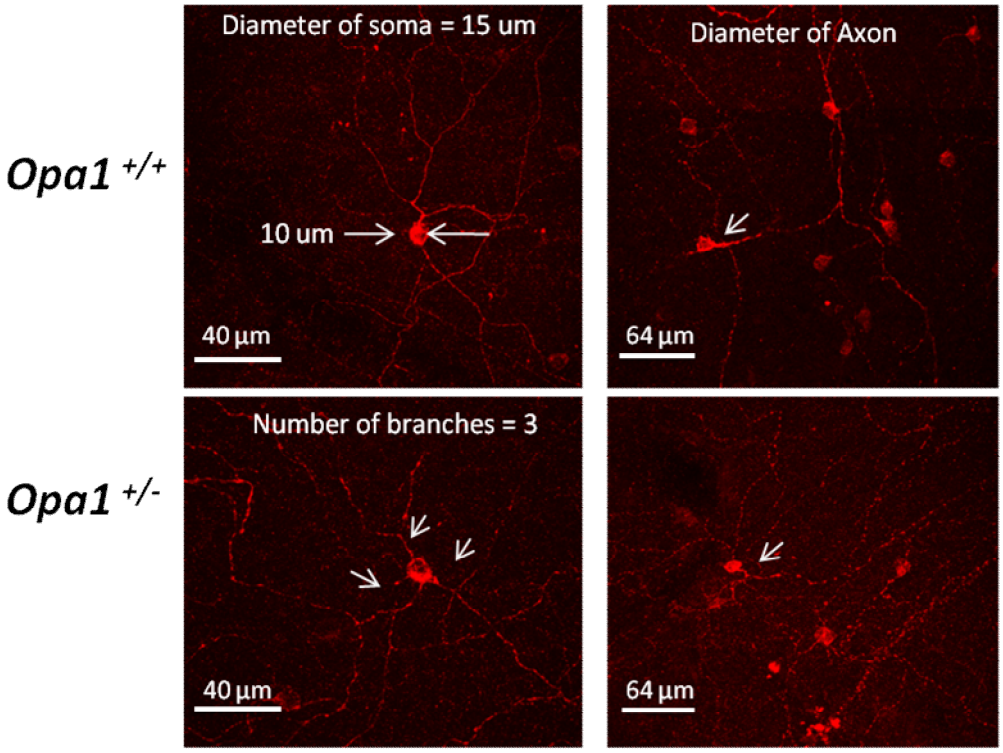

Figure 3.11: Melanopsin cell morphology in *Opa1*$^{+/+}$ and *Opa1*$^{+/Q285STOP}$ retina. Representative confocal images of melanopsin-immunostained cells from *Opa1*$^{+/+}$ and *Opa1*$^{+/Q285STOP}$ retinas showing the parameters. which were measured in terms of morphology assessment. Polyclonal rabbit melanopsin antibody (PAS8331) (Pires et al., 2009) was used for immunostaining. The diameter of soma, the number of primary dendrites emerging from the soma and the mean diameter of axon (3µm distance from soma) were determined for each genotype.

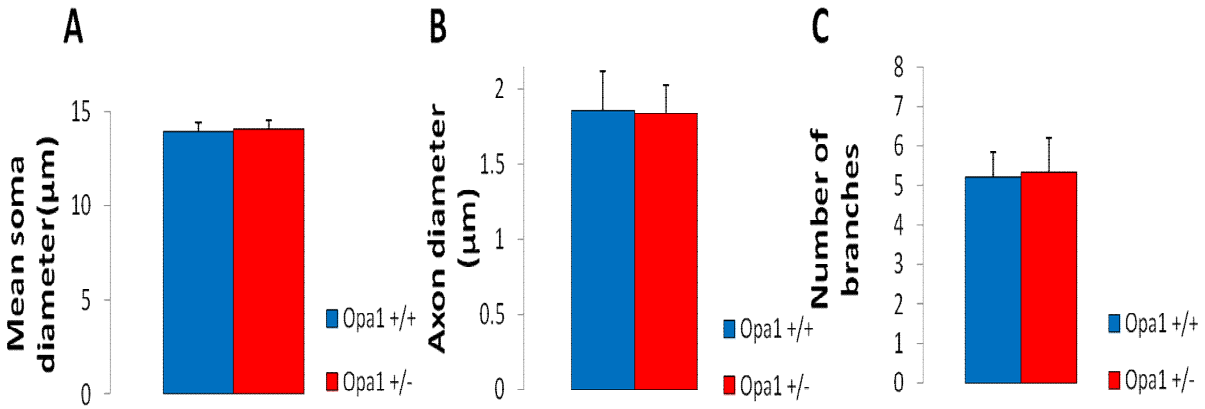

Figure 3.12 Quantification of melanopsin cell morphological parameters in *Opa1*$^{+/+}$ and *Opa1*$^{+/Q285STOP}$ retina. A. Average soma diameter (n = 30 for both genotypes) (p = 0.88) **B**. Average axon diameter in *Opa1*$^{+/+}$ and *Opa1*$^{+/Q285STOP}$ mouse retinae (n = 10 for both genotypes) (p = 0.94) and **C**. Average number of branches coming from cell body (n = 22 for both genotypes) (p = 0.96) .All data represent mean ± SEM, n represent the number of melanopsin positive cells, p = unpaired Student's test.

3.5.3 *Opa1* defect has no effect on melanopsin transcript levels

Real time qPCR was carried out to compare the relative expression levels of melanopsin transcripts in *Opa1*$^{+/+}$ (n = 5) and *Opa1*$^{+/Q285STOP}$ (n = 5) animals at 11-13 months of age (see section 2.5). No significant difference in melanopsin mRNA expression was found between genotypes. (p = 0.87)**.** RT qPCR was also carried out to quantify mRNA for retinal ganglion cell markers such as Brn3b and Thy1. During retinal ganglion cell differentiation, Brn3b is expressed first and plays an essential role in the survival of retina and Thy1.2 is critical for the normal retinal development. We also compared expression of rhodopsin as an outer retinal marker. All these genes were expressed in *Opa1* mutant mice with no significant difference to wildtype controls (p -values: rhodopsin expression p = 0. 33, Thy1.2 expression p = 0, 7, Brn3b expression p = 0. 52, unpaired Student's t-test). As a positive control, we assessed *Opa1* transcript levels. We detected an approximately 50 % reduction in expression in *Opa1*$^{+/Q285STOP}$ mice relative to wildtype controls (p = 0.003) This was predicted and has been previously reported by Davies et al., 2007 (Fig 3.13).

We also assessed melanopsin transcript levels in younger *Opa1*$^{+/+}$ (n = 5) and *Opa1*$^{+/Q285STOP}$ *(n = 5)* mice at 5 months of age in order to identify possible differences in melanopsin RNA expression at an early stage before the onset of visual symptoms. No significant differences in melanopsin expression were detected between genotypes (p = 0.9). The expression of the control retinal markers was also similar between heterozygous mice and wildtype controls (p values: rhodopsin expression p = 0.44, Thy1.2 expression p = 0.65, Brn3b expression p = 0.65; unpaired Student's t-test). Similar to *Opa1* mutant mice at 11-13 months, a reduction in *Opa1* transcript was observed by almost 50 % in the younger animals (p = 0.03; Fig 3.14).

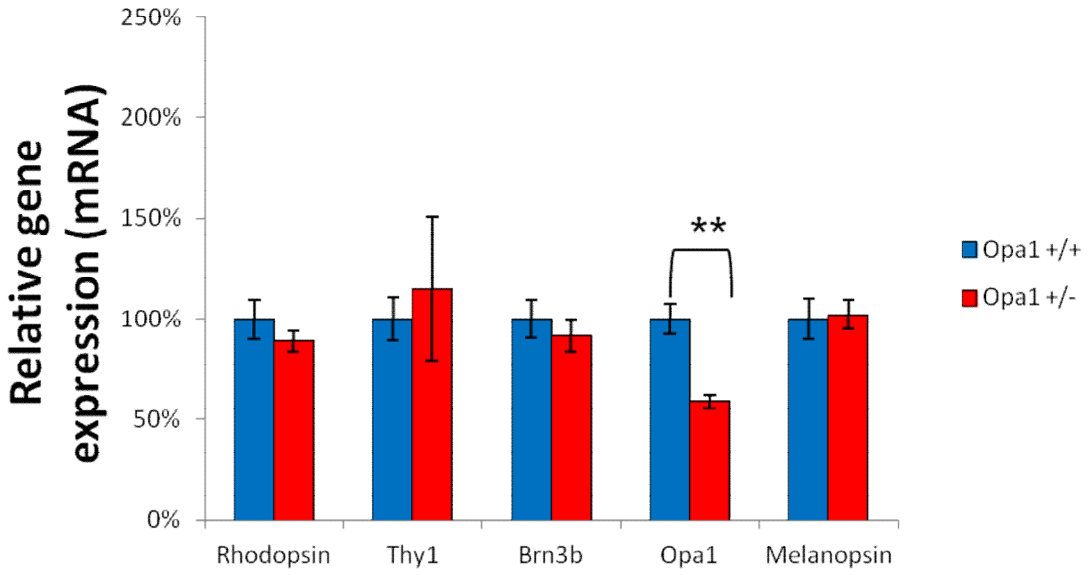

Figure 3.13 Relative quantification of *Rhodopsin, Thy1, Brn3b, Opa1* and Melanopsin in *Opa1*$^{+/+}$ and *Opa1*$^{+/Q285STOP}$ mice by real time quantitative PCR. The only gene that demonstrated significant differences between *Opa1*$^{+/+}$ (n = 5) and *Opa1*$^{+/Q285STOP}$ (n =5) retinae was Opa1. *p*-values: rhodopsin $p = 0.33$, Thy1.2 $p = 0.7$, Brn3b $p = 0.52$, *Opa1* $p = 0.003$, Melanopsin p = 0.87 (Asterisk indicate a statistically significant difference, ** $p < 0.01$, unpaired Student's t-test). All data represent mean ± SEM (n = 5 for both genotypes).

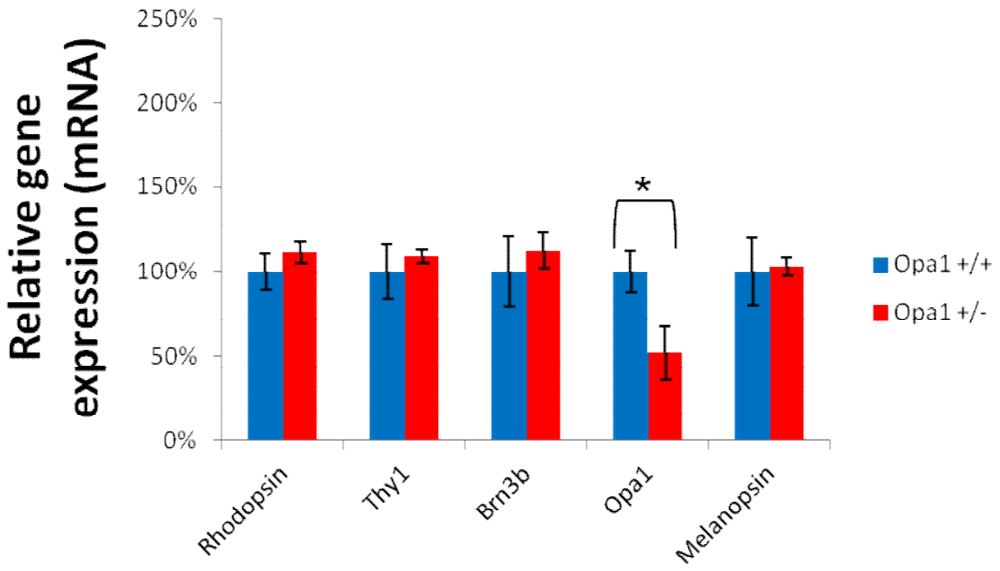

Figure 3.14 Relative quantification of *Rhodopsin, Thy1, Brn3b Opa1* and Melanopsin in *Opa1*$^{+/+}$ and *Opa1*$^{+/Q285STOP}$ mice (5 months old) by real time quantitative PCR. The only gene that demonstrated significant differences between *Opa1*$^{+/+}$ (n = 5) and *Opa1*$^{+/Q285STOP}$ (n =5) retinae was *Opa1*. *p*-values: rhodopsin $p = 0.44$, Thy1.2 $p = 0.65$, Brn3b $p = 0.65$, *Opa1* $p = 0.03$, Melanopsin $p = 0.9$. (Asterisk indicate a statistically significant difference, * $p < 0.05$, unpaired Student's t-test). All data represent mean ± SEM (n = 5 for both genotypes).

Finally we investigated whether there were significant differences in RNA expression of all tested genes between *Opa1* mutant mice > one year and 5 months old. Both the young and old samples were processed in the same way and run at the same time on the same qPCR plates. The only significant change was an increase in *Rhodopsin* transcript expression in *Opa1*$^{+/Q285STOP}$ mice of one year compared to younger animals (One-way ANOVA, p = 0.004).

Chapter 4

Discussion

We investigated non-image-forming visual behaviour in a mouse model of *OPA1* ADOA (*Opa1*^{Q285STOP} exon 8 mutation) with particular regard to photoentrainment, phase shift behaviour, negative masking response and sleep induction. This in turn would contribute towards a better understanding of how light induced circadian behaviours and sleep might be altered in patients with dominant optic atrophy. We also investigated whether or not the melanopsin ganglion cell population is preferentially affected or spared by the *Opa1* mutant phenotype. To the best of our knowledge this is the first report of an extensive functional assessment of light induced circadian/sleep behaviour in a mouse model of *OPA1* ADOA.

Autosomal dominant optic atrophy is caused by a defect in the *OPA1* gene and characterized by optic nerve degeneration and a variable loss of visual acuity. Mouse models of *OPA1* ADOA also display RGC and optic nerve abnormalities with associated visual deficits. Barnard et al., noted a significant reduction in the photopic negative response (PhNR) of the electroretinogram in *Opa1*$^{+/Q285STOP}$ animals at 1 year (Barnard et al., 2011). The PhNR is belived to reflect RGC function. This is the first description of a functional visual deficit detectable by ERG in mouse models of ADOA. A deficit in the VEP was also detected (Barnard et al., 2011). We have found that despite visual dysfunction, the photic regulation of circadian and sleep behaviours is unaffected in *Opa1* mutant mice. The melanopsin expressing RGCs which regulate these non-image-forming responses are also preserved.

Assessment of photentrainment in *Opa1* mutant and wildtype mice using wheel running activity monitoring found that both genotypes entrained to a normal light/dark cycle. Mice lacking melanopsin expressing RGCs demonstrate reduced entrainment to normal LD cycles (Guler et al., 2008, Hatori et al., 2008, Goz et al., 2008). This would suggest that functional output of the melanopsin expressing RGCs regulating photoentrainment is preserved in *Opa1* mutants. Further assessment of the circadian system can be probed using phase shift paradigms. Mice lacking melanopsin cells demonstrate a complete loss of phase shifting responses (Guler et al., 2008). We observed no difference between *Opa1* mutant and wildtype mice in phase shift responses to photon matched 480 nm and 525 nm pulses. The pulse at 480 nm was applied to maximally stimulate the melanopsin RGCs (λmax = 480 nm) and 525 nm to maximally stimulate the rod (λmax = 505nm) and medium wavelength MW-sensitive cones (λmax = 510nm) contributions to phase shift responses. No significant difference in the magnitude of the phase shift was found between genotypes at 480 nm or 525 nm. The data suggest preservation of melanopsin cell function and are suggestive of preservation of rod and cone pathway inputs to the melanopsin-expressing RGCs.

The suppressing influence of bright light at night is called negative masking (Mrosovsky, 1999). Mrosovsky and Hattar (2003) noted impaired masking responses to light in melanopsin–knockout mice and demonstated that melanopsin is important in maintaining masking responses over long periods. Mice lacking melanopsin cells demonstrate a complete loss of negative masking behavior (Hatori et al., 2008, Goz et al., 2008). *Opa1*$^{+/Q285STOP}$ mice similar to wild type controls refrained from running for the first hour of a 3 hour negative masking pulse suggesting that negative masking is preserved in *Opa1*$^{+/Q285STOP}$ mice. Activity levels increased in the subsequent hours mirroring published data in wildtype animals (Mrosovsky and Hattar, 2003). One study, by Davies et al. (2007) suggested that the masking

response is suppressed in *Opa1* mutant mice. These experiments were conducted on the same mouse model but the masking pulse data was not normalised to the baseline from the previous night. Therefore the difference observed by Davies et al. (2007) may reflect differences in baseline activity as we have also observed (but these differences were not significant).

A main further finding of our study is that acute light exposure induced sleep in *Opa1*$^{+/Q285STOP}$ mice and the time required for the immobility –defined sleep (sleep latency) was identical for both wild type and mutant mice. Moreover light not only induced sleep but sustained the response as all *Opa1* animals slept for the full period of light exposure. It is known that light promotes sleep in nocturnal animals and this direct photic regulation of sleep in mice is mainly dependent on melanopsin–based pRGC input (Lupi et al., 2008). (Altimus et al., 2008)) demonstrated also that mice lacking melanopsin cells do not demonstrate the acute-light induced sleep phenomenon.

The results from the quantification of melanopsin expressing RGCs in *Opa1* mutant mice revealed normal expression of melanopsin despite *Opa1* dysfunction. The number of melanopsin expressing RGCs was almost the same in both genotypes suggesting that there was no degeneration of these cells in *Opa1*$^{+/Q285STOP}$ mice of one year. qPCR was carried out to compare the relative expression levels of melanopsin transcripts in *Opa1*$^{+/+}$ and *Opa1*$^{+/Q285STOP}$ animals and the data further confirmed the normal expression of melanopsin in *Opa1* mouse model of ADOA. There were also no differences in melanopsin cell morphology including soma size, axon diameter or number of primary dendrites. Therefore we propose the melanopsin cells are preserved in *Opa1* mutant mice.

According to Williams et al. (2010) (Williams et al., 2010) the RGC population of *Opa1* animals does not demonstrate cell loss but exhibits a progressive dendropathy from 10 months before the onset of visual loss. There is specifically dendritic pruning localised to sublamina b (ON centre-RGCs) of the IPL. Melanopsin expressing RGCs are divided into M1 cells stratifying in sublamina a, M2 cells stratifying in sublamina b and M3 cells stratifying in both IPL sublaminae (Hattar et al., 2002, Hattar et al., 2006). According to Echer et al., (2010) there are also "M4" cells, an entirely new subtype of pRGC with large soma and wide, radiate dendritic arbor as well as "M5" cells. Both M4 and M5 cells express melanopsin at low levels.

M1 cells form the primary projection to the SCN regulating circadian behaviours while M1 and M2 cells project to the OPN in approximately equivalent proportions driving the pupil light reflex (Baver et al., 2008, Chen et al., 2011). The dendritic pruning observed in *Opa1* mutant mice is restricted to sublamina b (Williams et al., 2010) (Williams et al., 2010) and therefore could manifest as a specific deficit in the pupil light reflex. However assessment of pupillometry (which was performed during the light phase of the normal LD cycle) identified a robust light reflex in *Opa1*$^{+/Q285STOP}$ mice that was indistinguishable from wildtypes at all irradiance levels tested across a 6 log unit range (Prof Ron Douglas, personal communication). In this study, mice were dark adapted for at least 1 hr before a light stimulus was delivered for 20 seconds. Pupil areas after illumination were expressed relative to the area of the pupil in darkness immediately preceding the light exposure. Animals were subjected to 14 different light intensities presented in ascending order of brightness. No significant differences were found between genotypes at each intensity tested. The morphological and functional data would suggest that in Opa1 mutant mice, the melanopsin expressing RGCs are not subject to the dendritic pruning observed in the general RGC population.

There are several studies in patients with *OPA1* ADOA suggesting a preservation of pupil light responses despite visual deficits. According to Bremner et al. (2001) patients suffering from ADOA have normal pupil responses. La Morgia et al. (2010) also found normal pupillary light reaction in ADOA patients. There is also evidence of preservation of pupil light reflex in Lebers hereditary optic neuropathy, another mitochondrial retinopathy (Wakakura and Yokoe, 1995, Bremner et al., 1999, Kawasaki et al., 2010, La Morgia et al., 2010). Additionally, La Morgia et al. (2010) suggested an increased resistance of melanopsin cells in mitochondrial optic neuropathies (ADOA and LHON) by assessing melanopsin expression in post-mortem eyes from patients. In these optic neuropathies there is RGC loss due to neurodegeneration caused by mitochondrial dysfunction but pRGCs are lost in these patients at a much slower rate compared to regular RGCs. Therefore in both patient studies and mouse models of ADOA, a preservation of non image forming functions and the melanopsin expressing RGCs has been observed.

There are several studies supporting the La Morgia et al. (2010) findings in terms of melanopsin RGC survival in conditions of stress. Li et al., (2006) found pRGC survival in an animal model of glaucoma and Robinson and Madison (2004) found a preservation of pRGCs in a model of axotomy. There is also further earlier evidence from Chambille and Serviere (1993) suggesting that a damaged retinohypothalamic tract can still assume the photic entrainment of the circadian clock despite the toxic effect of monosodium glutamate to cells.

An important question that needs to be addressed is what makes melanopsin RGCs less vulnerable to injury and mitochondrial impairment? Do melanopsin cells have a unique characteristic which renders these cells resistant to damage in mitochondrial retinopathies?

OPA1 is widely expressed throughout the body (Delettre et al., 2001) but RGCs are preferentially affected in ADOA (Kjer, 1959). OPA1 plays important roles for the normal function of mitochondria. It has been proposed that RGCs have an increased susceptibility to mitochondrial impairment due to their axons which have long unmyelinated stretches with slower conduction velocities and therefore require far greater energy to restore the electrical potential. These unmyelinated regions are enriched with mitochondria (Carelli et al., 2004). It is possible that melanopsin expressing RGCs have a lower energy demand. However, ultrastructural characterisation of these cells has revealed dendritic varicosities packed with mitochondria (Belenky et al., 2003). Furthermore, in general photosensitive cells have high energy demands to cope with the phototransduction process.

Future aims would be to determine if there are neuroprotective mechanisms present in melanopsin expressing RGCs that could provide tools for therapeutic intervention for many neurodegenerative diseases. PACAP is co-expressed with glutamate in melanopsin expressing RGCs innervating the SCN and its neuroprotective potential has been investigated in numerous animal models. Therefore, it is possible that PACAP expression confers neuroprotection to the melanopsin expressing RGCs. It would be interesting to assess whether PACAP could be neuroprotective in mitochondrial diseases. This area of research could lead to exciting new therapeutic strategies.

References

ALAVI, M. V., BETTE, S., SCHIMPF, S., SCHUETTAUF, F., SCHRAERMEYER, U., WEHRL, H. F., RUTTIGER, L., BECK, S. C., TONAGEL, F., PICHLER, B. J., KNIPPER, M., PETERS, T., LAUFS, J. & WISSINGER, B. 2007. A splice site mutation in the murine Opa1 gene features pathology of autosomal dominant optic atrophy. Brain, 130, 1029-42.

ALBRECHT, U. & FOSTER, R. G. 2002. Placing ocular mutants into a functional context: a chronobiological approach. Methods, 28, 465-77.

ALEXANDER, C., VOTRUBA, M., PESCH, U. E., THISELTON, D. L., MAYER, S., MOORE, A., RODRIGUEZ, M., KELLNER, U., LEO-KOTTLER, B., AUBURGER, G., BHATTACHARYA, S. S. & WISSINGER, B. 2000. OPA1, encoding a dynamin-related GTPase, is mutated in autosomal dominant optic atrophy linked to chromosome 3q28. Nat Genet, 26, 211-5.

ALTIMUS, C. M., GULER, A. D., VILLA, K. L., MCNEILL, D. S., LEGATES, T. A. & HATTAR, S. 2008. Rods-cones and melanopsin detect light and dark to modulate sleep independent of image formation. Proc Natl Acad Sci U S A, 105, 19998-20003.

AMATI-BONNEAU, D. MILEA, D. BONNEAU, A. CHEVROLLIER, M. FERRE, V. GUILLET. 2009. OPA1-associated disorders: Phenotypes and pathophysiology. The International Journal of Biochemistry & Cell Biology, 41 (10), pp. 1855–1865

BAILES, H. J. & LUCAS, R. J. 2010. Melanopsin and inner retinal photoreception. Cell Mol Life Sci, 67, 99-111.

BARNARD, A. R., CHARBEL ISSA, P., PERGANTA, G., WILLIAMS, P. A., DAVIES, V. J., SEKARAN, S., VOTRUBA, M. & MACLAREN, R. E. 2011. Specific deficits in visual electrophysiology in a mouse model of dominant optic atrophy. Exp Eye Res, 93, 771-7.

BAVER, S. B., PICKARD, G. E. & SOLLARS, P. J. 2008. Two types of melanopsin retinal ganglion cell differentially innervate the hypothalamic suprachiasmatic nucleus and the olivary pretectal nucleus. Eur J Neurosci, 27, 1763-70.

BELENKY, M. A., SMERASKI, C. A., PROVENCIO, I., SOLLARS, P. J. & PICKARD, G. E. 2003. Melanopsin retinal ganglion cells receive bipolar and amacrine cell synapses. J Comp Neurol, 460, 380-93.

BELLINGHAM, J., WHITMORE, D., PHILP, A. R., WELLS, D. J. & FOSTER, R. G. 2002. Zebrafish melanopsin: isolation, tissue localisation and phylogenetic position. Brain Res Mol Brain Res, 107, 128-36.

BERSON, D. M., DUNN, F. A. & TAKAO, M. 2002. Phototransduction by retinal ganglion cells that set the circadian clock. Science, 295, 1070-3.

BERSON, D. M. 2003. Strange vision: ganglion cells as circadian photoreceptors. Trends Neurosci, 26, 314-20.

BERSON, D. M., CASTRUCCI, A. M. & PROVENCIO, I. 2010. Morphology and mosaics of melanopsin-expressing retinal ganglion cell types in mice. J Comp Neurol, 518, 2405-22.

BETTE, S., SCHLASZUS, H., WISSINGER, B., MEYERMANN, R. & MITTELBRONN, M. 2005. OPA1, associated with autosomal dominant optic atrophy, is widely expressed in the human brain. Acta Neuropathol, 109, 393-9.

BREMNER, F. D., SHALLO-HOFFMANN, J., RIORDAN-EVA, P. & SMITH, S. E. 1999. Comparing pupil function with visual function in patients with Leber's hereditary optic neuropathy. Invest Ophthalmol Vis Sci, 40, 2528-34.

BREMNER, F. D., TOMLIN, E. A., SHALLO-HOFFMANN, J., VOTRUBA, M. & SMITH, S. E. 2001. The pupil in dominant optic atrophy. Invest Ophthalmol Vis Sci, 42, 675-8.

CALDWELL, J. B., HOWARD, R. O. & RIGGS, L. A. 1971. Dominant juvenile optic atrophy. A study in two families and review of hereditary disease in childhood. Arch Ophthalmol, 85, 133-47.

CARELLI, V., ROSS-CISNEROS, F. N. & SADUN, A. A. 2004. Mitochondrial dysfunction as a cause of optic neuropathies. Prog Retin Eye Res, 23, 53-89.

CHAMBILLE, I. & SERVIERE, J. 1993. Neurotoxic effects of neonatal injections of monosodium L-glutamate (L-MSG) on the retinal ganglion cell layer of the golden hamster: anatomical and functional consequences on the circadian system. J Comp Neurol, 338, 67-82.

CHAURASIA, S. S., ROLLAG, M. D., JIANG, G., HAYES, W. P., HAQUE, R., NATESAN, A., ZATZ, M., TOSINI, G., LIU, C., KORF, H. W., IUVONE, P. M. & PROVENCIO, I. 2005. Molecular cloning, localization and circadian expression of chicken melanopsin (Opn4): differential regulation of expression in pineal and retinal cell types. J Neurochem, 92, 158-70.

CHEN, S. K., BADEA, T. C. & HATTAR, S. 2011. Photoentrainment and pupillary light reflex are mediated by distinct populations of ipRGCs. Nature, 476, 92-5.

CIPOLAT, S., MARTINS DE BRITO, O., DAL ZILIO, B. & SCORRANO, L. 2004. OPA1 requires mitofusin 1 to promote mitochondrial fusion. Proc Natl Acad Sci U S A, 101, 15927-32.

CIPOLAT, S., RUDKA, T., HARTMANN, D., COSTA, V., SERNEELS, L., CRAESSAERTS, K., METZGER, K., FREZZA, C., ANNAERT, W., D'ADAMIO, L., DERKS, C., DEJAEGERE, T., PELLEGRINI, L., D'HOOGE, R., SCORRANO, L. & DE STROOPER, B. 2006. Mitochondrial rhomboid PARL regulates cytochrome c release during apoptosis via OPA1-dependent cristae remodeling. Cell, 126, 163-75.

DACEY, D. M., LIAO, H. W., PETERSON, B. B., ROBINSON, F. R., SMITH, V. C., POKORNY, J., YAU, K. W. & GAMLIN, P. D. 2005. Melanopsin-expressing ganglion cells in primate retina signal colour and irradiance and project to the LGN. Nature, 433, 749-54.

DAVIES, V. J., HOLLINS, A. J., PIECHOTA, M. J., YIP, W., DAVIES, J. R., WHITE, K. E., NICOLS, P. P., BOULTON, M. E. & VOTRUBA, M. 2007. Opa1 deficiency in a mouse model of autosomal dominant optic atrophy impairs mitochondrial morphology, optic nerve structure and visual function. Hum Mol Genet, 16, 1307-18.

DEBOER, T. & TOBLER, I. 2000. Running wheel size influences circadian rhythm period and its phase shift in mice. J Comp Physiol A, 186, 969-73.

DELETTRE, C., LENAERS, G., GRIFFOIN, J. M., GIGAREL, N., LORENZO, C., BELENGUER, P., PELLOQUIN, L., GROSGEORGE, J., TURC-CAREL, C., PERRET, E., ASTARIE-DEQUEKER, C., LASQUELLEC, L., ARNAUD, B., DUCOMMUN, B., KAPLAN, J. & HAMEL, C. P. 2000. Nuclear gene OPA1, encoding a mitochondrial dynamin-related protein, is mutated in dominant optic atrophy. Nat Genet, 26, 207-10.

DELETTRE, C., GRIFFOIN, J. M., KAPLAN, J., DOLLFUS, H., LORENZ, B., FAIVRE, L., LENAERS, G., BELENGUER, P. & HAMEL, C. P. 2001. Mutation spectrum and splicing variants in the OPA1 gene. Hum Genet, 109, 584-91.

DELETTRE, C., LENAERS, G., PELLOQUIN, L., BELENGUER, P. & HAMEL, C. P. 2002. OPA1 (Kjer type) dominant optic atrophy: a novel mitochondrial disease. Mol Genet Metab, 75, 97-107.

DE ZAVALIA, N., PLANO, S. A., FERNANDEZ, D. C., LANZANI, M. F., SALIDO, E., BELFORTE, N., SARMIENTO, M. I., GOLOMBEK, D. A. & ROSENSTEIN, R. E. 2011. Effect of experimental glaucoma on the non-image forming visual system. J Neurochem, 117, 904-14.

DRIVENES, O., SOVIKNES, A. M., EBBESSON, L. O., FJOSE, A., SEO, H. C. & HELVIK, J. V. 2003. Isolation and characterization of two teleost melanopsin genes and their differential expression within the inner retina and brain. J Comp Neurol, 456, 84-93.

DROUYER, E., DKHISSI-BENYAHYA, O., CHIQUET, C., WOLDEMUSSIE, E., RUIZ, G., WHEELER, L. A., DENIS, P. & COOPER, H. M. 2008. Glaucoma alters the circadian timing system. PLoS One, 3, e3931.

DUMITRESCU, O. N., PUCCI, F. G., WONG, K. Y. & BERSON, D. M. 2009. Ectopic retinal ON bipolar cell synapses in the OFF inner plexiform layer: contacts with dopaminergic amacrine cells and melanopsin ganglion cells. J Comp Neurol, 517, 226-44.

DUNLAP, J. C. 1999. Molecular bases for circadian clocks. Cell, 96, 271-90.

ECKER, J. L., DUMITRESCU, O. N., WONG, K. Y., ALAM, N. M., CHEN, S. K., LEGATES, T., RENNA, J. M., PRUSKY, G. T., BERSON, D. M. & HATTAR, S. 2010. Melanopsin-expressing retinal ganglion-cell photoreceptors: cellular diversity and role in pattern vision. Neuron, 67, 49-60.

EIBERG, H., KJER, B., KJER, P. & ROSENBERG, T. 1994. Dominant optic atrophy (OPA1) mapped to chromosome 3q region. I. Linkage analysis. Hum Mol Genet, 3, 977-80.

FISHER, S. P., GODINHO, S. I., POTHECARY, C. A., HANKINS, M. W., FOSTER, R. G. & PEIRSON, S. N. 2012. Rapid assessment of sleep-wake behavior in mice. J Biol Rhythms, 27, 48-58.

FOSTER, R. G., PROVENCIO, I., HUDSON, D., FISKE, S., DE GRIP, W. & MENAKER, M. 1991. Circadian photoreception in the retinally degenerate mouse (rd/rd). J Comp Physiol A, 169, 39-50.

FREEDMAN, M. S., LUCAS, R. J., SONI, B., VON SCHANTZ, M., MUNOZ, M., DAVID-GRAY, Z. & FOSTER, R. 1999. Regulation of mammalian circadian behavior by non-rod, non-cone, ocular photoreceptors. Science, 284, 502-4.

GALANI, R., DUCONSEILLE, E., BILDSTEIN, O. & CASSEL, J. C. 2001. Effects of room and cage familiarity on locomotor activity measures in rats. Physiol Behav, 74, 1-4.

GOOLEY, J. J., LU, J., CHOU, T. C., SCAMMELL, T. E. & SAPER, C. B. 2001. Melanopsin in cells of origin of the retinohypothalamic tract. Nat Neurosci, 4, 1165.

GOZ, D., STUDHOLME, K., LAPPI, D. A., ROLLAG, M. D., PROVENCIO, I. & MORIN, L. P. 2008. Targeted destruction of photosensitive retinal ganglion cells with a saporin conjugate alters the effects of light on mouse circadian rhythms. PLoS One, 3, e3153.

GREEN, C. B., TAKAHASHI, J. S. & BASS, J. 2008. The meter of metabolism. Cell, 134, 728-42.

GULER, A. D., ECKER, J. L., LALL, G. S., HAQ, S., ALTIMUS, C. M., LIAO, H. W., BARNARD, A. R., CAHILL, H., BADEA, T. C., ZHAO, H., HANKINS, M. W., BERSON, D. M., LUCAS, R. J., YAU, K. W. & HATTAR, S. 2008. Melanopsin cells are the principal conduits for rod-cone input to non-image-forming vision. Nature, 453, 102-5.

HANNIBAL, J., HINDERSSON, P., KNUDSEN, S. M., GEORG, B. & FAHRENKRUG, J. 2002. The photopigment melanopsin is exclusively present in pituitary adenylate cyclase-activating polypeptide-containing retinal ganglion cells of the retinohypothalamic tract. J Neurosci, 22, RC191.

HATORI, M., LE, H., VOLLMERS, C., KEDING, S. R., TANAKA, N., BUCH, T., WAISMAN, A., SCHMEDT, C., JEGLA, T. & PANDA, S. 2008. Inducible ablation of melanopsin-expressing retinal ganglion cells reveals their central role in non-image forming visual responses. PLoS One, 3, e2451.

HATTAR, S., LIAO, H. W., TAKAO, M., BERSON, D. M. & YAU, K. W. 2002. Melanopsin-containing retinal ganglion cells: architecture, projections, and intrinsic photosensitivity. Science, 295, 1065-70.

HATTAR, S., LUCAS, R. J., MROSOVSKY, N., THOMPSON, S., DOUGLAS, R. H., HANKINS, M. W., LEM, J., BIEL, M., HOFMANN, F., FOSTER, R. G. & YAU, K. W. 2003. Melanopsin and rod-cone photoreceptive systems account for all major accessory visual functions in mice. Nature, 424, 76-81.

HATTAR, S., KUMAR, M., PARK, A., TONG, P., TUNG, J., YAU, K. W. & BERSON, D. M. 2006. Central projections of melanopsin-expressing retinal ganglion cells in the mouse. J Comp Neurol, 497, 326-49.

HEIDUSCHKA, P., SCHNICHELS, S., FUHRMANN, N., HOFMEISTER, S., SCHRAERMEYER, U., WISSINGER, B. & ALAVI, M. V. 2010. Electrophysiological and histologic assessment of retinal ganglion cell fate in a mouse model for OPA1-associated autosomal dominant optic atrophy. Invest Ophthalmol Vis Sci, 51, 1424-31.

HOSHI, H., LIU, W. L., MASSEY, S. C. & MILLS, S. L. 2009. ON inputs to the OFF layer: bipolar cells that break the stratification rules of the retina. J Neurosci, 29, 8875-83.

HUANG, T., SANTARELLI, R., STARR, A .2009.Mutation of OPA1 gene causes deafness by affecting function of auditory nerve terminals Brain Research, 1300, pp. 97–104

HUDSON G, AMATI-BONNEAU P, BLAKELY EL, STEWART JD, HE L, et al. 2008.Mutation of OPA1 causes dominant optic atrophy with external ophthalmoplegia, ataxia, deafness and multiple mitochondrial DNA deletions: a novel disorder of mtDNA maintenance. Brain 131: 329–337

HUGHES S., WELSH L., KATTI C., GONZALEZ-MENENDEZ I., TURTON M., HALFORD S., SEKARAN S., PEIRSON SN. 2012. Differential expression of melanopsin isoforms Opn4L and Opn4S during postnatal development of the mouse retina. PLoS One, 7(4):e 34531

JAEGER, W. 1974. [Hereditary degenerative diseases of the optic nerve]. Ber Zusammenkunft Dtsch Ophthalmol Ges, 72, 505-20.

JEAN-LOUIS, G., ZIZI, F., LAZZARO, D. R. & WOLINTZ, A. H. 2008. Circadian rhythm dysfunction in glaucoma: A hypothesis. J Circadian Rhythms, 6, 1.

JOHNSTON, P. B., GASTER, R. N., SMITH, V. C. & TRIPATHI, R. C. 1979. A clinicopathologic study of autosomal dominant optic atrophy. Am J Ophthalmol, 88, 868-75.

JUD, C., SCHMUTZ, I., HAMPP, G., OSTER, H. & ALBRECHT, U. 2005. A guideline for analyzing circadian wheel-running behavior in rodents under different lighting conditions. Biol Proced Online, 7, 101-16.

JUSUF, P. R., LEE, S. C., HANNIBAL, J. & GRUNERT, U. 2007. Characterization and synaptic connectivity of melanopsin-containing ganglion cells in the primate retina. Eur J Neurosci, 26, 2906-21.

KAWASAKI, A., HERBST, K., SANDER, B. & MILEA, D. 2010. Selective wavelength pupillometry in Leber hereditary optic neuropathy. Clin Experiment Ophthalmol, 38, 322-4.

KING, D. P. & TAKAHASHI, J. S. 2000. Molecular genetics of circadian rhythms in mammals. Annu Rev Neurosci, 23, 713-42.

KJER, P. 1959. Infantile optic atrophy with dominant mode of inheritance: a clinical and genetic study of 19 Danish families. Acta Ophthalmol Suppl, 164, 1-147.

KJER, P., JENSEN, O. A. & KLINKEN, L. 1983. Histopathology of eye, optic nerve and brain in a case of dominant optic atrophy. Acta Ophthalmol (Copenh), 61, 300-12.

KLINE, L. B. & GLASER, J. S. 1979. Dominant optic atrophy. The clinical profile. Arch Ophthalmol, 97, 1680-6.

KOYANAGI, M., KUBOKAWA, K., TSUKAMOTO, H., SHICHIDA, Y. & TERAKITA, A. 2005. Cephalochordate melanopsin: evolutionary linkage between invertebrate visual cells and vertebrate photosensitive retinal ganglion cells. Curr Biol, 15, 1065-9.

LA MORGIA, C., ROSS-CISNEROS, F. N., SADUN, A. A., HANNIBAL, J., MUNARINI, A., MANTOVANI, V., BARBONI, P., CANTALUPO, G., TOZER, K. R., SANCISI, E., SALOMAO, S. R., MORAES, M. N., MORAES-FILHO, M. N., HEEGAARD, S., MILEA, D., KJER, P., MONTAGNA, P. & CARELLI, V. 2010. Melanopsin retinal ganglion cells are resistant to neurodegeneration in mitochondrial optic neuropathies. Brain, 133, 2426-38.

LAPOSKY, A. D., BASS, J., KOHSAKA, A. & TUREK, F. W. 2008. Sleep and circadian rhythms: key components in the regulation of energy metabolism. FEBS Lett, 582, 142-51.

LEE, Y. J., JEONG, S. Y., KARBOWSKI, M., SMITH, C. L. & YOULE, R. J. 2004. Roles of the mammalian mitochondrial fission and fusion mediators Fis1, Drp1, and Opa1 in apoptosis. Mol Biol Cell, 15, 5001-11.

LEWY, A. 1980. Light supresses melatonin secretion in humans Science.

LI, R. S., CHEN, B. Y., TAY, D. K., CHAN, H. H., PU, M. L. & SO, K. F. 2006. Melanopsin-expressing retinal ganglion cells are more injury-resistant in a chronic ocular hypertension model. Invest Ophthalmol Vis Sci, 47, 2951-8.

LORENZ, B. 1994. [Hereditary optic atrophy]. Ophthalmologe, 91, 831-50.

LUCAS, R. J., FREEDMAN, M. S., MUNOZ, M., GARCIA-FERNANDEZ, J. M. & FOSTER, R. G. 1999. Regulation of the mammalian pineal by non-rod, non-cone, ocular photoreceptors. Science, 284, 505-7.

LUCAS, R. J., DOUGLAS, R. H. & FOSTER, R. G. 2001. Characterization of an ocular photopigment capable of driving pupillary constriction in mice. Nat Neurosci, 4, 621-6.

LUCAS, R. J., HATTAR, S., TAKAO, M., BERSON, D. M., FOSTER, R. G. & YAU, K. W. 2003. Diminished pupillary light reflex at high irradiances in melanopsin-knockout mice. Science, 299, 245-7.

LUPI, D., OSTER, H., THOMPSON, S. & FOSTER, R. G. 2008. The acute light-induction of sleep is mediated by OPN4-based photoreception. Nat Neurosci, 11, 1068-73.

MALPAUX, B., MIGAUD, M., TRICOIRE, H. & CHEMINEAU, P. 2001. Biology of mammalian photoperiodism and the critical role of the pineal gland and melatonin. J Biol Rhythms, 16, 336-47.

MARC, R. E., JONES, B. W., WATT, C. B., VAZQUEZ-CHONA, F., VAUGHAN, D. K. & ORGANISCIAK, D. T. 2008. Extreme retinal remodeling triggered by light damage: implications for age related macular degeneration. Mol Vis, 14, 782-806.

MARCHBANK, N. J., CRAIG, J. E., LEEK, J. P., TOOHEY, M., CHURCHILL, A. J., MARKHAM, A. F., MACKEY, D. A., TOOMES, C. & INGLEHEARN, C. F. 2002. Deletion of the OPA1 gene in a dominant optic atrophy family: evidence that haploinsufficiency is the cause of disease. J Med Genet, 39, e47.

MELYAN, Z., TARTTELIN, E. E., BELLINGHAM, J., LUCAS, R. J. & HANKINS, M. W. 2005. Addition of human melanopsin renders mammalian cells photoresponsive. Nature, 433, 741-5.

MILONE, M., YOUNGE, B.R., WANG, J., ZHANG, S., WONG, L.-J.2009. Mitochondrial disorder with OPA1 mutation lacking optic atrophy.Mitochondrion, 9(4) pp. 279-281

MOORE, R. Y. 1996. Neural control of the pineal gland. Behav Brain Res, 73, 125-30.

MROSOVSKY, N. 1999. Masking: history, definitions, and measurement. Chronobiol Int, 16, 415-29.

MROSOVSKY, N., LUCAS, R. J. & FOSTER, R. G. 2001. Persistence of masking responses to light in mice lacking rods and cones. J Biol Rhythms, 16, 585-8.

MROSOVSKY, N. & HATTAR, S. 2003. Impaired masking responses to light in melanopsin-knockout mice. Chronobiol Int, 20, 989-99.

MURE, L. S., RIEUX, C., HATTAR, S. & COOPER, H. M. 2007. Melanopsin-dependent nonvisual responses: evidence for photopigment bistability in vivo. J Biol Rhythms, 22, 411-24.

NAKAI, M., ENDOT T., HASE T., MATSUBARA H. 1993. Isolation and characterization of the yeast MSP1 gene which belongs to a novel family of putative ATRase. J Biol Chem, 24262-24269.

NOSEDA, R., KAINZ, V., JAKUBOWSKI, M., GOOLEY, J. J., SAPER, C. B., DIGRE, K. & BURSTEIN, R. 2010. A neural mechanism for exacerbation of headache by light. Nat Neurosci, 13, 239-45.

OLICHON, A., EMORINE, L. J., DESCOINS, E., PELLOQUIN, L., BRICHESE, L., GAS, N., GUILLOU, E., DELETTRE, C., VALETTE, A., HAMEL, C. P., DUCOMMUN, B., LENAERS, G. & BELENGUER, P. 2002. The human dynamin-related protein OPA1 is anchored to the mitochondrial inner membrane facing the inter-membrane space. FEBS Lett, 523, 171-6.

OLICHON, A., BARICAULT, L., GAS, N., GUILLOU, E., VALETTE, A., BELENGUER, P. & LENAERS, G. 2003. Loss of OPA1 perturbates the mitochondrial inner membrane structure and integrity, leading to cytochrome c release and apoptosis. J Biol Chem, 278, 7743-6.

PANDA, S., SATO, T. K., CASTRUCCI, A. M., ROLLAG, M. D., DEGRIP, W. J., HOGENESCH, J. B., PROVENCIO, I. & KAY, S. A. 2002. Melanopsin (Opn4) requirement for normal light-induced circadian phase shifting. Science, 298, 2213-6.

PANDA, S., NAYAK, S. K., CAMPO, B., WALKER, J. R., HOGENESCH, J. B. & JEGLA, T. 2005. Illumination of the melanopsin signaling pathway. Science, 307, 600-4.

PEIRSON SN, BUTLER JN, FOSTER RG. 2003. Experimental validation of novel and conventional approaches to quantitative real-time PCR data analysis. Nucleic Acids Res; 31:e73.

PEIRSON S, and BUTLER J (2007). Quantitative polymerase chain reaction. Methods Mol Biol, 362:349-62.

PELLOQUIN, L., BELENGUER, P., MENON, Y., GAS, N. & DUCOMMUN, B. 1999. Fission yeast Msp1 is a mitochondrial dynamin-related protein. J Cell Sci, 112 (Pt 22), 4151-61.

PEREZ-LEON, J. A., WARREN, E. J., ALLEN, C. N., ROBINSON, D. W. & BROWN, R. L. 2006. Synaptic inputs to retinal ganglion cells that set the circadian clock. Eur J Neurosci, 24, 1117-23.

PEREZ-RICO, C., DE LA VILLA, P., ARRIBAS-GOMEZ, I. & BLANCO, R. 2010. Evaluation of functional integrity of the retinohypothalamic tract in advanced glaucoma using multifocal electroretinography and light-induced melatonin suppression. Exp Eye Res, 91, 578-83.

PESCH UE, LEO-KOTTLER B, MAYER S, JURKLIES B, KELLNER U, APFELST- EDT-SYLLA E, ZRENNER E, ALEXANDER C, WISSINGER B (2001) OPA1 mutations in patients with autosomal dominant optic atrophy and evidence for semi-dominant inheritance. Hum Mol Genet 10:1359–1368

PIRES, S. S., HUGHES, S., TURTON, M., MELYAN, Z., PEIRSON, S. N., ZHENG, L., KOSMAOGLOU, M., BELLINGHAM, J., CHEETHAM, M. E., LUCAS, R. J., FOSTER, R. G., HANKINS, M. W. & HALFORD, S. 2009. Differential expression of two distinct functional isoforms of melanopsin (Opn4) in the mammalian retina. J Neurosci, 29, 12332-42.

PITTENDRIGH, C. 1976. A functional analysis of circadian pacemakers in nocturnal rodents: V. Pacemaker structure : A clock for all seasons
J Comp Physiol A, 106:333-355.

PROVENCIO, I., JIANG, G., DE GRIP, W. J., HAYES, W. P. & ROLLAG, M. D. 1998. Melanopsin: An opsin in melanophores, brain, and eye. Proc Natl Acad Sci U S A, 95, 340-5.

PROVENCIO, I., RODRIGUEZ, I. R., JIANG, G., HAYES, W. P., MOREIRA, E. F. & ROLLAG, M. D. 2000. A novel human opsin in the inner retina. J Neurosci, 20, 600-5.

PROVENCIO, I., ROLLAG, M. D. & CASTRUCCI, A. M. 2002. Photoreceptive net in the mammalian retina. This mesh of cells may explain how some blind mice can still tell day from night. Nature, 415, 493.

REID, K. J. & ZEE, P. C. 2009. Circadian rhythm disorders. Semin Neurol, 29, 393-405.

RENSING, L. & RUOFF, P. 2002. Temperature effect on entrainment, phase shifting, and amplitude of circadian clocks and its molecular bases. Chronobiol Int, 19, 807-64.

ROBINSON, G. A. & MADISON, R. D. 2004. Axotomized mouse retinal ganglion cells containing melanopsin show enhanced survival, but not enhanced axon regrowth into a peripheral nerve graft. Vision Res, 44, 2667-74.

ROECKLEIN, K. A., ROHAN, K. J., DUNCAN, W. C., ROLLAG, M. D., ROSENTHAL, N. E., LIPSKY, R. H. & PROVENCIO, I. 2009. A missense variant (P10L) of the melanopsin (OPN4) gene in seasonal affective disorder. J Affect Disord, 114, 279-85.

ROGGEVEEN, H. C., DE WINTER, A. P. & WENT, L. N. 1985. Studies in dominant optic atrophy. Ophthalmic Paediatr Genet, 5, 103-9.

RUBY, N. F., BRENNAN, T. J., XIE, X., CAO, V., FRANKEN, P., HELLER, H. C. & O'HARA, B. F. 2002. Role of melanopsin in circadian responses to light. Science, 298, 2211-3.

SAHAR, S. & SASSONE-CORSI, P. 2009. Metabolism and cancer: the circadian clock connection. Nat Rev Cancer, 9, 886-96.

SATOH, M., HAMAMOTO, T., SEO, N., KAGAWA, Y. & ENDO, H. 2003. Differential sublocalization of the dynamin-related protein OPA1 isoforms in mitochondria. Biochem Biophys Res Commun, 300, 482-93.

SCHMIDT, T. M., TANIGUCHI, K. & KOFUJI, P. 2008. Intrinsic and extrinsic light responses in melanopsin-expressing ganglion cells during mouse development. J Neurophysiol, 100, 371-84.

SCHMIDT, T. M. & KOFUJI, P. 2009. Functional and morphological differences among intrinsically photosensitive retinal ganglion cells. J Neurosci, 29, 476-82.

SCHMIDT, T. M. & KOFUJI, P. 2011. Structure and function of bistratified intrinsically photosensitive retinal ganglion cells in the mouse. J Comp Neurol, 519, 1492-504.SEKARAN, S., FOSTER, R. G., LUCAS, R. J. & HANKINS, M. W. 2003. Calcium imaging reveals a network of intrinsically light-sensitive inner-retinal neurons. Curr Biol, 13, 1290-8.

SHEARMAN, L. P., SRIRAM, S., WEAVER, D. R., MAYWOOD, E. S., CHAVES, I., ZHENG, B., KUME, K., LEE, C. C., VAN DER HORST, G. T., HASTINGS, M. H. & REPPERT, S. M. 2000. Interacting molecular loops in the mammalian circadian clock. Science, 288, 1013-9.

TAKAHASHI, J. S., HONG, H. K., KO, C. H. & MCDEARMON, E. L. 2008. The genetics of mammalian circadian order and disorder: implications for physiology and disease. Nat Rev Genet, 9, 764-75.

TERMAN, M. & TERMAN, J. S. 2005. Light therapy for seasonal and nonseasonal depression: efficacy, protocol, safety, and side effects. CNS Spectr, 10, 647-63; quiz 672.

TOOMES C, MARCHBANK N, MACKEY D, CRAIG J, NEWBURY-ECOB R, et al. (2001) Spectrum, frequency and penetrance of OPA1 mutations in dominant optic atrophy. Hum Mol Genet 10: 1369–1378.

VAN DEN POL, A. N., CAO, V. & HELLER, H. C. 1998. Circadian system of mice integrates brief light stimuli. Am J Physiol, 275, R654-7.

VANDESOMPELE JO, KATLEEN DE PRETER, FILIP PATTYN, BRUSE POPPE, NADINE VAN ROY, ANNE DE PAEPE, FRANK SPELEMAN. 2002. Accurate normalization of real-time quantitative RT-PCR data by geometric averaging of multiple internal control genes. Genome Biol. 2002; 3(7).

VINEY, T. J., BALINT, K., HILLIER, D., SIEGERT, S., BOLDOGKOI, Z., ENQUIST, L. W., MEISTER, M., CEPKO, C. L. & ROSKA, B. 2007. Local retinal circuits of melanopsin-containing ganglion cells identified by transsynaptic viral tracing. Curr Biol, 17, 981-8.

VOTRUBA, M., FITZKE, F. W., HOLDER, G. E., CARTER, A., BHATTACHARYA, S. S. & MOORE, A. T. 1998. Clinical features in affected individuals from 21 pedigrees with dominant optic atrophy. Arch Ophthalmol, 116, 351-8.

WAKAKURA, M. & YOKOE, J. 1995. Evidence for preserved direct pupillary light response in Leber's hereditary optic neuropathy. Br J Ophthalmol, 79, 442-6.

WALKER, M. T., BROWN, R. L., CRONIN, T. W. & ROBINSON, P. R. 2008. Photochemistry of retinal chromophore in mouse melanopsin. Proc Natl Acad Sci U S A, 105, 8861-5.

WANG, H. Z., LU, Q. J., WANG, N. L., LIU, H., ZHANG, L. & ZHAN, G. L. 2008. Loss of melanopsin-containing retinal ganglion cells in a rat glaucoma model. Chin Med J (Engl), 121, 1015-9.

WHITE, K. E., DAVIES, V. J., HOGAN, V. E., PIECHOTA, M. J., NICHOLS, P. P., TURNBULL, D. M. & VOTRUBA, M. 2009. OPA1 deficiency associated with increased autophagy in retinal ganglion cells in a murine model of dominant optic atrophy. Invest Ophthalmol Vis Sci, 50, 2567-71.

WILLIAMS, P. A., MORGAN, J. E. & VOTRUBA, M. 2010. Opa1 deficiency in a mouse model of dominant optic atrophy leads to retinal ganglion cell dendropathy. Brain, 133, 2942-51.

WONG, K. Y., DUNN, F. A., GRAHAM, D. M. & BERSON, D. M. 2007. Synaptic influences on rat ganglion-cell photoreceptors. J Physiol, 582, 279-96.

XU, H. P. & TIAN, N. 2007. Retinal ganglion cell dendrites undergo a visual activity-dependent redistribution after eye opening. J Comp Neurol, 503, 244-59.

YU-WAI-MAN, P., GRIFFITHS, P.G., GORMAN, G.S., LOURENCO, C.M., WRIGHT,A.F., MAUER-GRUMBAC, M .2010. Multi-system neurological disease is common in patients with OPA1 mutations. Brain, 133, pp. 771-786

YOSHIMURA, T., NISHIO, M., GOTO, M. & EBIHARA, S. 1994. Differences in circadian photosensitivity between retinally degenerate CBA/J mice (rd/rd) and normal CBA/N mice (+/+). J Biol Rhythms, 9, 51-60.

Appendix A

Non-image-forming light driven functions are preserved in visually impaired *Opa1* mutant mice

Georgia Perganta[1], Alun R. Barnard[1], Christiana Katti[1], Athanasios Vachtsevanos[1], Ron H. Douglas[3], Robert E. MacLaren[1,4], Marcela Votruba[2], Sumathi Sekaran[1]

[1]Nuffield Department of Clinical Neurosciences, Nuffield Laboratory of Ophthalmology, University of Oxford, Level 6 West Wing, John Radcliffe Hospital, Headley Way, Oxford OX3 9DU, UK. [2]School of Optometry and Vision Sciences, Cardiff University, Cardiff CF24 4LU, UK, [3]Optometry and Visual Science, City University London, London EC1V 0HB. [4]Moorfields Eye Hospital NHS Foundation Trust and NIHR Biomedical Research Centre.

Corresponding author: Sumathi Sekaran, Nuffield Laboratory of Ophthalmology, Nuffield Department of Clinical Neurosciences, University of Oxford, Level 6 West Wing, John Radcliffe Hospital, Headley Way, Oxford OX3 9DU, UK. Tel: 0044 1865 234705. Fax: 0044 1865 234795. E-mail: sumathi.sekaran@eye.ox.ac.uk

Abbreviated title: Non-image-forming vision in *Opa1* mutants.

Number of pages: 34; Number of figures: 6

Word count: Abstract 243; Introduction 382; Discussion 827.

Key words: autosomal dominant optic atrophy; *OPA1;* melanopsin; circadian behaviour; pupil light reflex

Research Support: This work was supported by the Biotechnology and Biological Sciences Research Council (BB/G003602/1 to S.S), the Wellcome Trust (090684 to S.S; 091984 to R.E.M), the Royal College of Surgeons of Edinburgh (A.R.B), the Health Foundation (R.E.M, G.P, A.V), and the Oxford NIHR Biomedical Research Centre (R.E.M, A.R.B).

Abstract

Purpose: Autosomal dominant optic atrophy (ADOA) is a slowly progressive optic neuropathy that has been associated mutations of the *OPA1* gene. The disease primarily affects the retinal ganglion cells (RGCs) and causes optic nerve atrophy and visual loss. A subset of RGCs is intrinsically photosensitive, express the photopigment melanopsin and drive non-image-forming (NIF) visual functions including circadian photoentrainment and the pupil light reflex. Given the RGC pathology in ADOA, disruption of NIF functions might be predicted. We studied the NIF visual system in a mouse model of ADOA.

Methods: Wheel running activity monitoring, videotracking and pupillometry were used to assess NIF functions in 11-13 month old *Opa1*$^{+/-}$ (B6; C3-*Opa1*^{Q285STOP}) mice and littermate wildtype controls. Melanopsin expression was quantified by immunohistochemistry and real time quantitative PCR.

Results: *Opa*1$^{+/-}$ mice retained the ability to entrain their activity rhythm to the external light/dark cycle, maintained the suppression of activity in response to acute light exposure at night (negative masking), generated equivalent circadian phase shift responses to littermate controls and demonstrated induction of sleep by exposure to brief light pulses. The pupil light reflex was also preserved in *Opa1* mutants at all intensities tested. Furthermore, there was no significant difference in the number of melanopsin-expressing RGCs, cell morphology or in melanopsin transcript levels between genotypes.

Conclusions: Taken together, these findings suggest a preservation of the NIF visual system in *Opa1* mutants. The results provide support to growing evidence that melanopsin-expressing RGCs are protected in mitochondrial optic neuropathies.

Introduction

Autosomal dominant optic atrophy (ADOA) is the most common form of inherited optic neuropathy[1-3]. It is clinically characterized by a moderate to severe decrease in visual acuity, central visual field deficits, colour vision defects and temporal or diffuse optic nerve pallor[1, 3, 4]. ADOA is associated with a specific degeneration of retinal ganglion cells (RGCs)[4, 5]. Mutations in the optic atrophy 1 (*OPA1*) gene have been identified in most of patients with ADOA[6, 7]. The OPA1 protein is a dynamin-related guanosine triphosphatase (GTPase) anchored to the inner mitochondrial membrane.

Mouse models of *OPA1* ADOA have been generated to characterise further the pathophysiology of the disease[8, 9]. In the B6; C3-*Opa1*^{Q285STOP} model, abnormalities in the optic nerve were detected by 9 months[8] without significant RGC loss[10]. Evidence of dendritic pruning localized to sublamina b of the inner plexiform layer was observed from 10 months[10]. By 24 months, severe optic nerve degeneration was found[11]. A specific deficit in the photopic negative response of the electroretinogram which reflects ganglion cell function, was detected in *Opa1* mutants from 12 months[12]. Importantly, deficits in the visual evoked potential (VEP) suggested light information was not being correctly relayed to the brain. Concordantly, a reduction in visual acuity detectable by optokinetic drum screening has been described[8].

A subset of RGCs is intrinsically photosensitive and expresses the photopigment melanopsin[13-15]. These cells are primarily responsible for driving non-image-forming (NIF) visual behaviours. Ablation of the melanopsin expressing RGCs results in: (i) reduced entrainment to normal light/dark (LD) cycles[16-18], (ii) complete loss of circadian phase shift responses[16], (ii) absence of the suppression of locomotor activity to acute light exposure at night ('negative masking')[17, 18], iii) loss of the acute induction of sleep to brief light pulses[19, 20] and iv) severe attenuation of the pupil light reflex (PLR)[16, 17]. Although considerable research has been devoted to describing visual dysfunction in ADOA, NIF responses to light have not been extensively investigated. Given the pathophysiology of the RGCs in *OPA1* ADOA, deficits in NIF visual functions might be predicted. Interestingly, the PLR is preserved in patients with *OPA1* ADOA[21, 22], although light driven circadian behaviours were not assessed.

To investigate the NIF visual system in *OPA1* ADOA we assessed light-driven circadian behaviour, acute light-induced sleep, the pupil light reflex and melanopsin expression in *Opa1* mutant mice.

Methods

Animals

Experiments were conducted on male heterozygous B6; C3-*Opa1*^{Q285STOP} (*Opa1*$^{+/-}$) mice and age matched male littermate controls (*Opa1*$^{+/+}$). B6; C3-*Opa1*^{Q285STOP} mice carry a heterozygous nonsense mutation in exon 8 of the *Opa1* gene (C-T transition at 1051 bp) resulting in protein truncation[8]. The mutation is embryonic lethal in homozygous animals. Food and water were available *ad libitum* and all animal procedures were performed in accordance with the ARVO Statement for the Use of Animals in Ophthalmic and Vision Research and U.K. Home Office guidelines.

Circadian behaviour

Mice *(Opa1*$^{+/+}$: n = 6; *Opa1*$^{+/-}$: n = 7; 11 - 13 months old) were individually placed in cages equipped with a steel running wheel and exposed to a 12:12 light/dark (LD) cycle for 10 days. The light intensity used throughout (unless otherwise stated) was 200 lux (equivalent to ~ 60 $\mu W/cm^2/s$ or 14.2 log quanta/cm^2/s). Activity levels, the length of the active phase and period were calculated. A masking light pulse was presented in the dark phase of the normal LD cycle. A 3-h pulse of white fluorescent light (200 lux) was given at zeitgeber time (ZT) 14 (2h after the lights were switched off). The masking

response was scored as the number of wheel revolutions during the light pulse expressed as a percentage of the number of revolutions made by the same animal during the same period on the previous night when there was no light pulse[23]. Total activity levels and activity levels in 1 hr bins during the light pulse were also calculated. Animals were re-entrained to the normal LD cycle for 10 days.

Mice were subsequently released into constant darkness (DD) for 10 days. To induce phase shift responses animals were exposed to a 15-min monochromatic 480 nm or 525 nm (half peak bandwidth 10 nm) pulse of 1 x 10^{11} photons/s/cm^2 irradiance at circadian time (CT) 16 (4 hr after the onset of daily activity). The 480 nm pulse was applied to maximally stimulate the melanopsin-RGCs (λ_{max} ~ 480 nm) and the 525 nm pulse to maximally stimulate rod (λ_{max} ~ 498 nm) and MW-sensitive cone (λ_{max} ~ 508 nm) contributions to phase shift behaviour. Monochromatic light stimuli were applied in a specialised chamber with full internal reflectance using an LED light source (Honig Lichttechnik). In the control sham condition animals were handled in a similar way to the light pulse condition but maintained in darkness. There were at least 10 days between pulses. The magnitudes of the phase shifts were calculated using the difference between a regression line through steady state activity onsets prior to and after the pulse. Transient responses in the first 2-3 days after the pulse were excluded.

Data were analysed with ClockLab software (Actimetrics). ANOVA or unpaired students t-tests were used to test for significance ($p < 0.05$). All data are expressed as mean ± SEM. Light measurements were made with a lux meter (Macam Photometrics) or a spectrometer (Ocean Optics Inc).

Sleep screening

Mice (*Opa1*$^{+/+}$: n = 5; *Opa1*$^{+/-}$: n = 6; 11 - 13 months old) were placed in cages equipped with infrared cameras for monitoring activity (Sentient Mini-night vision CCTV camera, Maplin, UK). The output was recorded on a 16-channel digital hard-drive recorder (VXM4B-16, Videcon. PLC) at 25 frames per second with a resolution of 704 x 576 pixels. Animals were exposed to a 12:12 LD cycle (200 lux) for 15 days. To determine the modulation of sleep behaviour by light, animals were exposed to a 1-h white light pulse (200 lux) at ZT14[24]. The immobility-defined sleep period for each mouse was assessed using video tracking software (ANY-maze, Stoelting). Sleep was defined as a period of immobility greater than 40 sec. A previous study has confirmed that monitoring of immobility with videotracking has extremely high concordance (>95%) with EEG recordings for sleep determination[24]. Sleep latency (defined as the time between the onset of the light exposure and the first 2 min of continuous immobility) and total sleep, were also determined.

Pupillometry

Pupillometry was performed on *Opa1*$^{+/+}$ (n = 5) and *Opa1*$^{+/-}$ (n = 5) at 24 months of age. Experiments were conducted during the light phase of the normal LD cycle to avoid any effects of circadian variation in the PLR[25]. The right eyes of unanaesthetised animals, restrained by hand, were filmed under infrared illumination by an infrared-sensitive camera (Cohu, San Diego, USA) fitted with a zoom lens (giving a field of view of 8.7x6.9 mm), positioned in a plane parallel to the pupil. Various intensities of white light, filtered by a heat glass and neutral density filters and controlled by a shutter, were delivered to the eye being filmed through a fibre optic from a Leica CLS 100x light source. The spectral irradiance at the animal's cornea for each neutral density filter was measured in 1nm steps (200-870nm) using an Ocean Optics USB2000 fibre optic spectrometer and CC3-UV cosine collector calibrated with an Ocean Optics DH-2000-Cal light source. Since the action spectrum of wildtype mouse pupil constriction is described by the mouse's scotopic sensitivity, measured spectral irradiances were weighted by the spectral absorbance of the murine rod visual pigment.

After at least 1 hr of dark adaptation, a light stimulus was delivered for 20 seconds. The animal was then released and returned to darkness for at least 2 min before exposure to subsequent stimuli. Animals were subjected to 14 different light intensities presented in ascending order of brightness. VHS video images were digitised and the area of the pupil both before light exposure and 5 sec after

illumination was determined using Image J software. Pupil areas after illumination were expressed relative to the area of the pupil in darkness immediately preceding the light exposure. Average irradiance/response curves were constructed for each genotype and fitted by a four term sigmoid relationship (SigmaPlot, Systat Software Inc., San Jose, USA). Data were compared using ANOVA.

Melanopsin Immunohistochemistry

Animals were sacrificed at ZT8 - ZT10 (*Opa1*$^{+/+}$: n = 3; *Opa1*$^{+/-}$: n = 3; 11 - 13 months old). Retinae were dissected and fixed in 4% paraformaldehyde (PFA) overnight. Retinae were incubated with an N-terminal polyclonal melanopsin antibody (PAS8331; rabbit anti-mouse (1:500) in 1% Donkey serum, 0.1% Triton X-100 in PBS)[26]. Retinae were subsequently incubated with an Alexa Fluor 488 secondary antibody (donkey anti-rabbit IgG (1:400) in 0.1 % Triton X-100 in PBS; Invitrogen). A fluorescent microscope (Zeiss Axioskop) was used to view the retinal flatmounts and images were captured with a Hamamatsu Orca camera. Cell counts were performed using Adobe Photoshop software. Confocal images were captured using a Laser scanning confocal microscope (Zeiss LSM510). Soma diameter was measured using Image J software.

Real-time Quantitative PCR

Animals were sacrificed at ZT8 - ZT10 (*Opa1*$^{+/+}$: n = 5; *Opa1*$^{+/-}$: n = 5; 11 - 13 months old). RNA was extracted using the AllPrep RNA/Protein Kit (QIAGEN) according to the manufacturer's instructions. Before RNA elution, on-column DNase treatment was performed in order to eliminate genomic DNA contamination. 500 μg RNA was subsequently reverse transcribed to cDNA with Superscript III Reverse Transcriptase (Invitrogen) using random hexamers as primers. Quantitative PCR (qPCR) was performed using Brilliant II Fast SYBR Green Master Mix and following the manufacturer's instructions. The reading temperature for each gene was determined empirically. Transcript levels are expressed relative to the geometric mean of three house-keeping genes (GAPDH, B2M and PSMB2). Primers used were: melanopsin (*Opn4*) - Forward: TCACAGGGATGCTGGGCAATC, Reverse: TTCTTGTAGAGGCTGCTGGCAAAG; *Opa1* - Forward: TGACAAACTTAAGGAGGCTGTG, Reverse: CATTGTGCTGAATAACCCTCAA.

Results

NIF visual functions in *Opa1*$^{+/-}$ B6; C3-*Opa1*^{Q285STOP} mice and littermate controls were assessed by wheel running, videotracking and pupillometry. Melanopsin expression was examined at the RNA and protein level.

***Opa1* mutation has no influence on entrainment to a normal LD cycle**

In normal lighting conditions, photic information from the retina is relayed to the central circadian clock located in the suprachiasmatic nucleus. The light signal entrains the internal clock to the external lighting conditions. The ability of *Opa1*$^{+/-}$ and *Opa1*$^{+/+}$ mice to entrain to a 12:12 LD cycle was assessed (Figure 1A,B). Both genotypes confined their activity to the dark phase suggesting the animals were entrained to the normal LD cycle. The period length (τ) and length of the active phase were equivalent for wildtype and heterozygous mice (Figure 1C). The total activity (average number of wheel revolutions per day) was slightly higher in *Opa1*$^{+/-}$ animals relative to the wildtype controls but this difference was not significant (Figure 1C). When released into constant darkness (DD), the phase of activity onset was coincident with lights OFF of the previous LD cycle for both genotypes (Figure 1A,B) again suggesting that the mice were entrained to the light signal.

Negative masking is preserved in *Opa1* $^{+/-}$ mice

Ambient lighting information is relayed to the central circadian oscillator to entrain the clock and modulate behaviour. In addition, light can directly affect activity levels. The suppression of locomotor activity by acute light exposure at night is termed negative masking. Negative masking in *Opa1*$^{+/-}$ and *Opa1*$^{+/+}$ mice was assessed by administering a 3 hr 200 lux light pulse 2 hr after lights off (zeitgeber time (ZT) 14)[23]. *Opa1*$^{+/+}$ *and Opa1*$^{+/-}$ mice significantly decreased their activity during the 3 hr light pulse period (data normalised to baseline from previous night; Figure 2A). Both genotypes acutely stopped running during the first hour of the light pulse and activity levels subsequently increased, as has been previously shown[23]. The baseline corrected activity levels during the light pulse was not significantly different between genotypes. An hourly breakdown of the number of wheel revolutions during the light pulse also showed no significant difference between genotypes (Figure 2B).

Phase shift responses are maintained in *Opa1*$^{+/-}$ mice

A more direct assessment of the effect of light on circadian activity is typically tested by phase shifting paradigms where animals are exposed to pulses of light when otherwise in constant darkness (DD). A light pulse administered in the early subjective night, delays the onset of activity. We assessed phase shift responses in *Opa1*$^{+/+}$ and *Opa1*$^{+/-}$ mice to 480 nm or 525 nm pulses at circadian time (CT) 16 (4 hr after the onset of activity; Figure 3A,B).

In DD mice display a wheel running activity rhythm with a period (τ) of less than 24 hr. We observed an almost identical τ for wildtype and heterozygous mice in constant darkness (Figure 1C). The total activity and length of the active phase were also similar between genotypes in DD (Figure 1C). The pulse of 480 nm light induced a delay in the phase of activity onset in both *Opa1*$^{+/+}$ and *Opa1*$^{+/-}$ mice. The average magnitude of the phase shifts was not significantly different between genotypes (Figure 3C). In both genotypes, the period of the activity rhythm was not altered following the light pulse (τ after 480 nm pulse*: Opa1*$^{+/+}$ 23.6 ± 0.09 hr; *Opa1*$^{+/-}$ 23.6 ± 0.07 hr). The pulse of 525 nm also successfully induced a phase delay in activity onset in *Opa1*$^{+/+}$ and *Opa1*$^{+/-}$ mice. There was no significant difference in the size of the phase shifts between genotypes (Figure 3C). Again the period length was not altered after the light pulse for each genotype (τ after 525 nm pulse*: Opa1*$^{+/+}$ 23.6 ± 0.09 hr; *Opa1*$^{+/-}$ 23.6 ± 0.06 hr). Importantly in a control sham pulse exposure, no obvious phase shift was observed in either wildtype or heterozygous animals (Figure 3C).

Acute light induction of sleep is present in *Opa1* $^{+/-}$ mice

Acute light exposure at night reduces activity levels ('masking') and also induces sleep in nocturnal species [19, 20, 27]. Sleep induction is believed to involve a direct projection from the melanopsin RGCs to sleep/wake regulatory brain centres including the ventrolateral preoptic nucleus and superior

colliculus[19, 20]. The acute effects of light on sleep were investigated in *Opa1* mutant mice and wild-type controls by administering a 1 hr light pulse 2 hr after the onset of dark (ZT 14), when the homeostatic and circadian drives for wakefulness are high. Videotracking was used to assess sleep behaviour. *Opa1*$^{+/+}$ and *Opa1*$^{+/-}$ mice exhibited low immobility (i.e. high activity) during the dark period of a normal 12:12 LD cycle as would be expected for a nocturnal species (Figure 4A). In response to the light pulse, a sharp increase in immobility was observed in both genotypes (Figure 4B). The latency to the first 2 minutes of continuous immobility (sleep latency) was not significantly different between genotypes (Figure 4C). During acute light exposure, the total time spent asleep was also similar for both wild type and mutant mice (Figure 4D) suggesting that both genotypes sustain the inhibitory response to light.

Pupil light reflex is preserved in *Opa1*$^{+/-}$ mice

Both wildtype mice and *Opa1* mutant mice demonstrated a graded pupil response to illumination. The average irradiance response curve for animals with mutations of the *Opa1* gene was very similar to that of wildtype littermates (Figure 5). A 2-way ANOVA using intensity and genotype as factors showed a significant effect of light intensity ($p < 0.0001$) but no significant effect of genotype ($p = 0.51$) and no significant interaction between genotype and intensity ($p = 0.99$).

Opa1 defect has no effect on melanopsin expression

To assess whether melanopsin-RGCs are affected by the *Opa1* mutation we used immunohistochemistry in wholemount retinae. Melanopsin expressing cells were observed in both $Opa1^{+/+}$ and $Opa1^{+/-}$ eyes. As expected, cells appeared to be randomly distributed throughout the retinae (Figure 6A,B). Quantitative assessment of total melanopsin cell numbers revealed no significant differences between genotypes (average cell count per retina: $Opa1^{+/+}$: 900 ± 28.9 cells; $Opa1^{+/-}$: 810 ± 37.9 cells). Autosomal dominant optic atrophy is often associated with central visual field defects. Therefore melanopsin cell numbers in the central retina (2mm radius from optic nerve) was assessed. Again, there was no significant difference between genotypes (central retina cell count: $Opa1^{+/+}$: 97.5 ± 3.4 cells; $Opa1^{+/-}$: 94.3 ± 3.4 cells). Morphological characterisation of the melanopsin cells also revealed no significant differences in the mean soma diameter ($Opa1^{+/+}$: 13.9 ± 0.5 μm, n = 30; $Opa1^{+/-}$: 14.0 ± 0.5 μm, n = 30). Finally, we observed no obvious differences in the stratification patterns of the melanopsin cells between genotypes (Figure 6C). Melanopsin positive dendrites were observed in both sublamina a (OFF) and sublamina b (ON) of the innerplexiform layer in both $Opa1^{+/+}$ and $Opa1^{+/-}$ retinae.

To characterise further melanopsin expression in *Opa1*$^{+/+}$ and *Opa1*$^{+/-}$ mice, we assessed melanopsin transcript levels (Figure 6D). No significant difference in melanopsin RNA expression level was detected between genotypes. As a control, we assessed *Opa1* transcript levels and found a significant reduction in expression by almost half in *Opa1*$^{+/-}$ mice ($p < 0.005$) as expected[8, 9].

Discussion

Mouse models of *OPA1* ADOA exhibit RGC and optic nerve abnormalities with associated visual dysfunction. Surprisingly despite the insult to the RGC population, we have found that photic regulation of circadian activity, sleep behaviour and the pupil light reflex are preserved in *Opa1* mutant mice. The melanopsin-expressing intrinsically photosensitive RGCs which primarily drive these NIF responses to light were found to be unaffected in *Opa1*$^{+/-}$ animals.

ADOA is characterised by loss of RGCs and optic nerve atrophy[4, 5]. Ocular electrophysiological testing in ADOA patients have demonstrated an abnormal pattern electroretinogram (ERG)[3, 28, 29] and reduced photopic negative response (PhNR)[30], which reflect RGC dysfunction. Output of photic information to central visual pathways is also disrupted. Reduced cortical visual evoked potential (VEP) amplitudes and increased VEP latencies have been recorded in ADOA patients[3, 29, 31]. The functional visual outcome includes a reduction in visual acuity, central visual field defects and colour vision disruption[1, 3, 4]. Similarly in mouse models of *OPA1* ADOA, abnormal ERGs[12], VEPs[12, 32] and visual behaviour[8] have been described.

With these substantial visual deficits in ADOA, it would seem likely that NIF visual behaviours including circadian photoentrainment and sleep induction might be similarly disrupted. However, this has not been examined in patients or extensively in animal models. The results from the current study

overwhelmingly support a preservation of NIF visual behaviour in *Opa1* mutant mice. *Opa1*$^{+/-}$ mice displayed normal photoentrainment to a LD cycle, negative masking, phase shift behaviour to 480 nm and 525 nm stimuli, and sleep induction. A previous study also assessed masking behaviour in the same *Opa1* mutant line[8] and suggested that masking in *Opa1*$^{+/-}$ mice was impaired. It is likely that this discrepancy is due to the fact that the data was not corrected for individual differences in baseline activity. This may be important as we have noted that the *Opa1*$^{+/-}$ animals display a slightly higher baseline activity level relative to wildtype controls, although in the present study this difference was not significant.

NIF functions are primarily driven by melanopsin-expressing photosensitive RGCs. Melanopsin-RGCs stratify in sublamina a (M1 cells), sublamina b (M2, M4 and M5 cells) or in both sublaminae (M3) of the innerplexiform layer (IPL)[13, 33, 34]. The melanopsin cell classes project to different brain centres and thus drive different NIF visual functions[13, 33]. The suprachiasmatic nucleus, which controls circadian behaviour, receives projections mainly from M1 cells[35, 36]. The olivary pretectal nucleus, which controls the PLR, receives projections from both M1 and M2 cells[35, 36]. The RGCs in *Opa1*$^{+/-}$ mice demonstrate a progressive dendropathy from 10 months restricted to sublamina b and without associated cell loss[10]. A specific deficit in the pupil light reflex may therefore be predicted. The pupil light reflex is primarily driven by melanopsin at high irradiance and by rod and cone input to the melanopsin cells at lower irradiances[37, 38]. Presently, a robust pupil light reflex was recorded in *Opa1*$^{+/-}$

mice that was equivalent to wildtype controls, in response to a full irradiance series. This evidence suggests that the melanopsin cells are receiving normal functional dendritic inputs from the rod and cone pathways are not perhaps subject to the dendritic reorganisation observed in other RGCs that stratify in sublamina b[10]. In support of this, we also observed no obvious differences in melanopsin cell stratification patterns between wildtype and *Opa1* mutant mice.

In patients with *OPA1* ADOA, preservation of pupil responses in the presence of visual acuity defects have also been described[22, 39]. Interestingly, several studies have suggested that the PLR is also preferentially preserved in another mitochondrial optic atrophy condition – Leber's hereditary optic neuropathy (LHON)[39-42]. Thus evidence from both mouse and human studies suggest that the PLR is preserved in mitochondrial retinopathies. Morgia et al. (2010) also reported a relative sparing of melanopsin RGCs relative to the total RGC population in ADOA and LHON patients[21]. Preservation of melanopsin ganglion cells has been reported in other models of retinal disease/damage[43, 44]. This may suggest that melanopsin RGCs are resistant in models of inner retinal damage, particularly in mitochondrial retinopathies.

It is unclear as to why melanopsin-expressing photosensitive RGCs may be less susceptible to mitochondrial impairment than other ganglion cells. It has been predicted that cells with a low energy

demand may be affected least by loss of normal mitochondrial morphology or function. However, ultrastructural characterisation of the melanopsin cells has identified dendritic varicosities packed with mitochondria[45] arguing against this simple explanation. Melanopsin RGCs express the neuropeptide pituitary adenylate cyclise activating polypeptide (PACAP)[46]. Several studies have found that *in vivo* application of PACAP has retinoprotective effects[47-49]. However, it is unknown if cellular expression of PACAP is neuroprotective in mitochondrial retinopathies.

We conclude that photic regulation of circadian behaviour, sleep induction and the pupil light reflex are preserved in a mouse model of ADOA despite previous reports of visual dysfunction[8, 12]. Melanopsin-expressing RGCs, which drive these behaviours, may be resistant to damage in mitochondrial retinopathies. Identification of the possible neuroprotective mechanism involved could lead to exciting therapeutic strategies.

Acknowledgements

The videotracking system was kindly supplied by Russell Foster and Stuart Peirson with technical assistance provided by Simon Fisher and Sofia Godhino. Julian Partridge kindly performed irradiance calibration for the pupil studies and Chris Hull and David Crabb helped with pupillometry data analysis and statistics.

Figure Legends

Figure 1. Circadian behaviour in wildtype and *Opa1* mutant mice. Representative actograms from (A) *Opa1* $^{+/+}$ and (B) *Opa1* $^{+/-}$ mice entrained to a 12/12 LD cycle which were subsequently released into constant darkness (DD). Each horizontal line corresponds to one day and the data has been double plotted. The black vertical bars represent activity (i.e. wheel revolutions). The shaded region represents lights ON. (C) Table showing average period (τ), total activity levels and length of the active phase in LD and in DD for *Opa1*$^{+/+}$ (n = 6) and *Opa1*$^{+/-}$ (n = 7) mice. There were no significant differences between genotypes (unpaired students t-test; p values are shown). All data are presented as mean ± SEM.

Figure 2. Masking response in *Opa1*$^{+/+}$ and *Opa1*$^{+/-}$ mice. (A) A 200 lux white light pulse was applied for 3 hr (ZT 14-17; white background) during the night phase of the normal LD cycle (gray background). The average wheel running revolutions on the night of the light pulse are plotted relative to the baseline levels (the night before the pulse) for *Opa1*$^{+/+}$ (n = 6) and *Opa1*$^{+/-}$ (n = 7) mice. The masking pulse completely suppressed activity in both genotypes immediately after lights ON. ANOVA analysis found no significant effect of genotype on the baseline corrected activity levels (p = 0.468)

(B) Bar graph showing hourly breakdown of activity during masking pulse. A 2-way ANOVA using activity in each hour of light pulse and genotype as factors found a significant effect of hour of light pulse ($p < 0.005$) but no significant effect of genotype ($p = 0.143$) and no interaction between genotype and light pulse hour ($p = 0.359$). All data are presented as mean ± SEM.

Figure 3. Phase shift behaviour in *Opa1*$^{+/+}$ and *Opa1*$^{+/-}$ mice. Representative actograms from (A) *Opa1*$^{+/+}$ and (B) *Opa1*$^{+/-}$ mice in constant dark (DD) conditions. Animals were exposed to 15 min light pulses every ~15 days. Photon matched pulses at 480 nm (black arrow) or 525 nm (white arrow; 1 x 10^{11} photons/s/cm^2) were applied at CT16. Animals were also exposed to a dark sham pulse condition (grey arrow). (C) The size of the phase shift response are plotted for the 525 nm, 480 nm and sham conditions for *Opa1*$^{+/+}$ (n = 6) and *Opa1*$^{+/-}$ (n = 7) mice. A two-way ANOVA with genotype and wavelength as factors was performed. There was no significant effect of wavelength ($p = 0.66$) or genotype ($p = 0.17$) and the interaction of genotype and wavelength was not significant ($p = 0.91$).

Figure 4. Induction of sleep by acute light in *Opa1*$^{+/+}$ and *Opa1*$^{+/-}$ mice. (A) The average immobility-defined sleep is plotted against zeitgeber time in a normal 12:12 hr LD cycle (1 hr resolution) for *Opa1*$^{+/+}$ (n = 5) and *Opa1*$^{+/-}$ (n = 6) mice. Animals were largely immobile in the day phase of the LD cycle. White background indicates the day portion and grey background the night

portion of the 24 hr LD cycle. (B) The effect of the administration of the 1-h light pulse (white background) at ZT 14 during the night phase is shown. Both genotypes demonstrated an increase in immobility during the light pulse (10 min resolution). Quantification of (C) sleep latency and (D) total sleep during light exposure found no significant differences between genotypes *(*unpaired student's t-test). All data are presented as mean ± SEM.

Figure 5. Pupil light reflex in *Opa1*$^{+/+}$ and *Opa1*$^{+/-}$ mice. The average minimum pupil area expressed as a percentage of maximum dilation following illumination with various intensities of white light for *Opa1*$^{+/+}$ (n = 5) and *Opa1*$^{+/-}$ (n = 5) mice. All data are fitted with four term sigmoidal functions (solid lines) of the form y=y0+a/(1+exp(-(x-x0)/b)) (goodness of fit of fitted curve to actual data (R2): *Opa1*$^{+/+}$ = 0.993 and *Opa1*$^{+/-}$ = 0.995). A 2-way ANOVA using intensity and genotype as factors showed a significant effect of light intensity ($p < 0.0001$) but no significant effect of genotype ($p = 0.51$) and no significant interaction between genotype and intensity ($p = 0.99$).

Figure 6. Melanopsin expression in *Opa1*$^{+/+}$ and *Opa1*$^{+/-}$ retinae. Overall distribution of melanopsin-positive RGCs in a flatmount retina from (A) *Opa1*$^{+/+}$ and (B) *Opa1*$^{+/-}$ mice. Each cell body is represented by a black dot in the periphery and a white dot in the central retina. There was no significant difference between the average total number of melanopsin expressing cells or the number

of melanopsin cells within 2 mm of the optic nerve between *Opa1*$^{+/+}$ (n = 3) and *Opa1*$^{+/-}$ (n = 3) retinae. (C) Confocal images of melanopsin positive neurons in *Opa1*$^{+/+}$ and *Opa1*$^{+/-}$ retinae.. A projected image of a confocal stack (from the inner plexiform layer to the ganglion cell layer) is shown for each genotype. An image at the plane of the outermost region of sublamina a and an image at the plane of the innermost region of sublamina b from the same image stacks is also shown. (D) Quantification of melanopsin (*Opn4*) and *Opa1* gene expression by real time quantitative PCR. Expression levels in *Opa1*$^{+/-}$ animals are plotted relative to wildtype data. No significant difference in expression was detected for *Opn4* between genotypes. A significant reduction in *Opa1* expression was observed in *Opa1*$^{+/-}$ mice relative to wildtype controls (student's t-test. * = $p < 0.005$). All data are presented as mean ± SEM.

References

1. Kjer P. Infantile optic atrophy with dominant mode of inheritance: a clinical and genetic study of 19 Danish families. *Acta Ophthalmol Suppl* 1959;164:1-147.

2. Kline LB, Glaser JS. Dominant optic atrophy. The clinical profile. *Arch Ophthalmol* 1979;97:1680-1686.

3. Votruba M, Fitzke FW, Holder GE, Carter A, Bhattacharya SS, Moore AT. Clinical features in affected individuals from 21 pedigrees with dominant optic atrophy. *Arch Ophthalmol* 1998;116:351-358.

4. Johnston PB, Gaster RN, Smith VC, Tripathi RC. A clinicopathologic study of autosomal dominant optic atrophy. *Am J Ophthalmol* 1979;88:868-875.

5. Kjer P, Jensen OA, Klinken L. Histopathology of eye, optic nerve and brain in a case of dominant optic atrophy. *Acta Ophthalmol (Copenh)* 1983;61:300-312.

6. Alexander C, Votruba M, Pesch UE, et al. OPA1, encoding a dynamin-related GTPase, is mutated in autosomal dominant optic atrophy linked to chromosome 3q28. *Nat Genet* 2000;26:211-215.

7. Delettre C, Lenaers G, Griffoin JM, et al. Nuclear gene OPA1, encoding a mitochondrial dynamin-related protein, is mutated in dominant optic atrophy. *Nat Genet* 2000;26:207-210.

8. Davies VJ, Hollins AJ, Piechota MJ, et al. Opa1 deficiency in a mouse model of autosomal dominant optic atrophy impairs mitochondrial morphology, optic nerve structure and visual function. *Hum Mol Genet* 2007;16:1307-1318.

9. Alavi MV, Bette S, Schimpf S, et al. A splice site mutation in the murine Opa1 gene features pathology of autosomal dominant optic atrophy. *Brain* 2007;130:1029-1042.

10. Williams PA, Morgan JE, Votruba M. Opa1 deficiency in a mouse model of dominant optic atrophy leads to retinal ganglion cell dendropathy. *Brain* 2010;133:2942-2951.

11. White KE, Davies VJ, Hogan VE, et al. OPA1 deficiency associated with increased autophagy in retinal ganglion cells in a murine model of dominant optic atrophy. *Invest Ophthalmol Vis Sci* 2009;50:2567-2571.

12. Barnard AR, Issa PC, Perganta G, et al. Specific deficits in visual electrophysiology in a mouse model of dominant optic atrophy. *Exp Eye Res* 2011.

13. Hattar S, Liao HW, Takao M, Berson DM, Yau KW. Melanopsin-containing retinal ganglion cells: architecture, projections, and intrinsic photosensitivity. *Science* 2002;295:1065-1070.

14. Berson DM, Dunn FA, Takao M. Phototransduction by retinal ganglion cells that set the circadian clock. *Science* 2002;295:1070-1073.

15. Sekaran S, Foster RG, Lucas RJ, Hankins MW. Calcium imaging reveals a network of intrinsically light-sensitive inner-retinal neurons. *Curr Biol* 2003;13:1290-1298.

16. Guler AD, Ecker JL, Lall GS, et al. Melanopsin cells are the principal conduits for rod-cone input to non-image-forming vision. *Nature* 2008;453:102-105.

17. Hatori M, Le H, Vollmers C, et al. Inducible ablation of melanopsin-expressing retinal ganglion cells reveals their central role in non-image forming visual responses. *PLoS One* 2008;3:e2451.

18. Goz D, Studholme K, Lappi DA, Rollag MD, Provencio I, Morin LP. Targeted destruction of photosensitive retinal ganglion cells with a saporin conjugate alters the effects of light on mouse circadian rhythms. *PLoS One* 2008;3:e3153.

19. Altimus CM, Guler AD, Villa KL, McNeill DS, Legates TA, Hattar S. Rods-cones and melanopsin detect light and dark to modulate sleep independent of image formation. *Proc Natl Acad Sci U S A* 2008;105:19998-20003.

20. Lupi D, Oster H, Thompson S, Foster RG. The acute light-induction of sleep is mediated by OPN4-based photoreception. *Nat Neurosci* 2008;11:1068-1073.

21. La Morgia C, Ross-Cisneros FN, Sadun AA, et al. Melanopsin retinal ganglion cells are resistant to neurodegeneration in mitochondrial optic neuropathies. *Brain* 2010;133:2426-2438.

22. Bremner FD, Tomlin EA, Shallo-Hoffmann J, Votruba M, Smith SE. The pupil in dominant optic atrophy. *Invest Ophthalmol Vis Sci* 2001;42:675-678.

23. Mrosovsky N, Hattar S. Impaired masking responses to light in melanopsin-knockout mice. *Chronobiol Int* 2003;20:989-999.

24. Fisher SP, Godinho SIH, Pothecary CA, Hankins MW, Foster RG, Peirson SN. Rapid assessment of sleep/wake behaviour in mice. . *Journal of Biological Rhythms* in press.

25. Zele AJ, Feigl B, Smith SS, Markwell EL. The circadian response of intrinsically photosensitive retinal ganglion cells. *PLoS One* 2011;6:e17860.

26. Pires SS, Hughes S, Turton M, et al. Differential expression of two distinct functional isoforms of melanopsin (Opn4) in the mammalian retina. *J Neurosci* 2009;29:12332-12342.

27. Benca RM, Gilliland MA, Obermeyer WH. Effects of lighting conditions on sleep and wakefulness in albino Lewis and pigmented Brown Norway rats. *Sleep* 1998;21:451-460.

28. Berninger TA, Jaeger W, Krastel H. Electrophysiology and colour perimetry in dominant infantile optic atrophy. *Br J Ophthalmol* 1991;75:49-52.

29. Holder GE, Votruba M, Carter AC, Bhattacharya SS, Fitzke FW, Moore AT. Electrophysiological findings in dominant optic atrophy (DOA) linking to the OPA1 locus on chromosome 3q 28-qter. *Doc Ophthalmol* 1998;95:217-228.

30. Miyata K, Nakamura M, Kondo M, et al. Reduction of oscillatory potentials and photopic negative response in patients with autosomal dominant optic atrophy with OPA1 mutations. *Invest Ophthalmol Vis Sci* 2007;48:820-824.

31. Granse L, Bergstrand I, Thiselton D, et al. Electrophysiology and ocular blood flow in a family with dominant optic nerve atrophy and a mutation in the OPA1 gene. *Ophthalmic Genet* 2003;24:233-245.

32. Heiduschka P, Schnichels S, Fuhrmann N, et al. Electrophysiological and histologic assessment of retinal ganglion cell fate in a mouse model for OPA1-associated autosomal dominant optic atrophy. *Invest Ophthalmol Vis Sci* 2010;51:1424-1431.

33. Hattar S, Kumar M, Park A, et al. Central projections of melanopsin-expressing retinal ganglion cells in the mouse. *J Comp Neurol* 2006;497:326-349.

34. Ecker JL, Dumitrescu ON, Wong KY, et al. Melanopsin-expressing retinal ganglion-cell photoreceptors: cellular diversity and role in pattern vision. *Neuron* 2011;67:49-60.

35. Baver SB, Pickard GE, Sollars PJ. Two types of melanopsin retinal ganglion cell differentially innervate the hypothalamic suprachiasmatic nucleus and the olivary pretectal nucleus. *Eur J Neurosci* 2008;27:1763-1770.

36. Chen SK, Badea TC, Hattar S. Photoentrainment and pupillary light reflex are mediated by distinct populations of ipRGCs. *Nature* 2011;476:92-95.

37. Lucas RJ, Hattar S, Takao M, Berson DM, Foster RG, Yau KW. Diminished pupillary light reflex at high irradiances in melanopsin-knockout mice. *Science* 2003;299:245-247.

38. Lucas RJ, Douglas RH, Foster RG. Characterization of an ocular photopigment capable of driving pupillary constriction in mice. *Nat Neurosci* 2001;4:621-626.

39. La Morgia C, Ross-Cisneros FN, Sadun AA, et al. Melanopsin retinal ganglion cells are resistant to neurodegeneration in mitochondrial optic neuropathies. *Brain* 2011;133:2426-2438.

40. Wakakura M, Yokoe J. Evidence for preserved direct pupillary light response in Leber's hereditary optic neuropathy. *Br J Ophthalmol* 1995;79:442-446.

41. Bremner FD, Shallo-Hoffmann J, Riordan-Eva P, Smith SE. Comparing pupil function with visual function in patients with Leber's hereditary optic neuropathy. *Invest Ophthalmol Vis Sci* 1999;40:2528-2534.

42. Kawasaki A, Herbst K, Sander B, Milea D. Selective wavelength pupillometry in Leber hereditary optic neuropathy. *Clin Experiment Ophthalmol* 2009;38:322-324.

43. Li RS, Chen BY, Tay DK, Chan HH, Pu ML, So KF. Melanopsin-expressing retinal ganglion cells are more injury-resistant in a chronic ocular hypertension model. *Invest Ophthalmol Vis Sci* 2006;47:2951-2958.

44. Robinson GA, Madison RD. Axotomized mouse retinal ganglion cells containing melanopsin show enhanced survival, but not enhanced axon regrowth into a peripheral nerve graft. *Vision Res* 2004;44:2667-2674.

45. Belenky MA, Smeraski CA, Provencio I, Sollars PJ, Pickard GE. Melanopsin retinal ganglion cells receive bipolar and amacrine cell synapses. *J Comp Neurol* 2003;460:380-393.

46. Hannibal J, Hindersson P, Knudsen SM, Georg B, Fahrenkrug J. The photopigment melanopsin is exclusively present in pituitary adenylate cyclase-activating polypeptide-containing retinal ganglion cells of the retinohypothalamic tract. *J Neurosci* 2002;22:RC191.

47. Seki T, Itoh H, Nakamachi T, et al. Suppression of rat retinal ganglion cell death by PACAP following transient ischemia induced by high intraocular pressure. *J Mol Neurosci* 2011;43:30-34.

48. Seki T, Nakatani M, Taki C, et al. Neuroprotective effect of PACAP against kainic acid-induced neurotoxicity in rat retina. *Ann N Y Acad Sci* 2006;1070:531-534.

49. Tamas A, Gabriel R, Racz B, et al. Effects of pituitary adenylate cyclase activating polypeptide in retinal degeneration induced by monosodium-glutamate. *Neurosci Lett* 2004;372:110-113.

Figure 1

A)

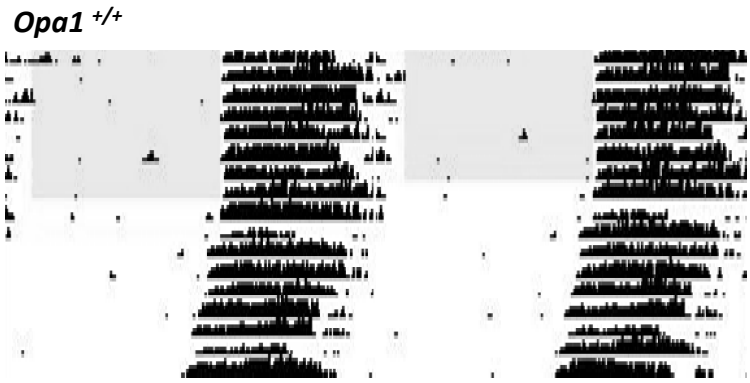

B)

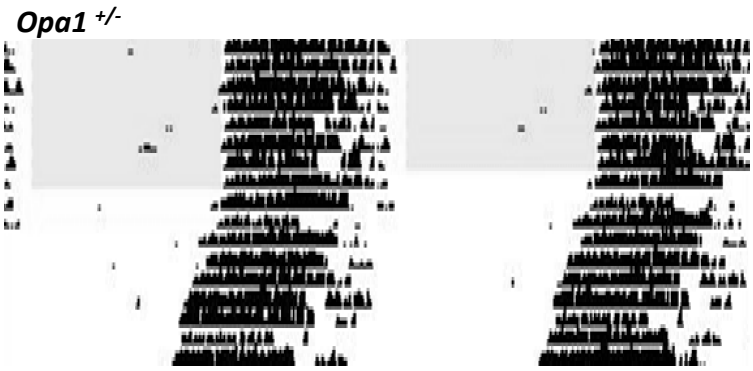

C)

Parameter	Condition	*Opa1*$^{+/+}$	*Opa1*$^{+/-}$	p value
Period (hr)	LD	23.98 ± 0.01	23.99 ± 0.01	0.44
	DD	23.69 ± 0.05	23.68 ± 0.05	0.97
Total activity (wheel rev.)	LD	14549 ± 3982	17244 ± 2717	0.58
	DD	14727 ± 4120	17323 ± 2304	0.58
Length of active phase (hr)	LD	10.32 ± 0.44	10.04 ± 0.88	0.80
	DD	9.15 ± 0.65	9.33 ± 0.65	0.85

Figure 2

A)

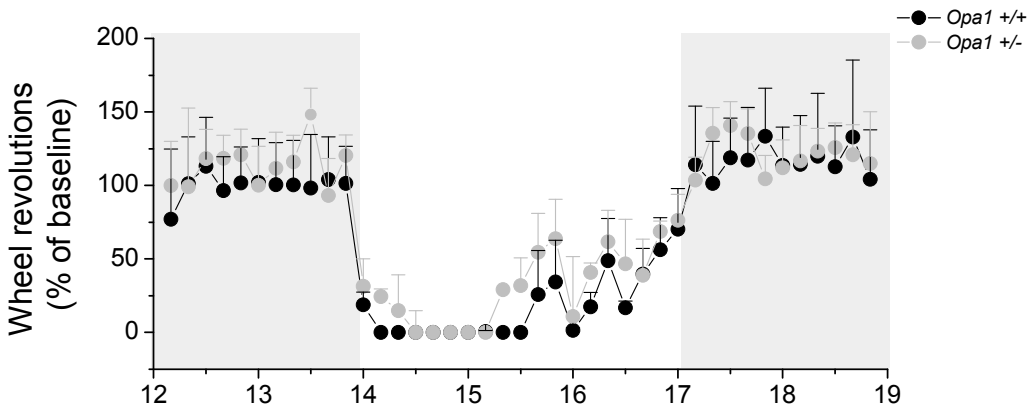
Opa1 +/+
Opa1 +/-
Wheel revolutions
(% of baseline)
200
150
100
50
0
12
13
14
15
16
17
18
19

B)

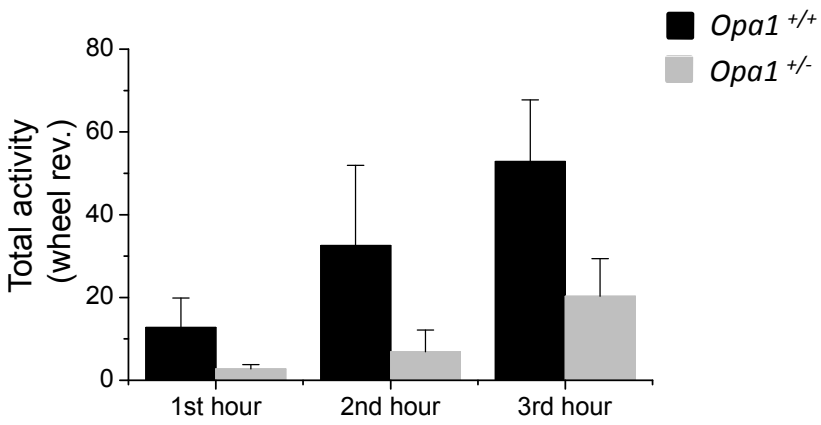
Opa1 +/+
Opa1 +/-
Total activity
(wheel rev.)
80
60
40
20
0
1st hour
2nd hour
3rd hour

Figure 3

A) ***Opa1*** $^{+/+}$

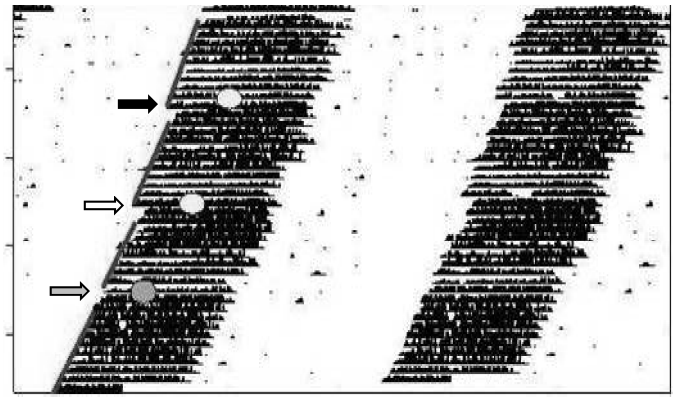

B) ***Opa1*** $^{+/-}$

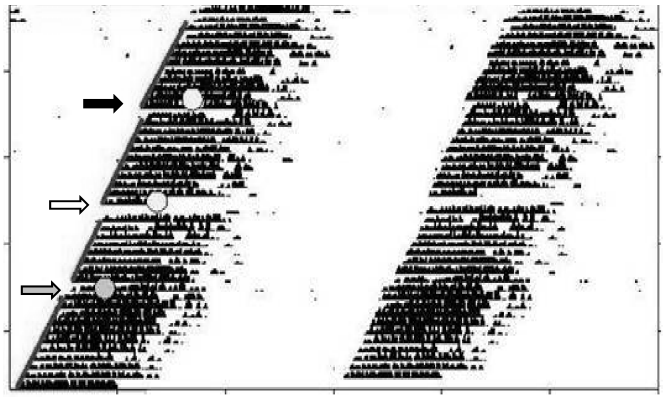

C)

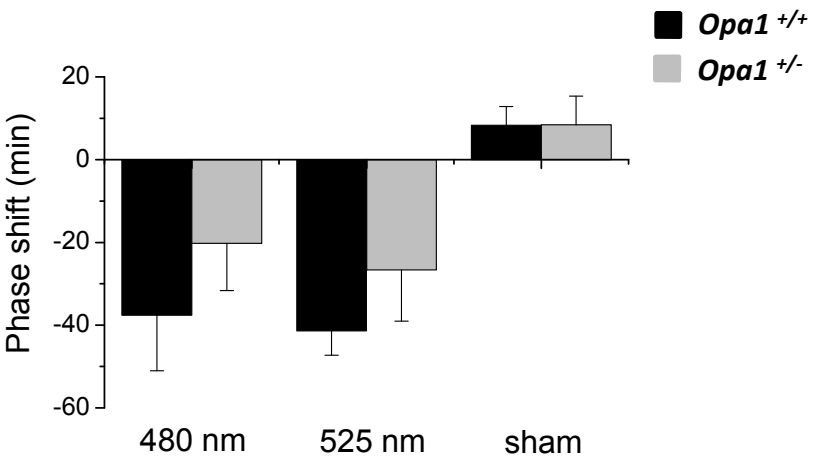

Figure 4

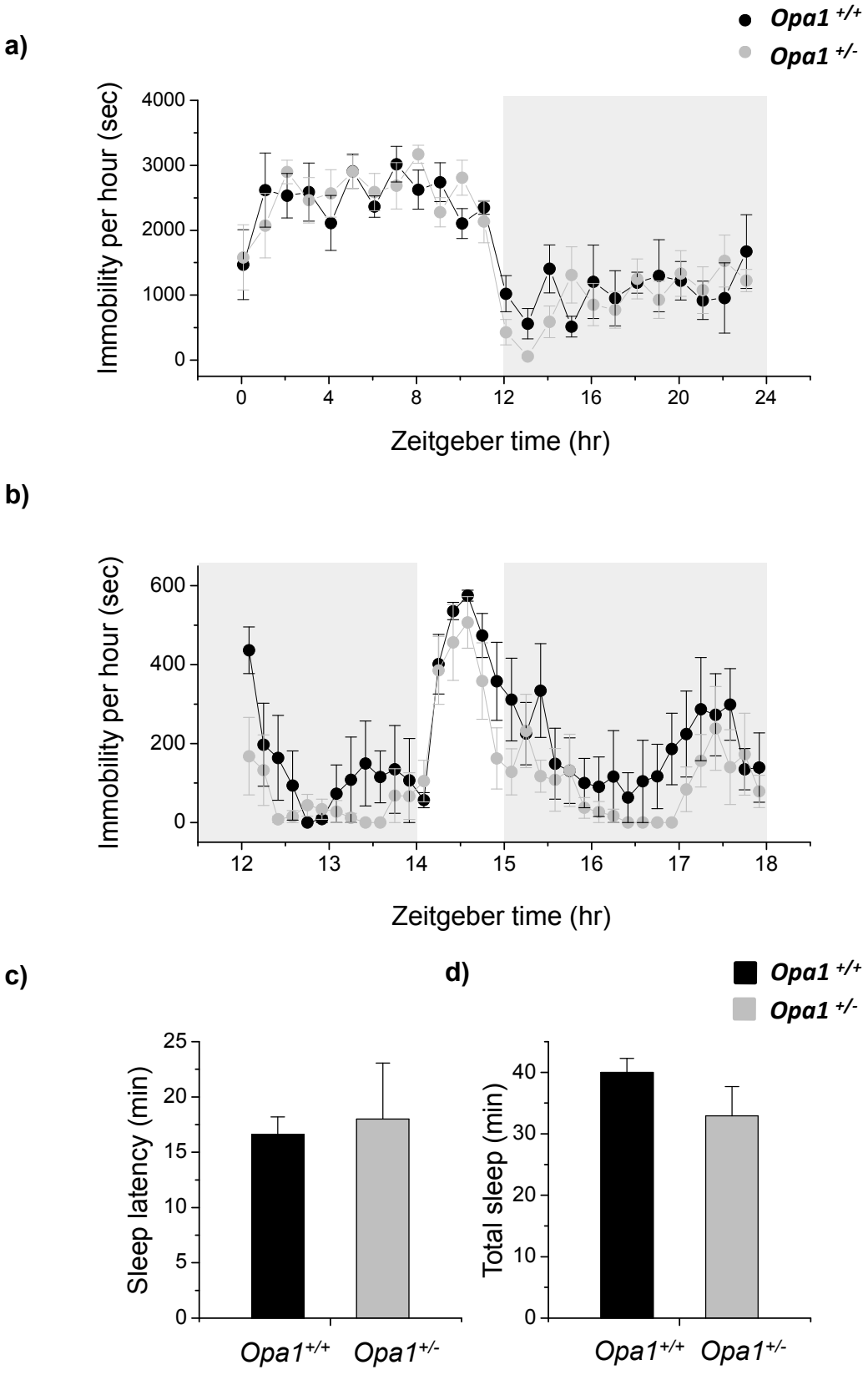
a)
Opa1 +/+
Opa1 +/-
Immobility per hour (sec)
4000
3000
2000
1000
0
0
4
8
12
16
20
24
Zeitgeber time (hr)
b)
Immobility per hour (sec)
600
400
200
0
12
13
14
15
16
17
18
Zeitgeber time (hr)
c)
Sleep latency (min)
25
20
15
10
5
0
Opa1+/+
Opa1+/-
d)
Opa1 +/+
Opa1 +/-
Total sleep (min)
40
30
20
10
0
Opa1+/+
Opa1+/-

Figure 5

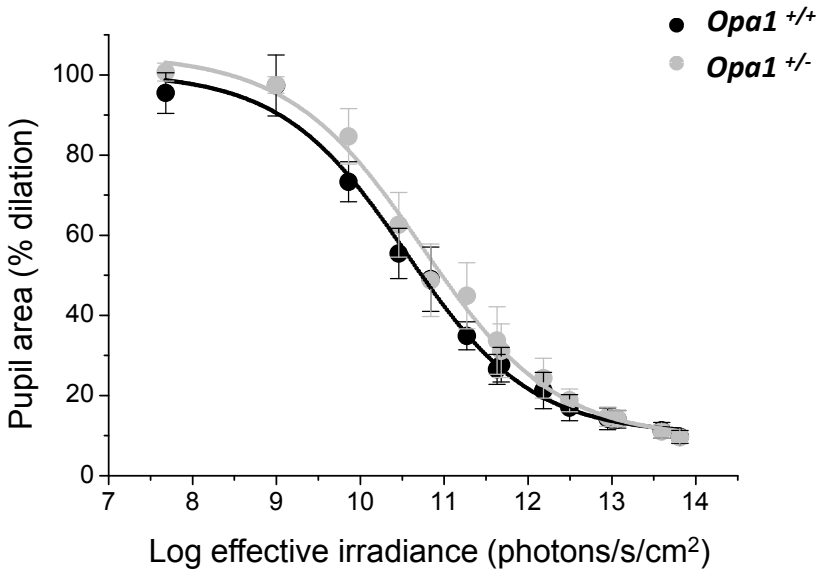
Opa1 +/+
Opa1 +/-
Pupil area (% dilation)
0
20
40
60
80
100
7
8
9
10
11
12
13
14
Log effective irradiance (photons/s/cm2)

Figure 6

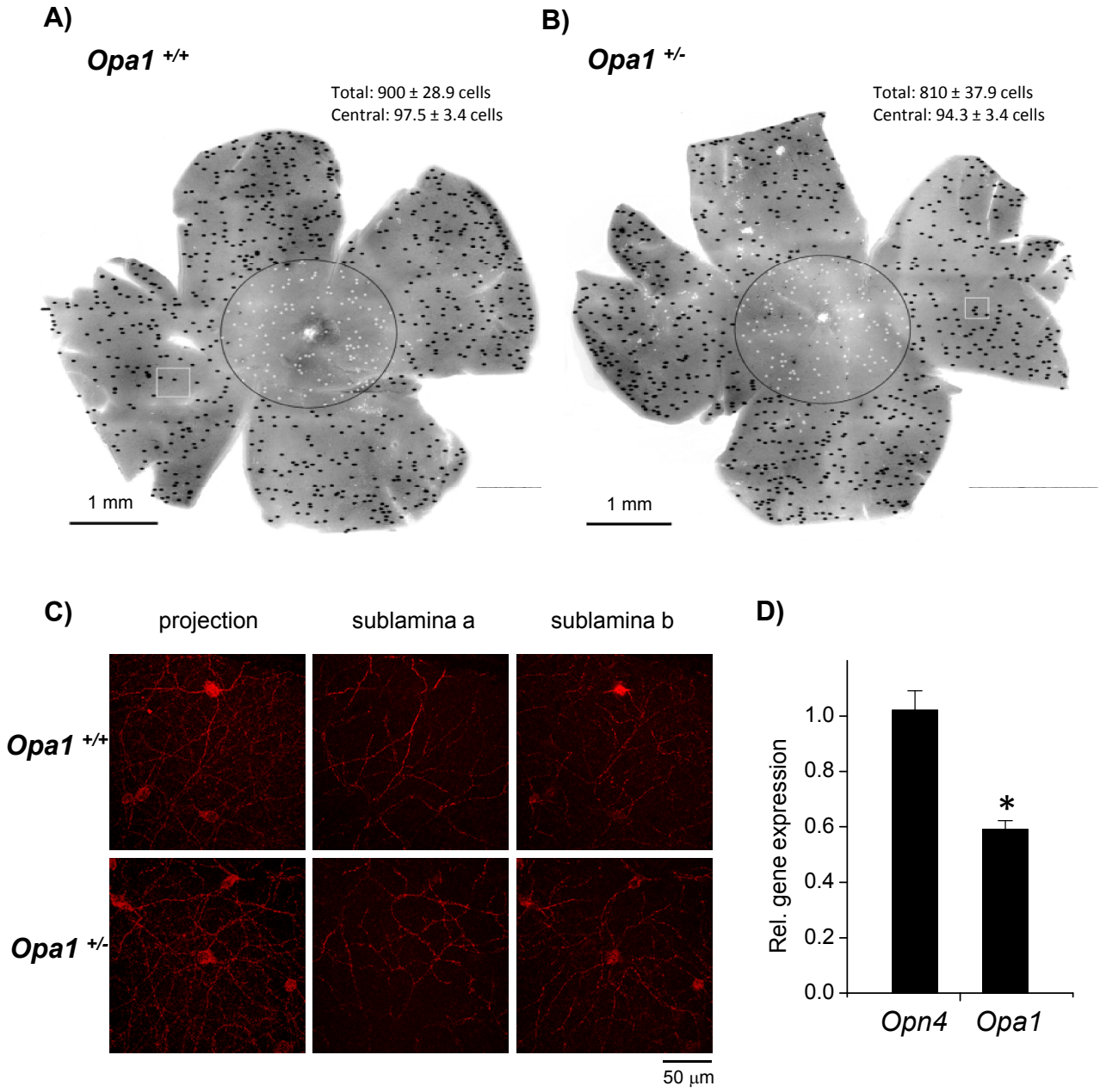
A)
Opa1 +/+
Total: 900 ± 28.9 cells
Central: 97.5 ± 3.4 cells
1 mm
B)
Opa1 +/-
Total: 810 ± 37.9 cells
Central: 94.3 ± 3.4 cells
1 mm
C)
projection
sublamina a
sublamina b
Opa1 +/+
Opa1 +/-
50 μm
D)
Rel. gene expression
1.0
0.8
0.6
0.4
0.2
0.0
*
Opn4
Opa1

Appendix B

Experimental Eye Research 93 (2011) 771–777

Contents lists available at ScienceDirect

Experimental Eye Research

journal homepage: www.elsevier.com/locate/yexer

Letter to the editor

Specific deficits in visual electrophysiology in a mouse model of dominant optic atrophy

Alun R. Barnard [a,*], Peter Charbel Issa [a], Georgia Perganta [a], Pete A. Williams [b], Vanessa J. Davies [b,c], Sumathi Sekaran [a], Marcela Votruba [b,d], Robert E. MacLaren [a,e,**]

[a] Nuffield Laboratory of Ophthalmology & Oxford NIHR Biomedical Research Centre, University of Oxford, John Radcliffe Hospital, Oxford OX3 9DU, UK
[b] School of Optometry and Vision Sciences, Cardiff University, Cardiff CF24 4LU, UK
[c] Cardiff Neuroscience Centre, Cardiff University, Cardiff, UK
[d] Cardiff Eye Unit, University Hospital Wales, Cardiff CF14 4XW, UK
[e] Moorfields Eye Hospital NIHR Biomedical Research Centre, London EC1V 2PD, UK

ARTICLE INFO

Article history:
Received 17 May 2011
Accepted in revised form 16 July 2011
Available online 22 July 2011

Keywords:
optic atrophy
Opa1
retina
ganglion cell
ERG
VEP
electrophysiology

ABSTRACT

Autosomal dominant optic atrophy (ADOA) is a slowly progressive optic neuropathy caused by mutations in the *OPA1* gene. *OPA1* is ubiquitously expressed and plays a key role in mitochondrial fusion. Heterozygous *Opa1* mutant mice (B6; C3-*Opa1*^{Q285STOP}), have previously been reported to develop visual defects and optic nerve changes. In this study, *in vivo* visual electrophysiological testing (ERGs and VEPs) was performed on 11–13 month old B6; C3-*Opa1*^{Q285STOP} mice ($n = 5$) and age/sex matched wildtype littermate controls. Full intensity series were recorded in response to brief (4 ms) single flash stimuli delivered in a Ganzfeld dome under dark- and light-adapted conditions. The major ERG components (a-wave and b-wave) showed no detectable difference from wildtype in the amplitude or implicit time of dark-adapted ERGs across the full intensity range tested. This was also true for the components of the dark-adapted VEP. However, the light-adapted ERG responses revealed a significant reduction in the photopic negative response (PhNR) amplitude in *Opa1*$^{+/-}$ animals relative to wildtypes at the brighter intensities tested. Elements of the light-adapted VEP were also abnormal in mutant mice. Overall *Opa1*$^{+/-}$ mice display functional deficits in electrophysiology that are consistent with ganglion cell dysfunction. These deficits may correlate with a reduction in the dendritic arborisation of retinal ganglion cells, which has been previously reported to occur at a similar age in the same mutant mouse line (Williams et al., 2010). The functional phenotype we have described in this mouse model may be useful in the robust and accurate assessment of potential treatments for ADOA.

1. Introduction

Autosomal dominant optic atrophy (ADOA, OMIM 165500) is the most common inherited optic neuropathy, presenting with variable loss of visual acuity, central visual field defects, colour vision abnormalities and optic atrophy. It is associated with optic nerve degeneration and the ultimate loss of retinal ganglion cells (Votruba, 2004). Heterozygous mutations in *OPA1* cause ADOA (Alexander et al., 2000), likely through haploinsufficiency. The gene product of *OPA1* is ubiquitously expressed and plays a key role in mitochondrial fusion (Davies and Votruba, 2006). Despite this broad cell and tissue distribution, retinal ganglion cells appear to be specifically susceptible to mutations in *OPA1*, although there is increasing evidence that other cell types and neurological systems may also be affected (Amati-Bonneau et al., 2009; Yu-Wai-Man et al., 2010). The coding sequence of the *OPA1* gene is 2.9 kb in size, which, including regulatory sequences, is small enough to fit into recombinant adeno-associated virus (AAV) serotype 2; known to transduce primate ganglion cells highly effectively (Yin et al., 2011). Taken together with the slow degeneration and presumed haploinsufficiency mechanism in ADOA, this makes the disease appealing for future clinical trials using AAV2 mediated gene replacement.

Heterozygous *Opa1* mutant mice have been generated that carry a nonsense mutation in exon 8, which inserts a STOP signal instead of a glutamine amino acid (Q285X), and causes premature protein

* Corresponding author. Nuffield Laboratory of Ophthalmology, University of Oxford, Level 5 and 6 West Wing, The John Radcliffe Hospital, Headley Way, Oxford OX3 9DU, UK. Tel.: +44 (0) 1865 234 701; fax: +44 (0) 1865 234 795.
** Corresponding author. Nuffield Laboratory of Ophthalmology, University of Oxford, Level 5 and 6 West Wing, The John Radcliffe Hospital, Headley Way, Oxford OX3 9DU, UK. Tel.: +44 (0) 1865 234 782; fax: +44 (0) 1865 234 795.
E-mail addresses: alun.barnard@eye.ox.ac.uk (A.R. Barnard), enquiries@eye.ox.ac.uk (R.E. MacLaren).

0014-4835/$ – see front matter © 2011 Elsevier Ltd. All rights reserved.
doi:10.1016/j.exer.2011.07.004

truncation (Davies et al., 2007). Anatomical changes have been previously reported in this line, and include slow optic nerve degeneration, abnormalities in mitochondrial ultrastructure in ganglion cell axons and a progressive ganglion cell dendropathy (Davies et al., 2007; White et al., 2009; Williams et al., 2010). Identifying functional changes in the retina of *Opa1* mutant mice has been significantly more challenging. There is evidence of a reduction in visual acuity in *Opa1* mutant mice, as tested by responses to an optokinetic drum stimulus (Davies et al., 2007). However, the detection of a phenotype using a more direct measure of retinal function, such as the electroretinogram (ERG), would aid considerably in the preclinical assessment of potential treatments such as AAV.*OPA1* gene replacement. This would be particularly true if the functional deficit appeared at relatively early stages. A recent assessment in a different mouse model of *OPA1*-associated ADOA revealed a subtle reduction in amplitude (but not latency) in the cortical visually evoked potential (VEP) at 20 months, but no changes in retinal function were seen (Heiduschka et al., 2010).

Therefore, the purpose of our study was to re-examine and extend visual electrophysiological investigation in *Opa1* mutant mice. Particular emphasis was placed on recording and analysing specific components of the ERG that have been linked to the activity of retinal ganglion cells, such as the scotopic threshold response (STR) and the photopic negative response (PhNR). In our ADOA mouse model, a recent morphological study has shown that retraction of retinal ganglion cell dendrites is apparent from around one year, which is before the onset of ganglion cell and optic nerve degenerative changes (Williams et al., 2010). With this in mind, we investigated mice at a similar age to explore whether a deficit in the ganglion cell associated ERG components might be correlated with these morphological changes and reveal evidence of RGC dysfunction.

2. Methods

2.1. Animals and experimental preparation

Experiments were conducted on five 11–13 month old heterozygous B6; C3-*Opa1*^{Q285STOP} mice (*Opa1*$^{+/-}$, $n = 5$) and an equal number of age/sex matched wildtype littermate controls (*Opa1*$^{+/+}$, $n = 5$). All animal breeding and experimental procedures were performed under approval of local and national ethical and legal authorities. Generation and propagation of the mutant line has been described previously (Davies et al., 2007). Mice were kept in a 12 h light (<100 lux)/12 h dark cycle with food and water available *ad libitum*. All recordings were conducted 5–9 h after the light onset (dawn). Prior to testing all animals were dark-adapted for >90 min. Animal preparation and electrode placement were conducted under dim red illumination. Mice were anaesthetized with a single intraperitoneal injection of Dormitor (medetomidine hydrochloride, 1 mg/kg body weight) and ketamine (60 mg/kg body weight) in water. Pupils were fully dilated (to around 2 mm^2 in both groups) using 1% tropicamide eye drops.

2.2. In vivo electrophysiology

Electroretinogram (ERG) and flash visual evoked potential (VEP) responses were recorded simultaneously from electrodes placed on the cornea and overlying the visual cortex, respectively. For ERG recordings a DTL-type silver-coated nylon thread active electrode was modified to include a custom-made contact lens of optically clear Aclar film (after (Sagdullaev et al., (2004)). This was positioned concentrically on the cornea with hypromellose eye drops (1% methylcellulose solution) pre-applied. The VEP active electrode was a subcutaneous platinum needle (Grass technologies Inc.) placed in the scalp approximately 2 mm lateral to lambda, overlying a large area of the right visual cortex. Platinum needles in the scruff and at the base of the tail served as reference and ground electrodes respectively. Signals were differentially amplified and digitized at a rate of 5 kHz (VEP bandpass filtered 0–100 Hz, ERG unfiltered) using an Espion E2 system (Diagnosys LLC, Cambridge, UK). The amplitude and timing of the major ERG and VEP components was measured with the Espion software (Diagnosys LLC, Cambridge, UK) by placing a cursor at a subjectively determined turning point (i.e. the peak or trough) for each component in individual records (without knowledge of the animal's genotype). The Espion E2 system also generated and controlled the light stimulus. Brief (4 ms) single flash stimuli were delivered in a Ganzfeld dome. Animals were situated on a heated platform, maintained at a constant temperature (38 °C) using a circulating pump-water bath. All recordings were made in a custom-made, light-tight Faraday cage.

For dark-adapted testing, responses were elicited by brief flashes of white light recorded on dark background. Stimulus intensity was increased in log unit steps across a 7 log unit range (−6 to 1 log cd s/m^2, approximate scotopic units can be obtained by adding 0.44 to these values). At each intensity tested, 50 responses were averaged per result. An interstimulus interval (ISI) of 2 s was used for dimmer stimuli (−6 to −3 log cd s/m^2) and for brighter intensities (−2 to 1 log cd s/m^2) an ISI of 5 s was used. For light-adapted testing, animals were pre-exposed to steady, full-field, white background illumination (30 cd/m^2) for 10 min. Responses were then recorded to brief light flashes of three intensities (0, 1 & 1.4 log cd s/m^2) superimposed on the stable background. In all cases an ISI of 1 s was used and 50 responses were averaged per result.

2.3. In vivo imaging

Immediately after electrophysiological recordings, the fundus was imaged with a confocal scanning laser ophthalmoscope (cSLO; Spectralis-HRA, Heidelberg Engineering, Heidelberg, Germany) using a 55° angle lens. The optic disc was positioned in the centre of the image and a series of images could be obtained of various retinal layers by changing the focus. Retinal infrared (IR) reflectance images were recorded using an 810 nm laser as light source. For fundus autofluorescence (FAF) imaging a 488 nm laser was used for excitation and recording of emitted light was limited by a barrier filter to wavelengths between 500 and 700 nm. Images were recorded using the inbuilt "automatic real time" (ART) mode and enhanced using the image normalisation option, if necessary.

3. Results

3.1. Dark-adapted visual responses are normal in *Opa1*$^{+/-}$ mice

Initially, mice were exposed to brief (4 ms) flashes of white light under otherwise dark conditions. Under these dark-adapted conditions, typical ERG and flash VEP waveforms could be recorded in *Opa1*$^{+/-}$ animals. Generally, as the intensity of the light stimulus was increased there was a concomitant increase in the size and speed of ERG responses. Such intensity dependent alterations are characteristic of normal responses in wildtype animals. Comparison of representative and group averaged responses showed no clear difference between wildtype and *Opa1*$^{+/-}$ animals (Fig. 1A). Quantification of the major ERG components (a-wave and b-wave) confirmed that there was no detectable difference in the size (amplitude) or speed (implicit time) of dark-adapted ERGs across the full intensity range tested (Fig. 1B and C). Visual comparison of the amplitude and timing of oscillatory potentials (OPs) in unfiltered and 75–300 Hz bandpass filtered records indicated that these were indistinguishable between genotypes and therefore were not further analysed.

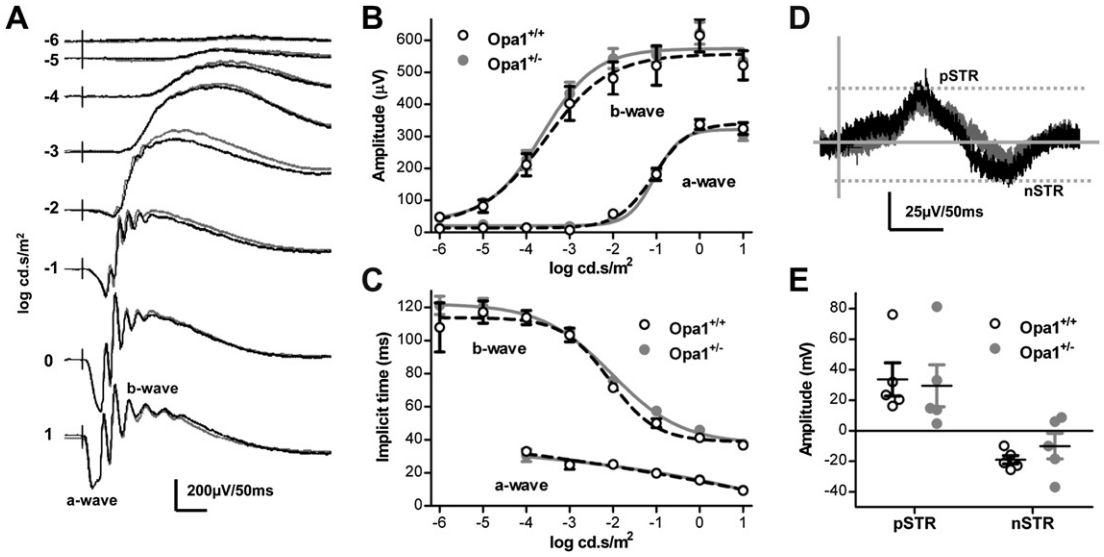

Fig. 1. Dark-adapted ERG recordings are not significantly affected in *Opa1*$^{+/-}$ mice. A. Averaged traces for each genotype ($n = 5$ for each). Stimulus intensity shown on left, values in log cd s/m^2. Quantification of B. Amplitude and C. Implicit Time of a- & b-waves. Plotted values are mean ± SEM, $n = 4$. D. Expanded view of genotype averaged ERG to dimmest stimulus (−6 log cd s/m^2) shows scotopic threshold response (STR) waveform. E. Amplitude of positive & negative STR components. Individual values plotted (n = 5), horizontal bars show group means with SEM. Wildtype control (*Opa1*$^{+/+}$) traces and values are shown in black/empty symbols, heterozygote mutants (*Opa1*$^{+/-}$) are in grey/filled symbols.

In response to very dim stimuli the dark-adapted ERG shows a very characteristic waveform known as the scotopic threshold response (STR). This waveform is thought to reflect activity of the proximal retina, i.e. amacrine and ganglion cell (Saszik et al., 2002). In response to the dimmest stimulus used (−6 log cd s/m^2) a STR could be seen in *Opa1*$^{+/-}$ and control animals (Fig. 1D). Indeed, quantification of the amplitude of the positive and negative components of the STR showed that there was no significant reduction in this waveform in heterozygous mutant mice (Fig. 1E).

Dark-adapted flash VEPs (Fig. 2A) were dominated by a strong negative component (N1) at all intensities tested. At higher intensities N1 was preceded by a small positive deflection (P1). A positive potential (P2) was also seen following the negative peak of N1. This was primarily apparent as an increasingly abrupt return to baseline (with increasing stimulus intensity) but sometimes at the highest stimuli resulted in a positive deflection above baseline. Again, as the intensity of the light stimulus was increased there was a concomitant increase in the size and speed of responses. As with the ERG, comparison of VEP responses showed no clear difference between genotypes at this age (Fig. 2A). Quantification of the size (amplitude) or speed (latency) of VEP components P1, N1 & P2 (Fig. 2B–G) confirmed that there was no significant difference between mutant and wildtype mice across the full intensity range tested.

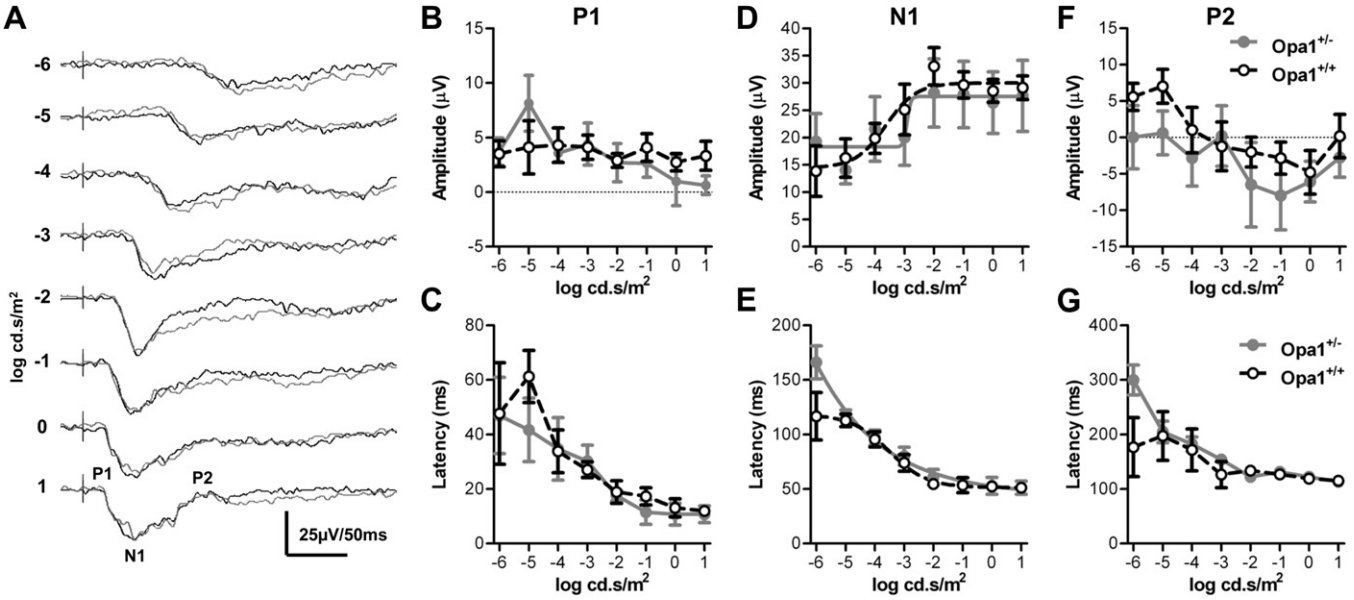

Fig. 2. Dark-adapted VEPs are not significantly affected in *Opa1*$^{+/-}$ mice. A. Averaged traces for each genotype ($n = 5$ for both). Stimulus intensity shown on left, values are log cd s/m^2. Quantification of B. Amplitude of P1. C. Latency of P1. D. Amplitude of N1. E. Latency of N1. F. Amplitude of P2. G. Latency of P2. In all graphs plotted values are mean ± SEM, $n = 5$. Wildtype control (*Opa1*$^{+/+}$) traces and values are shown in black/empty symbols, heterozygote mutants (*Opa1*$^{+/-}$) are in grey/filled symbols.

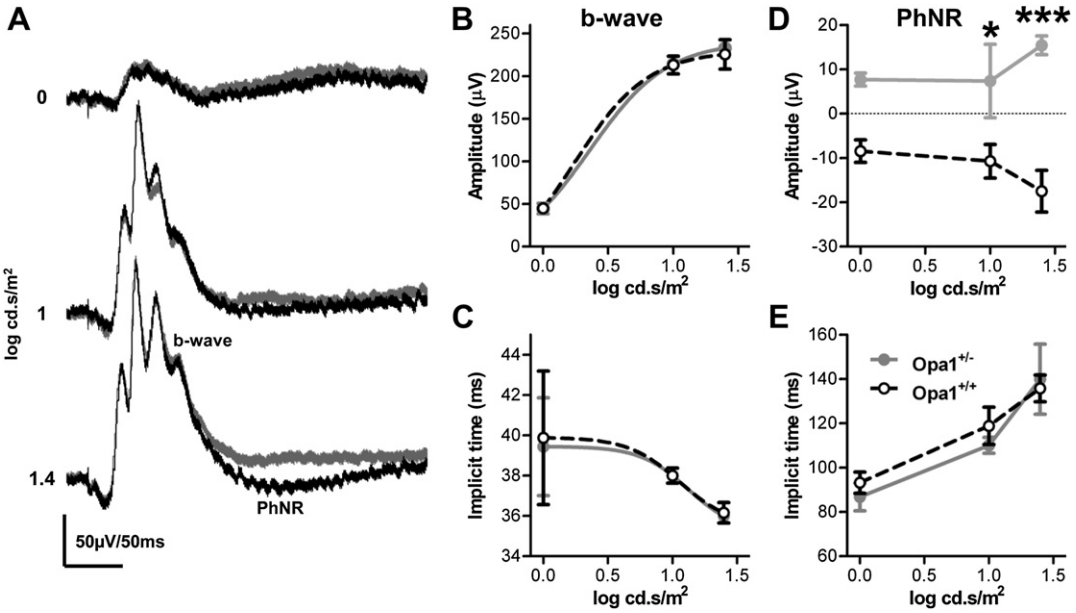

Fig. 3. *Opa1*$^{+/-}$ mice display a specific and significant reduction in the photopic negative response of the light-adapted ERG. A. Averaged traces for each genotype ($n = 5$ for both). Stimulus intensity shown on right, values are log cd s/m^2. Quantification of B. Amplitude of b-wave. C. Implicit time of b-wave. D. Amplitude of Photopic Negative Response (PhNR). E. Implicit time of PhNR. In all graphs plotted values are mean ± SEM, $n = 5$. * = $p < 0.05$, *** = $p < 0.001$: significance of Bonferroni posttests after Repeated measures Two-way ANONA with genotype and stimulus intensity as factors. Wildtype control (*Opa1*$^{+/+}$) traces and values are shown in black/empty symbols, heterozygote mutants (*Opa1*$^{+/-}$) are in grey/filled symbols.

3.2. *Opa1*$^{+/-}$ mice display specific and significant deficits in light-adapted visual responses

Following dark-adapted visual testing, mice were exposed to steady, full-field, white background illumination (30 cd/m^2). After 10 min continuous exposure, photopic visual responses were recorded to brief light flashes of different intensity, superimposed on the background. As with dark-adapted conditions, superficially normal ERG and VEP responses could be recorded from mutant animals. At all stimulus intensities, light-adapted ERGs predominantly consisted of a fast, positive b-wave with minor oscillatory potentials and little or no a-wave (Fig. 3A). Light-adapted VEPs (Fig. 4A) were similar to dark-adapted VEPs although all components were of smaller amplitude. Again, there was a clear intensity dependence of the shape, size and speed of ERG and VEP responses.

There were specific differences in the light-adapted ERG responses between heterozygous mutants and wildtype controls. Although the positive peak of the b-wave was indistinguishable between genotypes, there was a clear difference in the immediately following negative deflection – the photopic negative response (PhNR). The amplitudes and implicit times of b-waves were quantified and compared (Fig. 3B and C), which confirmed the absence of

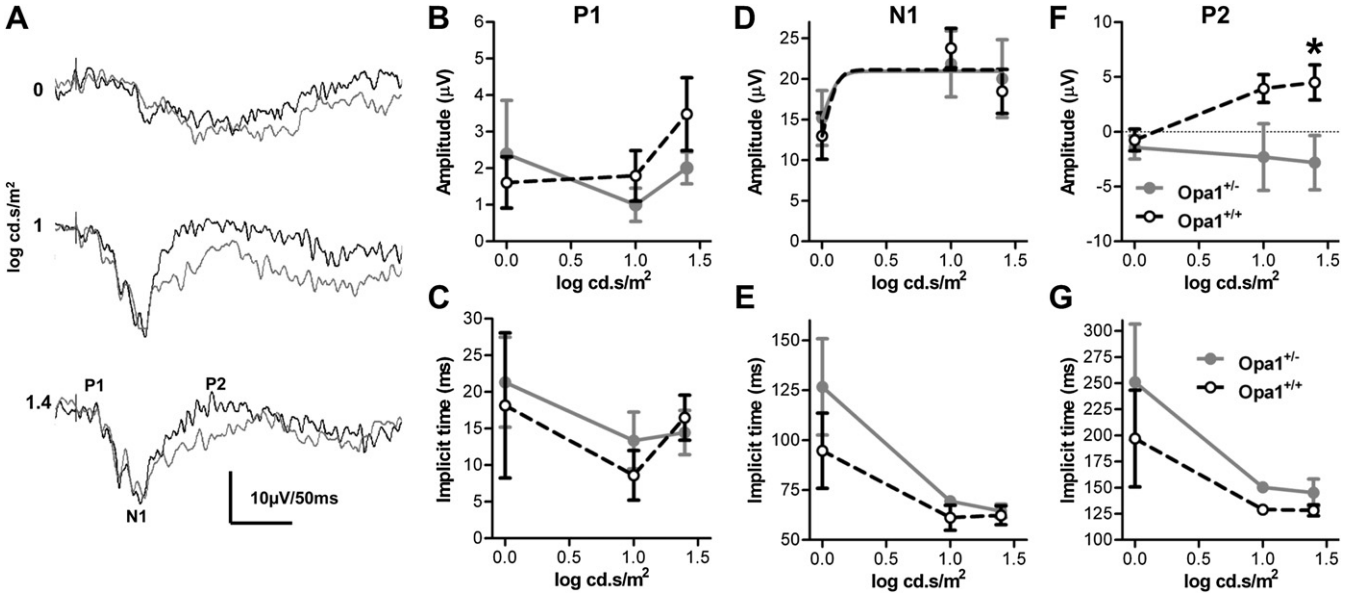

Fig. 4. *Opa1*$^{+/-}$ mice have a significant reduction in the P2 component of light-adapted VEP recordings. A. Averaged traces for each genotype ($n = 5$ for both). Stimulus intensity shown on left, values are log cd s/m^2. Quantification of B. Amplitude of P1. C. Latency of P1. D. Amplitude of N1. E. Latency of N1. F. Amplitude of P2. G. Latency of P2. In all graphs plotted values are mean ± SEM, $n = 5$. * = $p < 0.05$: significance of Bonferroni posttest after Repeated measures Two-way ANONA with genotype and stimulus intensity as factors. Wildtype control (*Opa1*$^{+/+}$) traces and values are shown in black/empty symbols, heterozygote mutants (*Opa1*$^{+/-}$) are in grey/filled symbols.

any significant difference between genotypes (Repeated measures Two-way ANOVA with genotype and stimulus intensity as factors, genotype factor $p = 0.77$, $F = 0.088$, $df = 1$ and $p = 0.90$, $F = 0.0156$, $df = 1$ for amplitude and implicit time respectively). Importantly, quantification of the PhNR amplitude (measured from baseline to negative peak) revealed a significant reduction in *Opa1*$^{+/-}$ animals relative to wildtypes at the two brightest intensities tested (Fig. 3D. Repeated measures Two-way ANOVA with genotype and stimulus intensity as factors: Interaction not significant ($p = 0.12$, $F = 2.40$, $df = 2$), stimulus intensity not significant ($p = 0.95$, $F = 0.0489$, $df = 2$), genotype highly significant ($p < 0.001$, $F = 31.3$, $df = 1$). Bonferroni posttests to compare genotypes at each stimulus intensity were as follows: 0 log cd s/m^2 not significantly different ($p > 0.05$, $t = 2.57$), 1 log cd s/m^2 significantly different ($p < 0.05$, $t = 2.88$), 1.4 log cd s/m^2 highly significantly different ($p < 0.001$, $t = 5.24$)). Quantification and comparison of the PhNR implicit times between genotypes showed that they were not different (Fig. 3E. Repeated measures Two-way ANOVA with genotype and stimulus intensity as factors, genotype factor not significant ($p = 0.60$, $F = 0.283$, $df = 2$)). Light-adapted oscillatory potentials appeared very similar between genotypes (in unfiltered and 75–300 Hz bandpass filtered records) and were not further analysed. Conversely, when we applied a 100 Hz lowpass filter to ERG records to reduce the effect of OPs, quantification of the b-wave and PhNR yielded very similar results as in unfiltered records and the statistical comparisons were equivalent to those described above (data not shown).

For light-adapted flash VEPs, another specific deficit was apparent. Although the negative N1 component appeared identical between genotypes, *Opa1*$^{+/-}$ animals showed a reduction in the subsequent positive deflection (P2 wave). Quantification of the VEP components (Fig. 4B–G) showed no significant difference in P1 and N1 amplitude or latency between *Opa1*$^{+/-}$ mice and their wildtype control at any of the stimulus intensities tested (Repeated measures Two-way ANOVA with genotype and stimulus intensity as factors, genotype factor not significant for P1 amplitude ($p = 0.50$, $F = 0.501$, $df = 1$), P1 latency ($p = 0.66$, $F = 0.212$, $df = 1$), N1 amplitude ($p = 0.89$, $F = 0.0213$, $df = 1$) or N1 latency ($p = 0.32$, $F = 1.16$, $df = 1$)). However, quantification of the P2 component (Fig. 4F and G) confirmed a significant amplitude reduction in *Opa1*$^{+/-}$ mice relative to wildtypes at the brightest intensity tested (Repeated measures Two-way ANOVA with genotype and stimulus intensity as factors: Interaction not significant ($p = 0.08$, $F = 3.08$, $df = 2$), stimulus intensity not significant ($p = 0.33$, $F = 1.19$, $df = 2$), genotype significantly different ($p < 0.05$, $F = 6.05$, $df = 1$). Bonferroni posttests to compare genotypes at each stimulus intensity were as follows: 0 log cd s/m^2 not significantly different ($p > 0.05$, $t = 0.265$), 1 log cd s/m^2 not significantly different ($p < 0.05$, $t = 2.46$), 1.4 log cd s/m^2 significantly different ($p < 0.05$, $t = 2.88$)). P2 latencies were not different between genotypes (Repeated measures Two-way ANOVA with genotype and stimulus intensity as factors, genotype factor not significant ($p = 0.29$, $F = 1.29$, $df = 2$)).

Taken together, the dark- and light-adapted recordings indicated that both rod and cone visual pathways remain largely intact and unaffected in heterozygous mutant animals at this age (one year). However, distinctive and significant differences were detected in late evolving components of the light-adapted ERG and flash VEP responses. Thus, we describe a specific and so far unreported functional visual deficit in a mouse model of ADOA.

3.3. The ocular fundi of *Opa1*$^{+/-}$ mice are indistinguishable from those of wildtype controls

Although a recent study showed no detectable retinal ganglion cell soma loss in these mice at one year (Williams et al., 2010), another study of *Opa1*$^{+/-}$ mice of a different origin identified a significant increase in retinal macrophages associated with ganglion cell loss at two years using a carbocyanine dye (Heiduschka et al., 2010). We were therefore interested to see if there was any change in macrophage distribution within the retina coincident with the above functional changes observed at one year. We used the cSLO which has recently been shown to be highly effective at identifying individual retinal macrophages *in vivo* (Luhmann et al., 2009; Xu et al., 2008). IR-reflectance images throughout the depth focus, from the retinal pigment epithelium (RPE)/outer retina to the nerve fibre layer, were comparable in mutant (Fig. 5A&B) and control animals (Fig. 5D and E). Fundus autofluorescence (FAF) imaging revealed a moderate level of background autofluorescence and the presence of a few bright foci of very high fluorescence signal. These foci were dispersed in the outer retina or distributed along retinal vessels in the inner retina/nerve fibre layer, as expected for subretinal and perivascular microglia. Although present in mutant mice, they were also found in similar locations and with similar numbers in age-matched littermate wildtype controls (Fig. 5C and F). Hence there was no evidence of low grade inflammation or signs of augmented macrophage recruitment in the retina of the *Opa1*$^{+/-}$ at this age.

4. Discussion

In this letter we describe a clear functional deficit in the PhNR of *Opa1*$^{+/-}$ mice at one year.

To our knowledge, is the first report of a phenotype detectable by ERG testing in a mouse model of ADOA. This finding is significant, because it represents an entirely retina-specific electrical response, whereas VEP recordings can be affected by mild impairment of central pathways (Lachapelle et al., 2004) where OPA1 is also widely expressed (Bette et al., 2005). Hence the PhNR may provide a useful biomarker for retinal dysfunction at early stages of dominant optic atrophy in these mice and might provide a useful measure against which to assess any retina-specific therapies, such as intravitreal gene delivery.

The precise cellular electrical generator of the PhNR has not yet been clearly identified. Although there is agreement that the potential must be derived from the proximal retina, there remains debate if it is predominantly amacrine cell or RGC in origin. There are species differences and even rodent studies have provided equivocal results; with some authors reporting a reduction in the PhNR (Li et al., 2005) while others report that it is unaffected (Mojumder et al., 2008) following optic nerve injury (to induce rapid RGC loss). Other optic nerve injury studies do not explicitly measure the PhNR (Alarcon-Martinez et al., 2010; Bui and Fortune, 2004) or are complicated by the inconsistent nature of the PhNR and the fact that it is not always reliably observed under baseline conditions, even in recording protocols that have previously been successful (Miura et al., 2009). The reasons for this are unclear, although we might speculate that factors such as time of day and long-term light history might influence the magnitude and reliability of the PhNR, as has been shown for the b-wave of the photopic ERG in mice (Barnard et al., 2006). In our study we were careful to keep these factors constant between experimental groups. These experimental precautions, combined with a prolonged recording epoch, may facilitate detection of the PhNR deficit.

Importantly, our results are phenotypically similar to the observation of a reduced PhNR in the flash ERG of patients with ADOA due to *OPA1* mutations (Miyata et al., 2007). In addition, glaucoma studies have found the PhNR to be attenuated in patients with ocular hypertension and open angle glaucoma and proposed that it can be used to quantify retinal ganglion cell dysfunction, which occurs prior to cell death in the glaucomas (Drasdo et al., 2001; North et al., 2010). Other human studies have predominantly used the pattern

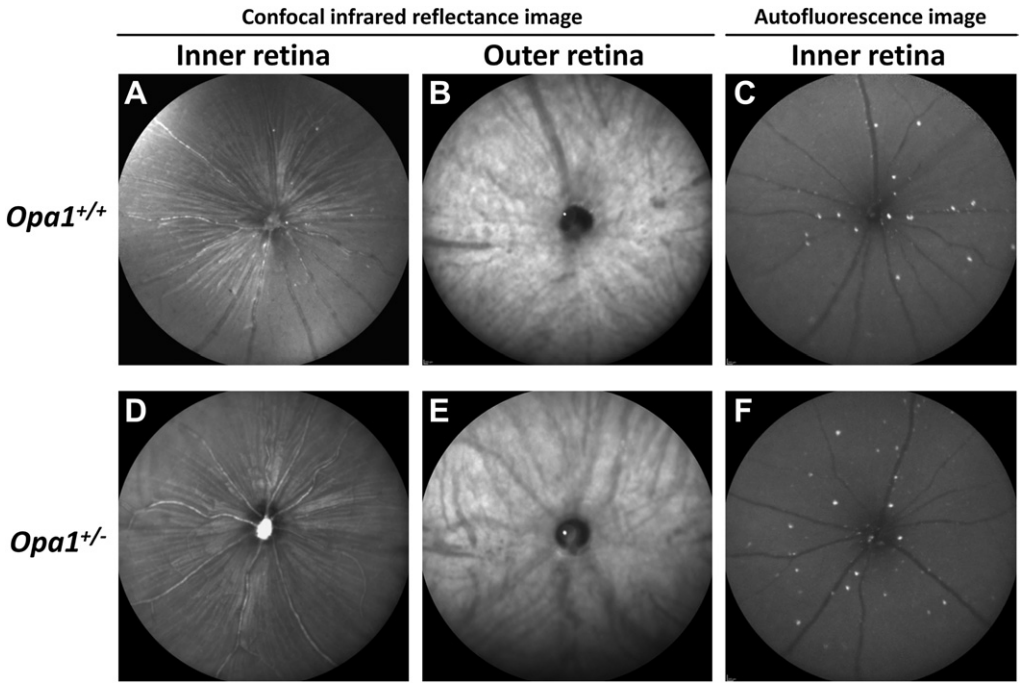

Fig. 5. The ocular fundi of *Opa1*$^{+/-}$ mice are indistinguishable from wildtype controls. Representative fundal images acquired using the cSLO. Reflectance infrared (IR) images acquired at the inner retina/nerve fibre layer confocal plane in wildtype control (A. *Opa1*$^{+/+}$) and heterozygote mutants (D. *Opa1*$^{+/-}$). Reflectance IR images acquired at the retinal pigment epithelium (RPE)/outer retina confocal plane in *Opa1*$^{+/+}$ (B.) and *Opa1*$^{+/-}$ (E.) mice. Fundus autofluorescence (FAF) images acquired at the inner retina/nerve fibre layer confocal plane in *Opa1*$^{+/+}$ (C.) and *Opa1*$^{+/-}$ (F.) mice.

electroretinogram (PERG), rather than the flash ERG used in our work. In ADOA patients the PERG shows an abnormal ratio of waveforms, with a reduction in the amplitude of the N95 waveform relative to the size of waveform P50 (Berninger et al., 1991; Holder et al., 1998; Votruba et al., 1998). As the PERG N95 component is very likely to be RGC in origin, these findings are consistent with predominantly ganglion cell death/dysfunction in ADOA. Work in non-human primates has led to the suggestion that the same cellular generators are responsible for the PhNR and the N95 of the PERG (Viswanathan et al., 2000). PERG recordings in mice are technically more demanding, the signals recorded are of very low amplitude and it is less clear how the components of the PERG relate to the flash ERG, if indeed they do (Miura et al., 2009; Porciatti, 2007). Nevertheless, PERG testing in *Opa1* mutant mice would now be useful to further explore ganglion cell function and should be attempted in future studies.

We did not observe any significant reduction in the dark-adapted scotopic threshold response (STR) in *Opa1*$^{+/-}$ mice. The STR, like the PhNR, is the subject of some discussion with regards to the most significant cellular generator (Saszik et al., 2002). Amacrine and ganglion cells are again likely contributors and the consensus of work involving pharmacology and optic nerve damage and genetic models in rodents seems to be that RGCs are relatively more important, particularly for the pSTR (Alarcon-Martinez et al., 2010, 2009; Bui and Fortune, 2004; Moshiri et al., 2008; Saszik et al., 2002). Given the proximal retinal origin, it is perhaps surprising that the STR is unaffected in *Opa1*$^{+/-}$ mice, especially given the reduction in PhNR amplitude. In fact, the observation that one amacrine/ganglion cell derived ERG component (PhNR) is affected while the other (STR) is not, is consistent with several alternative explanations. Perhaps the simplest is that the PhNR and STR are derived from separate and non-overlapping cell populations in the mouse retina that are differentially affected in heterozygous mutant mice. The observation that OPA1 is expressed in the ganglion cell layer (GCL), inner plexiform layer (IPL), and inner nuclear layer (INL) of the retina (Aijaz et al., 2004) may be relevant to this. Alternatively, at this age mutant mice may display a STR deficit which is too subtle to be detected in our recordings; stimulus paradigms that focus specifically on the range of stimuli eliciting n and pSTRs might show the differences more readily. It would be of great interest but, to our knowledge, the STR of the flash ERG has not yet been studied in ADOA patients.

Our principal finding in VEP recordings was that function is predominantly unaltered in *Opa1*$^{+/-}$ mice. N1, the main component of the mouse flash VEP, was not significantly different from controls, in terms of both amplitude and latency, under all conditions tested. In patients with ADOA, the amplitude and/or latency of multiple components of the VEP can be affected (Granse et al., 2003; Holder et al., 1998; Votruba et al., 1998). Differences in the stimuli used (flash vs. pattern) and large species differences in the resultant VEP waveforms belie a detailed comparison with our results. However, we did detect a defined VEP phenotype (significant reduction in the-amplitude of P2 in *Opa1*$^{+/-}$ mice relative to wildtype controls), further confirming the face validity of our mouse line as a model of ADOA. Although this deficit is subtle, it could foreshadow a more generalised impairment of the VEP, with increasing age/disease progression.

Heiduschka et al. (2010) reported a 50% reduction in the P1-N1 amplitudes of dark-adapted VEPs in *Opa1* mutant mice at higher light intensities and a statistically insignificant trend towards smaller amplitudes in light-adapted VEPs. They note that the P2 amplitudes showed no difference, but the quantitative data were not shown. VEP latency was not affected in mutant mice in their study, which is in agreement with our results. Mice used in their study were substantially older (>20 months old) than those used here (11–13 months old) which perhaps accounts for the difference in terms of P1-N1/N1 amplitude findings. However, the fact that they do not detect a significant reduction in P2 amplitude cannot be explained by age differences, but is perhaps due to differences in

the precise mouse model used or because of minor technical differences between the studies.

Taken together with normal ERG findings, Heiduschka et al. (2010) say that their VEP data indicate the number of RGCs that transmit the signal has to be reduced and also implies that the remaining RGCs function normally. This is applicable in the context of significant RGC loss but does not explain functional deficits when no death of RGC can be detected. This is important, as previous work shows that no significant loss of ganglion cells can be detected in the ADOA model used, at the age we tested or even older (White et al., 2009; Williams et al., 2010). Therefore, our preferred interpretation of the functional deficits we observe is that they are due to altered function in RGCs, rather than RGC death. Altered RGC function may be related to pathophysiology in cellular processes associated with defects in mitochondrial fusion. A morphological basis for altered RGC function is also provided by the recent finding of dendropathy and increased dendritic pruning specifically in ON-centre RGCs in the *Opa1*$^{+/-}$ mouse (Williams et al., 2010).

5. Conclusions

To our knowledge this is the first report of a functional deficit detectable with the ERG in a mouse model of ADOA. The reduction in PhNR amplitude is indicative of ganglion cell dysfunction and is similar to the phenotype observed in some ADOA patients (Miyata et al., 2007). The deficit is apparent in *Opa1*$^{+/-}$ mice at one year, which coincides with an increase in dendritic retraction/pruning in retinal ganglion cells, which has been previously reported to occur at a similar age in the same mutant mouse line (Williams et al., 2010). A functional phenotype that is detectable by ERG offers particular benefits as it is less invasive than cortical electrode VEP recording. Importantly, with ERG, treatments of one eye can be compared with the untreated partner eye in the same animal. Thus, the ERG phenotype we have described may be useful in the robust and accurate assessment of potential treatments for ADOA.

Acknowledgements

We would like to thank the following sources of funding: The Royal College of Surgeons of Edinburgh, the Health Foundation, the NIHR Biomedical Research Centres, Marie Curie Intra-European Fellowship (no.: 237238); the Seventh European Community Framework Program; European Commission, Fight for Sight, Medical Research Council UK (Grant no.: G0700949), the Biotechnology and Biological Sciences Research Council (Grant no.: BB/G003602/1) and the Wellcome Trust (Grant no.: 091984/Z/10/Z).

References

Aijaz, S., Erskine, L., Jeffery, G., Bhattacharya, S.S., Votruba, M., 2004. Developmental expression profile of the optic atrophy gene product: OPA1 is not localized exclusively in the mammalian retinal ganglion cell layer. Invest. Ophthalmol. Vis. Sci. 45, 1667–1673.

Alarcon-Martinez, L., Aviles-Trigueros, M., Galindo-Romero, C., Valiente-Soriano, J., Agudo-Barriuso, M., Villa Pde, L., Villegas-Perez, M.P., Vidal-Sanz, M., 2010. ERG changes in albino and pigmented mice after optic nerve transection. Vision Res. 50, 2176–2187.

Alarcon-Martinez, L., de la Villa, P., Aviles-Trigueros, M., Blanco, R., Villegas-Perez, M.P., Vidal-Sanz, M., 2009. Short and long term axotomy-induced ERG changes in albino and pigmented rats. Mol. Vis. 15, 2373–2383.

Alexander, C., Votruba, M., Pesch, U.E., Thiselton, D.L., Mayer, S., Moore, A., Rodriguez, M., Kellner, U., Leo-Kottler, B., Auburger, G., Bhattacharya, S.S., Wissinger, B., 2000. OPA1, encoding a dynamin-related GTPase, is mutated in autosomal dominant optic atrophy linked to chromosome 3q28. Nat. Genet. 26, 211–215.

Amati-Bonneau, P., Milea, D., Bonneau, D., Chevrollier, A., Ferre, M., Guillet, V., Gueguen, N., Loiseau, D., de Crescenzo, M.A., Verny, C., Procaccio, V., Lenaers, G., Reynier, P., 2009. OPA1-associated disorders: phenotypes and pathophysiology. Int. J. Biochem. Cell Biol. 41, 1855–1865.

Barnard, A.R., Hattar, S., Hankins, M.W., Lucas, R.J., 2006. Melanopsin regulates visual processing in the mouse retina. Curr. Biol. 16, 389–395.

Berninger, T.A., Jaeger, W., Krastel, H., 1991. Electrophysiology and colour perimetry in dominant infantile optic atrophy. Br. J. Ophthalmol. 75, 49–52.

Bette, S., Schlaszus, H., Wissinger, B., Meyermann, R., Mittelbronn, M., 2005. OPA1, associated with autosomal dominant optic atrophy, is widely expressed in the human brain. Acta Neuropathol. 109, 393–399.

Bui, B.V., Fortune, B., 2004. Ganglion cell contributions to the rat full-field electroretinogram. J. Physiol. 555, 153–173.

Davies, V., Votruba, M., 2006. Focus on molecules: the OPA1 protein. Exp. Eye Res. 83, 1003–1004.

Davies, V.J., Hollins, A.J., Piechota, M.J., Yip, W., Davies, J.R., White, K.E., Nicols, P.P., Boulton, M.E., Votruba, M., 2007. Opa1 deficiency in a mouse model of autosomal dominant optic atrophy impairs mitochondrial morphology, optic nerve structure and visual function. Hum. Mol. Genet. 16, 1307–1318.

Drasdo, N., Aldebasi, Y.H., Chiti, Z., Mortlock, K.E., Morgan, J.E., North, R.V., 2001. The s-cone PHNR and pattern ERG in primary open angle glaucoma. Invest. Ophthalmol. Vis. Sci. 42, 1266–1272.

Granse, L., Bergstrand, I., Thiselton, D., Ponjavic, V., Heijl, A., Votruba, M., Andreasson, S., 2003. Electrophysiology and ocular blood flow in a family with dominant optic nerve atrophy and a mutation in the OPA1 gene. Ophthalmic Genet. 24, 233–245.

Heiduschka, P., Schnichels, S., Fuhrmann, N., Hofmeister, S., Schraermeyer, U., Wissinger, B., Alavi, M.V., 2010. Electrophysiological and histologic assessment of retinal ganglion cell fate in a mouse model for OPA1-associated autosomal dominant optic atrophy. Invest. Ophthalmol. Vis. Sci. 51, 1424–1431.

Holder, G.E., Votruba, M., Carter, A.C., Bhattacharya, S.S., Fitzke, F.W., Moore, A.T., 1998. Electrophysiological findings in dominant optic atrophy (DOA) linking to the OPA1 locus on chromosome 3q 28-qter. Doc. Ophthalmol. 95, 217–228.

Lachapelle, J., Ouimet, C., Bach, M., Ptito, A., McKerral, M., 2004. Texture segregation in traumatic brain injury – a VEP study. Vision Res. 44, 2835–2842.

Li, B., Barnes, G.E., Holt, W.F., 2005. The decline of the photopic negative response (PhNR) in the rat after optic nerve transection. Doc. Ophthalmol. 111, 23–31.

Luhmann, U.F., Robbie, S., Munro, P.M., Barker, S.E., Duran, Y., Luong, V., Fitzke, F.W., Bainbridge, J.W., Ali, R.R., MacLaren, R.E., 2009. The drusenlike phenotype in aging Ccl2-knockout mice is caused by an accelerated accumulation of swollen autofluorescent subretinal macrophages. Invest. Ophthalmol. Vis. Sci. 50, 5934–5943.

Miura, G., Wang, M.H., Ivers, K.M., Frishman, L.J., 2009. Retinal pathway origins of the pattern ERG of the mouse. Exp. Eye Res. 89, 49–62.

Miyata, K., Nakamura, M., Kondo, M., Lin, J., Ueno, S., Miyake, Y., Terasaki, H., 2007. Reduction of oscillatory potentials and photopic negative response in patients with autosomal dominant optic atrophy with OPA1 mutations. Invest. Ophthalmol. Vis. Sci. 48, 820–824.

Mojumder, D.K., Sherry, D.M., Frishman, L.J., 2008. Contribution of voltage-gated sodium channels to the b-wave of the mammalian flash electroretinogram. J. Physiol. 586, 2551–2580.

Moshiri, A., Gonzalez, E., Tagawa, K., Maeda, H., Wang, M., Frishman, L.J., Wang, S.W., 2008. Near complete loss of retinal ganglion cells in the math5/brn3b double knockout elicits severe reductions of other cell types during retinal development. Dev. Biol. 316, 214–227.

North, R.V., Jones, A.L., Drasdo, N., Wild, J.M., Morgan, J.E., 2010. Electrophysiological evidence of early functional damage in glaucoma and ocular hypertension. Invest. Ophthalmol. Vis. Sci. 51, 1216–1222.

Porciatti, V., 2007. The mouse pattern electroretinogram. Doc. Ophthalmol. 115, 145–153.

Sagdullaev, B.T., DeMarco, P.J., McCall, M.A., 2004. Improved contact lens electrode for corneal ERG recordings in mice. Doc. Ophthalmol. 108, 181–184.

Saszik, S.M., Robson, J.G., Frishman, L.J., 2002. The scotopic threshold response of the dark-adapted electroretinogram of the mouse. J. Physiol. 543, 899–916.

Viswanathan, S., Frishman, L.J., Robson, J.G., 2000. The uniform field and pattern ERG in macaques with experimental glaucoma: removal of spiking activity. Invest. Ophthalmol. Vis. Sci. 41, 2797–2810.

Votruba, M., 2004. Molecular genetic basis of primary inherited optic neuropathies. Eye (Lond) 18, 1126–1132.

Votruba, M., Fitzke, F.W., Holder, G.E., Carter, A., Bhattacharya, S.S., Moore, A.T., 1998. Clinical features in affected individuals from 21 pedigrees with dominant optic atrophy. Arch. Ophthalmol. 116, 351–358.

White, K.E., Davies, V.J., Hogan, V.E., Piechota, M.J., Nichols, P.P., Turnbull, D.M., Votruba, M., 2009. OPA1 deficiency associated with increased autophagy in retinal ganglion cells in a murine model of dominant optic atrophy. Invest. Ophthalmol. Vis. Sci. 50, 2567–2571.

Williams, P.A., Morgan, J.E., Votruba, M., 2010. Opa1 deficiency in a mouse model of dominant optic atrophy leads to retinal ganglion cell dendropathy. Brain 133, 2942–2951.

Xu, H., Chen, M., Manivannan, A., Lois, N., Forrester, J.V., 2008. Age-dependent accumulation of lipofuscin in perivascular and subretinal microglia in experimental mice. Aging Cell 7, 58–68.

Yin, L., Greenberg, K., Hunter, J.J., Dalkara, D., Kolstad, K.D., Masella, B.D., Wolfe, R., Visel, M., Stone, D., Libby, R.T., Diloreto Jr., D., Schaffer, D., Flannery, J., Williams, D.R., Merigan, W.H., 2011. Intravitreal injection of AAV2 transduces macaque inner retina. Invest. Ophthalmol. Vis. Sci.

Yu-Wai-Man, P., Griffiths, P.G., Gorman, G.S., Lourenco, C.M., Wright, A.F., Auer-Grumbach, M., Toscano, A., Musumeci, O., Valentino, M.L., Caporali, L., Lamperti, C., Tallaksen, C.M., Duffey, P., Miller, J., Whittaker, R.G., Baker, M.R., Jackson, M.J., Clarke, M.P., Dhillon, B., Czermin, B., Stewart, J.D., Hudson, G., Reynier, P., Bonneau, D., Marques Jr., W., Lenaers, G., McFarland, R., Taylor, R.W., Turnbull, D.M., Votruba, M., Zeviani, M., Carelli, V., Bindoff, L.A., Horvath, R., Amati-Bonneau, P., Chinnery, P.F., 2010. Multi-system neurological disease is common in patients with OPA1 mutations. Brain 133, 771–786.